2013

MODELING OF CO2-WATER-ROCK INTERACTIONS IN A MISSISSIPPIAN SANDSTONE RESERVOIR OF KENTUCKY

Anne M. Schumacher
University of Kentucky, annemschumacher@gmail.com

STUDENT AGREEMENT:

I represent that my thesis or dissertation and abstract are my original work. Proper attribution has been given to all outside sources. I understand that I am solely responsible for obtaining any needed copyright permissions. I have obtained and attached hereto needed written permission statements(s) from the owner(s) of each third-party copyrighted matter to be included in my work, allowing electronic distribution (if such use is not permitted by the fair use doctrine).

I hereby grant to The University of Kentucky and its agents the non-exclusive license to archive and make accessible my work in whole or in part in all forms of media, now or hereafter known. I agree that the document mentioned above may be made available immediately for worldwide access unless a preapproved embargo applies.

I retain all other ownership rights to the copyright of my work. I also retain the right to use in future works (such as articles or books) all or part of my work. I understand that I am free to register the copyright to my work.

REVIEW, APPROVAL AND ACCEPTANCE

The document mentioned above has been reviewed and accepted by the student's advisor, on behalf of the advisory committee, and by the Director of Graduate Studies (DGS), on behalf of the program; we verify that this is the final, approved version of the student's dissertation including all changes required by the advisory committee. The undersigned agree to abide by the statements above.

Anne M. Schumacher, Student

Dr. Thomas M. Parris, Major Professor

Dr. Alan E. Fryar, Director of Graduate Studies

MODELING OF CO_2-WATER-ROCK INTERACTIONS IN A MISSISSIPPIAN SANDSTONE RESERVOIR OF KENTUCKY

THESIS

A thesis submitted in partial fulfillment of the
requirements for the degree of Master of Science in the
Department of Earth and Environmental Sciences
at the University of Kentucky

By

Anne Marie Schumacher

Co- Directors: Dr. Thomas M. Parris, Adjunct Assistant Professor of Earth and Environmental Sciences

and Dr. Alan E. Fryar, Associate Professor of Earth and Environmental Sciences

Lexington, Kentucky

2013

ABSTRACT OF THESIS

MODELING OF CO_2-WATER-ROCK INTERACTIONS IN A MISSISSIPPIAN SANDSTONE RESERVOIR OF KENTUCKY

This study examined CO_2-water-rock interactions occurring during a carbon sequestration pilot test into a Mississippian oil reservoir in western Kentucky. New samples (n=62) and archived data, both collected from oil wells, were used to characterize the chemistry of formation waters from the Sugar Creek field in Hopkins County. In addition, core and cuttings samples (n=17) from the reservoir and overlying cap-rocks in, or near, the field were analyzed for bulk and clay mineralogy using X-ray diffraction. Electric logs were used to select sample intervals within the overlying cap-rocks and the center of the producing zones in the Jackson Sandstone. Using the water chemistry and mineralogic data as inputs, speciation and reaction path models were created using the Geochemist's Workbench software (GWB) to predict the distribution of aqueous species at equilibrium, evolution of fluid chemistry, and reservoir mineralogy as CO_2 was injected into the reservoir. Formation water was primarily Na-Cl. Reservoir rock was predominantly quartz. GWB simulations at the injection wells, mid-point fugacity and production wells indicated a sharp decrease in pH and increase in CO_2 (aq). Delta mineral mass plots showed net dissolution for injection stages and net precipitation for post-CO_2 injection. Important minerals were carbonates and alumino-silicates.

KEYWORDS: Carbon Sequestration, Modeling Subsurface Interactions, CO_2 Enhanced Oil Recovery, Geochemical Modeling, Carbon Capture and Storage

Anne M. Schumacher

April 2013

MODELING OF CO_2-WATER-ROCK INTERACTIONS IN A MISSISSIPPIAN SANDSTONE RESERVOIR OF KENTUCKY

By

Anne Schumacher

Dr. Thomas M. Parris
Co-Director of Thesis

Dr. Alan E. Fryar
Co-Director of Thesis and
Director of Graduate Studies

April 2013

To Mom and Dad-
"The road to success is covered with parking spaces along the way."
Thanks for keeping me moving.

ACKNOWLEDGEMENTS

The following thesis, while an individual work, benefited from the knowledge, insights, and direction of several people. First, I would like to acknowledge my co-thesis director, Dr. Thomas M. Parris, who exemplifies they type of life-long learner mentality to which I aspire, provided countless hours of instructive commentary and evaluation at every juncture, and who patiently stuck by me throughout this long journey to completion. I must also acknowledge my co-thesis director, Dr. Alan E. Fryar, for his kindness, continued patience, and vastly important contributions to the project. Thank you to my committee member, Dr. J. Richard Bowersox, for constructive edits and helping to streamline the project to bring it toward a timelier close.

Thank you to the Department of Earth and Environmental Sciences as well as the Kentucky Geological Survey for their enrichment of my overall experience at the University of Kentucky. Thank you to Glynn Beck and Kathy Takacs for their hard work collecting field samples. This project would not have been possible without funding and technical assistance from the U.S. Department of Energy and Midwest Geological Sequestration Consortium. The Brown McFarlan Fund provided much needed financial assistance for traveling to present my thesis at several professional venues.

Last but certainly not least, I would like to acknowledge my family and friends for their rock-solid (pun intended) support over the years. My parents epitomize the definition of role models. I owe thanks to my wife, Sarah, who has been instrumental in providing me with the motivation necessary to finally bring this chapter in my life to a close. A single page of acknowledgements will never be enough to summarize how grateful I am to all those who have supported me along the way!

TABLE OF CONTENTS

Acknowledgements iii

List of Tables v

List of Figures viii

Chapter 1: Introduction 1
1.1 Previous Work 2
1.2 Statement of Purpose 3
Chapter 2: Background 6
2.1 Geologic Background 6
2.1.1 Illinois Basin 6
2.1.2 Chesterian Lithology 7
2.2 Hydrogeologic Background 8
2.3 Carbon Sequestration 10
2.3.1 Storage Reservoirs 10
2.3.2 CO_2 Properties 12
2.3.3 Storage Mechanisms and Potential Reactions 13
2.3.4 History of Enhanced Oil Recovery (EOR) in Kentucky 14
2.4 Study Area: Sugar Creek 15
Chapter 3: Methods 27
3.1 Formation Water Collection and Laboratory Analysis 27
3.2 Archived Water Data 29
3.3 Mineralogical Analysis 30
3.4 Other Measurements 31
3.5 Modeling: Geochemist's Workbench (GWB) Software 31
3.5.1 Conceptual Model and Strategies 32
3.5.2 Model Inputs and Calculations 35
Chapter 4: Water Chemistry and Mineralogy Results and Discussion 48
4.1 Formation Water Chemistry 48
4.2 Mineralogy and Petrography 50
Chapter 5: GWB Modeling Results 59
5.1 Pre-CO_2 Injection 61
5.2 CO_2-Injection Phase I 62
5.3 CO_2-Injection Phase II 63
5.4 Post-CO_2 Injection 65
Chapter 6: GWB Modeling Discussion 84
6.1 Porosity Effects 90
6.2 Model Predictions versus Field Measurements 91
Chapter 7: Conclusions 96
7.1 Limitations 99
7.2 Future Work 100
References 101
Vita 108

LIST OF TABLES

Table 3.1 Administrative information for wells from which water data were collected and/or analyzed. Record number refers to the KGS database identification number corresponding to each well. Dashes mean that no data were available 38

Table 3.2 Charge balance analysis (% electroneutrality) for Jackson formation waters collected in this study. WT3 samples are from a Pennsylvanian sandstone aquifer, which supplied some injection water in the field. Well abbreviations are defined in Table 3.1 39

Table 3.2 (continued) Charge balance analysis (% electroneutrality) for Jackson formation waters collected in this study. WT3 samples are from a Pennsylvanian sandstone aquifer, which supplied some injection water in the field. Well abbreviations are defined in Table 3.1 40

Table 3.3 Charge balance analysis (% electroneutrality) for archived water samples from the Jackson collected near Sugar Creek.....41

Table 3.4 Calculated CO_2 fugacity and CH_4 solubility for the pre-injection and CO_2-injection simulations. The CO_2 fugacity co-efficient (Duan *et al.*, 1992) and CH_4 solubility (Duan and Mao, 2006) were determined with an online calculator using input values of reservoir temperature, pressure, and molar concentration of NaCl in the formation water.....42

Table 3.5 Porosity and phase saturation data for reservoir and seal rocks. Total porosity represents an average based on core analysis of the Jackson in the area of Sugar Creek. Oil- and water-filled porosity values are based on phase saturation calculations by the field operator that yielded oil and water saturations equal to 65% and 35%, respectively (M. Gallagher [field operator], personal communication). Note: Values represent conditions at the onset of field development and before the water flood operation.....43

Table 3.6 Inputs for kinetic simulations included surface areas calculated in this study and rate constants compiled from the literature. Dolomite and Chlinochlore-14A were used as substitutes for ankerite and chlorite, respectively, due to lack on thermodynamic data available within the GWB software ([1]Brantley, 2008; [2]Arvidson *et al.*, 2003; [3]Pokrovsky and Schott, 2001; [4]Gunter *et al.*, 1997; [5]Rockware, Inc. GWB Short-course, unpublished, 2009; [6]Palandri and Kharaka, 2004; [7]White and Brantley, 1995)..... 44

Table 4.1a Average water properties for Jackson formation water sample. For each well name, the top line of the sample round column represents the samples collected before injection of CO_2 (before May 11, 2009) and the bottom line represents samples collected after CO_2 injection had occurred.....51

Table 4.1b Average water properties for Jackson formation water sample. For each well name, the top line of the sample round column represents the samples collected before injection of CO_2 (before May 11, 2009) and the bottom line represents samples collected after CO_2 injection had occurred. Important cation and anion concentrations are listed in milligrams per liter (mg/L) 52

Table 4.1c Average water properties for Jackson formation water sample. For each well name, the top line of the sample round column represents the samples collected before injection of CO_2 (before May 11, 2009) and the bottom line represents samples collected after CO_2 injection had occurred. Important cation and anion concentrations are listed in milligrams per liter (mg/L).....53

Table 4.2 Summary of XRD mineralogic characterization for the Jackson. Values for each mineral are listed in weight percent. *Jackson samples collected immediately above the sandstone reservoir have low porosity and permeability and are treated as the seal rocks for the formation. Abbreviations are as follows: Graden Osburn #1-A (GO1A), Gatlin Harris #3 (GH3), Thomason & Boyd #1 (TB1), Wilbur Todd #2 (WT2), and Dexter Laffoon #1 (DL1), quartz (Qtz), potassium feldspar (K-spar), plagioclase (Plag), ankerite (Ank), calcite (Cal), dolomite (Dol), pyrite (Pyr), gypsum (Gyp), kaolinite (Kao), and chlorite (Chlor). Abbreviations for mixed-layer clays are R0 M-L I/S 90S, randomly ordered mixed-layer illite/smectite with 90% smectite layers, and R1 M-L I/S 30S, randomly ordered mixed-layer illite/smectite with 30% smectite layers 54

Table 5.1a Variation in calculated fCO_2 during the four GWB simulation phases at different wells for Jackson formation waters in the reservoir. Changes in fCO_2 produce changes in aqueous CO_2, HCO_3^-, carbonated alkalinity, and pH.....67

Table 5.1b Variation in calculated fCO_2 during the four GWB simulation phases at different wells for Jackson formation waters in the seal rocks. Changes in fCO_2 produce changes in aqueous CO_2, HCO_3^-, carbonated alkalinity, and pH.....68

Table 5.2a Mineral saturation (log Q/K) values for minerals during each of the four GWB simulation phases at RG5 (injection well). GWB describes the saturation state of minerals with real numbers only for minerals with log Q/K greater than -3. Values greater than zero are super-saturated, equal to zero are at equilibrium, and less than zero are undersaturated. #Represents the saturation state for dolomite, and is a proxy for ankerite, which lakes thermodynamic data in GWB. *Denotes new minerals that precipitate in the system 69

Table 5.2b Mineral saturation (log Q/K) values for minerals during each of the four GWB simulation phases at the mid-fugacity. GWB describes the saturation state of minerals with real numbers only for minerals with log Q/K greater than -3. Values greater than zero are super-saturated, equal to zero are at equilibrium, and less than zero are undersaturated. #Represents the saturation state for dolomite, and is a proxy for ankerite, which lakes thermodynamic data in GWB. *Denotes new minerals that precipitate in the system 70

Table 5.2c Mineral saturation (log Q/K) values for minerals during each of the four GWB simulation phases at RG1-4/WT9. GWB describes the saturation state of minerals with real numbers only for minerals with log Q/K greater than -3. Values greater than zero are super-saturated, equal to zero are at equilibrium, and less than zero are undersaturated. #Represents the saturation state for dolomite, and is a proxy for ankerite, which lakes thermodynamic data in GWB. *Denotes new minerals that precipitate in the system.....71

Table 5.2d Mineral saturation (log Q/K) values for minerals during each of the four GWB simulation phases at PH1/WT4. GWB describes the saturation state of minerals with real numbers only for minerals with log Q/K greater than -3. Values greater than zero are super-saturated, equal to zero are at equilibrium, and less than zero are undersaturated. #Represents the saturation state for dolomite, and is a proxy for ankerite, which lakes thermodynamic data in GWB. *Denotes new minerals that precipitate in the system.....72

Table 5.3a Simulated mineral precipitation and dissolution for reservoir rocks. Positive values are precipitation and negative equal dissolution. *Represents dolomite and ankerite. Abbreviations: “nc” equals no change in mass or volume and “na” indicates mineral did not precipitate for simulation.....73

Table 5.3b New minerals precipitated in response to CO_2 injection and not part of the original reservoir mineralogy in reservoir rocks. Abbreviations: “nc” equals no change in mass or volume and “na” indicates mineral did not precipitate for simulation.....74

Table 5.3c Simulated mineral precipitation and dissolution for seal rocks. Positive values are precipitation and negative equal dissolution. *Represents dolomite and ankerite. Abbreviations: “nc” equals no change in mass or volume and “na” indicates mineral did not precipitate for simulation.....75

Table 5.3d New minerals precipitated in response to CO_2 injection and not part of the original mineralogy in seal rocks. Abbreviations: “nc” equals no change in mass or volume and “na” indicates mineral did not precipitate for simulation 76

Table 6.1 Calculated change in porosities after CO_2 injection phase II and post-CO_2 injection phase for Jackson reservoir and seal rocks. Positive values indicate a net dissolution (porosity increase) whereas negative values indicate a net precipitation (porosity decrease).....93

LIST OF FIGURES

Figure 2.1 Structural setting of Kentucky with faults abbreviated as follows: FD-Fluorspar District, RCFS- Rough Creek Fault System, PFS- Pennyroyal Fault System, LFS- Lexington Fault System, KRFS- Kentucky River Fault System, IPCFS- Irvine-Paint Creek Fault System, and PMTF- Pine Mountain Thrust Fault (Greb and Solis, 2009).....18

Figure 2.2 Mississippian rock units in eastern and western Kentucky. Bold arrow points to the Golconda Formation that contains the Jackson (Modified from S. Greb, unpublished).....19

Figure 2.3 Range of temperatures and pressures where CO_2 phases are stable. Circles represent temperatures and pressures for Kentucky oil and gas wells at increasing depths (Greb and Harris, 2009; data compiled by B. C. Nuttall).....20

Figure 2.4 Variation of CO_2 density with depth. The change in cube size represents a change in relative volume occupied by the CO_2, not absolute change (from IPCC, 2005).....21

Figure 2.5 CO_2 solubility at different temperatures and pressures (from Carr *et al.*, 2003; Greb and Harris, 2009).....22

Figure 2.6 Decreasing percent CO_2 solubility versus increasing salinity, which typically increases with depth (from Carr *et al.*, 2003).....23

Figure 2.7 CO_2 storage security in the reservoir depends on a combination of both physical and geochemical trapping mechanisms. As time increases, solubility and mineral trapping increase (from IPCC, 2005).....24

Figure 2.8 Location of the Sugar Creek oil reservoir in Hopkins County, Kentucky (courtesy of R. Locke, ISGS).....25

Figure 2.9 Isopach map at Sugar Creek showing thickness of the Jackson in feet. Wells from which formation water and other samples were collected are labeled with abbreviated names (see text). Production wells are shown as black dots and the injection well is a red dot. The WT3 well is not shown on the map (Courtesy of J. Damico *et al.*, ISGS).....26

Figure 3.1 Photo showing the field setup apparatus used to sample formation waters. Oil was separated from formation water in the separation carboy. The outflow water from the separation carboy was further filtered before entering the flow-through cell for the YSI multi-meter. The large waste carboy on the ground collects overflow (photo by G. Beck, 2009).....45

Figure 3.2 Sample calculations explaining how (a) water-saturated and rock volumes and masses in the reservoir were calculated, and (b) how mineral masses were estimated. The example in (b) is for quartz in the Jackson 46

Figure 3.3 Calculations of mineral surface area using quartz as an example 47

Figure 4.1 Piper plot showing major-ion concentrations in Jackson formation water samples collected before CO_2 injection 55

Figure 4.2 Piper plot showing major-ion concentrations for Jackson formation water samples collected during CO_2 injection 56

Figure 4.3 Sodium chloride (Na+Cl) versus TDS for Jackson and Pennsylvanian (WT3) formation water samples. Compartmentalization in the Jackson reservoir is evidenced by the distinct separation between RG1-RG5/WT9 and PH1/WT4. The four archived samples were collected from other oil fields near Sugar Creek. The dashed line represents a line of best fit for the archived data, creating a historic trend line for pristine Mississippian formation water in the Jackson 57

Figure 4.4 Piper plot showing major-ion concentrations for archived Jackson formation water from fields near Sugar Creek 58

Figure 5.1 pH versus GWB simulation phase for the Jackson reservoir rocks. The pH response within the seal rocks (not shown) follows an identical pattern to the pH change within the reservoir rocks for the first two simulation phases. For the final two phases, the pH in the seal rocks is slightly less than in the reservoir rocks at each of the well locations (Tables 5.1a, 5.1b) 77

Figure 5.2 Carbonate alkalinity (mg/kg) versus GWB simulation phase for the Jackson reservoir rocks. The carbonate alkalinity response within the seal rocks (not shown) follows an identical pattern to the change within the reservoir rocks for the first two simulation phases. For the final two phases, the carbonate alkalinity in the seal rocks is less than in the reservoir rocks at each of the well locations (Tables 5.1a, 5.1b).....78

Figure 5.3 pH versus time for mid-fugacity during the CO_2 injection phase II when kinetic minerals were titrated into the system. The model predicts a very rapid pH increase and a similar plot for carbonate alkalinity as well 79

Figure 5.4 Mass of calcite versus time for the mid-fugacity showing the rapid calcite dissolution during the CO_2 injection phase II when kinetic minerals were titrated into the system. The model predicts the dissolution of approximately 5.5 grams of calcite 80

Figure 5.5 Mass of dolomite versus time at the mid-fugacity showing the rapid precipitation of dolomite during CO_2 injection phase II when kinetic minerals were titrated into the system. The model predicts the precipitation of approximately 1.4 grams of dolomite 81

Figure 5.6 Change in mass (delta mass) versus time in days for reservoir rocks at the mid-point fugacity during CO_2 injection phase II. The model shows dissolution of calcite and precipitation of dolomite-ankerite and strontianite. The magnitude and rates of mass change associated with carbonates far exceeds those for alumino-silicate minerals (lines with low gradient slopes near the zero delta mass axis). The magnitude of calcite dissolution exceeds precipitation for all carbonate and alumino-silicate minerals leading to net dissolution. Mass changes for other simulation scenarios follow a similar pattern (Tables 5.3a, b) 82

Figure 5.7 Example of change in mass (delta mass) versus time for reservoir rocks at the mid-point fugacity during the post-CO_2 injection phase. The model shows net precipitation as controlled by precipitation of calcite, dolomite and strontianite. As in Figure 5.6, the magnitude and rates of mass change associated with carbonates far exceeds those for alumino-silicate minerals (lines with low gradient slopes near the zero delta mass axis). Mass changes for other simulation scenarios follow a similar pattern (Tables 5.3a, b) 83

Figure 6.1 Plot from GWB showing HCO_3^- species interactions as pH rapidly decreases during CO_2 injection phase I. Acetate (CH_3COO^-) combines with hydrogen ions (H^+) to form acetic acid (HCH_3COO).....94

Figure 6.2 Plot from GWB showing delta mass (grams) versus time in days for some alumino-silicate minerals during CO_2 injection phase II for the mid-point fugacity. Chlorite is represented as chlinochlor-14A in the plot 95

Chapter 1: Introduction

Increases in amounts of atmospheric concentrations of greenhouse gases, especially carbon dioxide (CO_2), have raised concerns over the potential adverse effects to life on Earth. Combustion of fossil fuels (natural gas, oil, and coal) to meet human energy needs is a large source of carbon emissions. As the atmospheric concentration of CO_2 increases, solar radiation is trapped in the atmosphere and the Earth's surface temperature rises (IPCC, 2001). The temperature increase from rising atmospheric greenhouse gas concentrations is also of concern because it is likely to increase global sea level and change weather patterns worldwide (IPCC, 2005). Ongoing research has ensued to address global climate change and investigate a wide variety of stabilizing mechanisms (IPCC, 2001). Pacala and Socolow (2004) discuss numerous stabilizing mechanisms, including improved fuel economy, use of nuclear and wind power, reduced deforestation, and substituting natural gas for coal. Another potential mitigating mechanism is carbon capture and storage (CCS) in subsurface geologic reservoirs. Prospective CCS reservoirs include depleted oil and gas fields, deep saline/non-potable aquifers, un-mineable coal beds, organic-rich shales, and basalts. The CCS process proposes to capture CO_2 directly from anthropogenic sources (e.g. flue gas from coal-fired power plants) and inject it into geologic reservoirs for storage over time periods on the order of 10^3 to 10^4 years. Numerous pilot- and commercial- scale projects (e.g. Frio, Weyburn, In-Salah, Sleipner) have investigated the efficacy and challenges associated with CCS (Gale, 2002).

Though technically feasible in the appropriate geologic settings, CCS still faces technical, socio-economic, and regulatory challenges. One of the main challenges associated with CCS is to document the fate of injected CO_2 in the subsurface. This

monitoring, verification, and accounting (MVA) protocol is especially important because CO_2 is potentially chemically reactive with reservoir fluids (e.g. water, oil, and gas) and reservoir minerals.

1.1 Previous Work

The fate of injected CO_2 in storage reservoirs and the subsurface geochemical interactions in those reservoirs are being investigated through theoretical modeling, laboratory experiments, and field demonstrations. Enhanced oil recovery (EOR) is a mature technology within the oil industry and thus provides an extensive history in handling and injection of CO_2 (Melzer and Miller, 2007). In addition to previous use of CO_2 for EOR, the Burlington Allison Unit pilot project has been underway since 1996 to study CO_2 injection for enhanced methane recovery from deep coal seams (Gale and Freund, 2001). EOR projects have the benefit of providing economic return in addition to storing carbon. EOR projects, such as Sleipner West in the North Sea, Weyburn in Saskatchewan, and West Pearl in New Mexico, along with CO_2 injection projects in saline formations, such as Frio in Texas, have provided considerable insight into the physical and chemical behavior of CO_2 in the subsurface and implications for geological storage of CO_2 (Gale, 2002). General studies regarding issues surrounding the viability of CO_2 sequestration are abundant, including work by Bergman and Winter (1995), Holloway and van der Straaten (1995), Cook (1999), Gale (2002), Bachu (2000, 2002, 2003), Wildenborg and van der Meer (2002), Pacala and Socolow (2004), and many others.

The scientific community (e.g. Czernichowski-Lauriol *et al.*, 1996 and Gunter *et al.,* 1997) recognized the potential geochemical implications of long-term carbon sequestration as soon as the technology emerged. Since then, much progress has been made with respect to geochemical and solute transport modeling. Model evolution progressed from simple batch models assuming interactions only between CO_2, formation water, and rocks to complex three-dimensional flow models (Gaus *et al.*, 2008). Some recent papers of importance include Kharaka *et al.* (2006), who report gas-water-rock interactions within the Frio Formation following CO_2 injection; Zhang *et al.* (2009), who describe a case study from the Songliao Basin in China in which long-term variations of CO_2 trapped by different mechanisms within saline formations were analyzed; and Allen *et al.* (2005), who explain the significance of elevated pressures and salinities when modeling CO_2 sequestration within saline aquifers. Funded by agencies such as the Intergovernmental Panel on Climate Change (IPCC) and the United States Department of Energy (DOE), these studies represent a small part of a body of research, which has rapidly grown since the mid-1990's, examining the impacts and factors of using CCS as a climate-change mitigation option.

1.2 Statement of Purpose

Kentucky House Bill 1 (August 2007) provided funding and legislative mandate to conduct geologic carbon sequestration studies in saline aquifers, organic-rich shales, and oil and gas reservoirs. The legislation also called for an assessment of the application of CO_2 enhanced oil recovery (CO_2—EOR) in existing oil and gas reservoirs. EOR using CO_2 is viewed as a possible bridge mechanism to commercial-scale CCS in saline

aquifers because developed oil and gas reservoirs are typically geologically well characterized and the incremental oil production could produce revenue to offset some of the costs. Though CO_2-EOR is a successful and mature technology in many petroleum-bearing basins, it has not been extensively applied in the Illinois or Appalachian basins of Kentucky. Consequently, little is known about how CO_2 interacts with fluids and rock-forming minerals in reservoirs of this region. The geochemical interactions are important because they buffer pH and dictate how CO_2 is trapped in the reservoir through time. Additionally, the reactions could affect porosity and permeability of the reservoir and seal rocks through mineral precipitation and dissolution reactions.

The need to address the geochemical issues outlined above provides the motivation for the research in this thesis. The overall objective of this thesis is to assess potential geochemical reactions occurring between CO_2, water, and rock-forming minerals within the Jackson Sandstone, which is an oil-bearing Mississippian sandstone reservoir in western Kentucky and elsewhere in the Illinois Basin. The Sugar Creek oil field, Hopkins County, where the study reservoir is located is noteworthy because it was the site for a pilot CO_2 injection project administered by the Midwest Geologic Sequestration Consortium (http://sequestration.org/). The reaction modeling software, Geochemist's Workbench (GWB), is used to predict aqueous speciation and mineral saturation states in the reservoir before CO_2 injection and then changes in these parameters as CO_2 is injected into the oil reservoir for EOR and CO_2 storage. The reservoir aqueous and gas chemistry, mineralogy, and reservoir pressure and temperature data were collected before, during, and after CO_2 injection to serve as inputs into GWB.

The Sugar Creek pilot project provided the opportunity to develop a robust data set to examine potential reactions related to CO_2 injection using the GWB geochemical modeling software. Within the context of this pilot project, the goals of this study were to: 1) characterize the mineralogy of reservoir and seal rocks, 2) characterize the composition of aqueous reservoir fluids, 3) use GWB to characterize aqueous speciation and mineral saturation states of aqueous fluids before CO_2 injection, 4) use GWB to model possible reactions occurring between CO_2, aqueous formation fluids, and rock-forming minerals under different CO_2 concentrations, 5) compare reactions predicted by GWB with actual changes documented in the field, and 6) use GWB to simulate the effects of geochemical reactions on reservoir and seal porosity. Because many Mississippian oil reservoirs in western Kentucky and the Illinois Basin have similar temperature and pressure conditions and mineral compositions, the modeling results of this study should provide a valuable guide for examining reactions in future CO_2-EOR storage projects.

Chapter 2: Background

2.1 Geologic Background

Kentucky is divided into four major geologic provinces that include regional deformation and fault zones. The Illinois and Appalachian basins are the dominant features in western and eastern Kentucky, respectively. The Cincinnati Arch in central Kentucky separates the two basins, while the Mississippi Embayment covers the very western edge of the state (Figure 2.1; McDowell, 2001). Since the Sugar Creek oil field is located in western Kentucky, it will be helpful to look more closely at the geologic history of the Illinois basin, including stratigraphy, structure, and hydrodynamics.

2.1.1 Illinois Basin

As described by Swann (1967), the Illinois basin is an intracratonic basin filled with approximately three miles of shallow marine Paleozoic strata. The basin is a broad, elongate, north-south depression extending from northern Illinois and western Indiana southward through western Kentucky into northern Tennessee. Strata in the basin dip 1° (few feet per mile) toward the basin axis, which trends northwest-southeast. The majority of the Ordovician through Pennsylvanian strata in the basin consist of dolostone and smaller amounts of limestone, shale, sandstone, chert, anhydrite and coal. The Paleozoic strata are underlain by igneous and metamorphic basement rocks, which are approximately 1.3 billion years old (Swann, 1967).

Deformation in the basin is largely restricted to the LaSalle and DuQuoin-Louden anticlinal belts in Illinois, and the Rough Creek-Shawneetown fault zone, most of which is in Kentucky (Swann, 1967). These zones of deformation resulted from compressive

stresses created from collisions among South America, Africa and Laurentia during the Late Mississippian Appalachian orogeny (Swann, 1967; Kolata and Nelson, 1991).

2.1.2 Chesterian Lithology

Reservoir and seal rock samples in this study come from the Middle to Late Mississippian (Chesterian) section. Potter *et al.* (1958) did extensive work on the Chester sandstone depositional systems in the Illinois basin, and found that the sandstones were deposited under both fluvial and shallow-marine shelf conditions with sediment derived from a northeastern source beyond the margins of the basin, likely a large river system flowing southwest. Overall, about half of Chesterian series rocks are shale by volume with the remaining half split evenly between sandstone and limestone (Potter *et al.*, 1958). Each clastic unit within the series represents the advance of the Michigan River delta and subsequent filling of the shallow sea occupying the basin. Interruptions to sedimentation by major marine transgressions occurred six or seven times (Potter *et al.*, 1958; Swann, 1967). Basin subsidence coupled with a decreased sediment load resulted in these cyclical returns of the sea and limestone deposition (Swann, 1967).

The samples were collected from the Big Clifty Member of the Golconda Formation (Figure 2.2). The Big Clifty Sandstone Member is also called the Jackson sandstone (informal driller's term) and is henceforth referred to as the Jackson. Thickness of the Jackson can be 50 feet or more, and it is well-cemented, fine- to medium-grained, and is often cross-bedded (Fritz, 1967; Grabowski, 2001).

2.2 Hydrogeologic Background

Subsurface fluids include more than just freshwater; thus, it is important to know the composition of saline reservoirs and the movement of and interactions among various fluids (including gases or liquid hydrocarbons). Regional and local structures play significant roles in controlling fluid flow and composition through recharge and mixing. Other factors affecting flow include permeability, time, and density variations (Stueber *et al.*, 1993). The origin of fluid salinity, water-rock interactions, the pathways of fluid migration, and the timing of migration can all affect the composition of formation water as well. In this study, formation water refers to the aqueous reservoir fluids present in the Jackson. The fate of CO_2 injected into saline aquifers and many oil and gas fields will be affected by fluid flow direction and rate, and the composition of subsurface formation waters. Although there is no flow or transport component incorporated into this research, the basic concepts are necessary to understand subsurface interactions between reservoir fluids.

Sedimentary basins are ideal for geological storage of carbon because of the thick sequences of porous and permeable rocks, which are important in the transmission of fluids with varying densities (Gupta and Bair, 1997). Basins in tectonically quiescent areas (e.g. intracratonic and passive margin basins) are better suited to sequestration because of the decreased risk in fault hazards and potential reservoir leakage (Bachu, 2000). There is a close correlation between the flow regime of formation waters and both the age and type of sedimentary basin involved (Bachu, 2000). Flow in continental basins, such as the Illinois basin, is commonly controlled by topography, with fluids being recharged at high elevations and discharged at low elevations. Basin maturity, or

time, also plays a role in controlling flow direction. In mature, non-subsiding basins such as the Illinois Basin, flow is directed into the center of the basin (Gupta and Bair, 1997).

As Hanor (1994) explains, the composition of waters in sedimentary basins is affected by both chemical and physical processes, such as the basin-scale flow mechanism discussed above, which is an example of advection. Other transport processes that affect fluid composition include dispersion (mechanical mixing) and diffusion (mass movement driven by solute concentration gradients). Because the mixing of formation waters occurs fairly slowly and inefficiently, dispersion causes spatial and temporal variations in salinity (Hanor, 1994).

In addition to the natural driving forces (e.g. topographic relief), fluid composition can be affected by anthropogenic injection of fluids, such as waste disposal and EOR. For example, in this study, the operator at Sugar Creek mixed together formation waters of varying composition from different stratigraphic units (Pennsylvanian and Mississippian) as part of the water-flooding EOR plan. Formation-water composition can be also be modified after deposition by diagenetic reactions, including redox and acid-base reactions, mineral hydrolysis, and exchange with other fluid phases. Understanding mineral hydrolysis reactions, including the dissolution and precipitation of silicate and carbonate minerals, can increase solute concentrations in addition to affecting porosity in reservoirs. Additionally, formation waters in contact with oil within the reservoir can have elevated concentrations of organic acids, dissolved methane and bromide concentrations (Kharaka *et al.*, 1986). Notwithstanding the previously mentioned processes, fluid composition in many basins, including the Illinois, show a somewhat regular trend of increasing salinity with depth (Hanor, 1994).

2.3 Carbon Sequestration

According to the U.S. Department of Energy (DOE), carbon sequestration into geologic reservoirs is one of the most auspicious technologies (U.S. DOE, 1999, 2004) to help mitigate atmospheric concentration of CO_2, the main greenhouse gas, which has increased since the Industrial Revolution. Although much of the necessary scientific, technical, and industrial knowledge already exists largely because of experience gained in the oil and gas industry, commercial-scale implementation of carbon sequestration has been slow due to high costs and the need to accurately document the fate of CO_2 in the subsurface (Wildenborg and van der Meer, 2002; Bachu, 2003).

2.3.1 Storage Reservoirs

Assurance of environmental safety and project effectiveness requires that particular attention be given to the selection of appropriate storage reservoirs in order to minimize leakage. An ideal reservoir would have a large capacity in which to store CO_2 and be overlain by low porosity and permeability rocks that would block the upward migration of CO_2 (Wildenborg and van der Meer, 2002). Mature sedimentary basins that formed in mid-continental settings or on the edge of stable cratons are ideal for sequestration due to their stability and structure. Because of their geologic and technical maturity, these basins will likely have: (1) a well-documented geologic framework; (2) hydrocarbon reservoirs, if present, that are near depletion or abandonment; and (3) some of the infrastructure necessary for the transport and injection of CO_2 (IPCC, 2005).

Worldwide, reservoirs that are being investigated for carbon storage include: (1) deep saline formations, (2) depleted or abandoned oil and gas fields, (3) unmineable coal beds, (4) organic-rich shales, and (5) basalts (U.S. DOE, 1999, 2004; Greb and Harris,

2009). In Kentucky, saline formations, oil and gas fields, and organic rich shales are considered prospective, although the shale potential is more speculative (Parris *et al*., 2010). Saline aquifers, which contain mostly non-potable water, have the greatest storage potential with an estimated capacity of 12 to 158 billion metric tons in the Illinois basin alone. Oil and gas reservoirs within the Illinois basin have an estimated storage volume of 140 to 440 million metric tons (U.S. DOE, 2012). However, the actual storage volume for CO_2 will be less than total reservoir pore volume because of reservoir heterogeneity, CO_2 buoyancy, and pore-level influences such as irreducible water saturation and capillary entry pressure (Bachu *et al.*, 2007).

Although they have less potential storage capacity than saline formations, a variety of factors make depleted oil and gas reservoirs excellent candidates for CO_2 sequestration. From a reservoir perspective, the most important attribute is the successful containment of hydrocarbons that were trapped for time periods in excess of the targeted 1,000 to 10,000 year time period for carbon storage. Moreover, throughout the life cycle of oil and gas development and production, the reservoirs were often extensively mapped and characterized, and engineering models were used in some fields to simulate subsurface fluid movement. Thus, the geometry and limits of the reservoir and trapping mechanisms are well documented. From a technology perspective, the methods used in the withdrawal of hydrocarbons, along with the injection and transportation of CO_2 in EOR projects, is directly transferable to sequestration projects (Wildenborg and van der Meer, 2002).

The use of CO_2 in a storage project to enhance oil and gas production can provide a revenue stream to offset injection costs, and thus the project can partly achieve both

economic and environmental goals (Wildenborg and van der Meer, 2002). However, it should be noted that combining these goals can be problematic for carbon sequestration goals because, for EOR to be economically viable, the field operator attempts to minimize the ratio of CO_2 injected relative to the incremental oil produced. Beyond economic considerations, infrastructure problems could occur in fields that have numerous abandoned wells that might be prone to leakage (IPCC, 2005).

2.3.2 CO_2 Properties

Knowledge of the physical and chemical properties of CO_2 is paramount to understanding potential fluid-rock-gas interactions once CO_2 is injected into the subsurface. CO_2 is a naturally occurring, colorless and odorless gas with an atmospheric concentration of approximately 392 parts per million (Voormeij and Simandl, 2002; Pacala and Socolow, 2004). When dissolved in water, CO_2 forms carbonic acid (H_2CO_3), which, as a weak acid, can affect both the chemical and physical properties of rocks in the reservoir and seal, and materials (e.g. cement) in injection and production wells (Gaus *et al.*, 2008). Other interactions will also occur elsewhere in the reservoir as CO_2 displaces formation fluids. For example, as CO_2 migrates as a free phase throughout the reservoir, it has the potential to cause a pressure perturbation depending on the rate of injection (Gaus, 2010).

The temperature and pressure of a prospective sequestration reservoir are important considerations because they will dictate the phase behavior of CO_2 and hence the storage efficiency. Generally, as temperature and pressure increase with depth, gaseous CO_2 becomes more liquid-like and liquid CO_2 becomes more gas-like. At the critical temperature of 87.8°F (31°C) and pressure of 1073 psi (75.11 bars or 7.38 MPa),

gaseous CO_2 is no longer distinguishable from liquid CO_2 and they form a single supercritical phase (Figure 2.3; IPCC, 2005; Greb and Harris, 2009). Formation of the supercritical phase is important because the density of the CO_2 increases significantly, which allows more CO_2 to be stored in a given volume (Figure 2.4; IPCC, 2005). Under hydrostatic conditions and a geothermal gradient of 25°C/km, the transition to supercritical CO_2 in many sedimentary basins occurs at depths of 800 to 1000 meters (Voormeij and Simandl, 2002; IPCC, 2005).

Temperature, pressure and salinity also affect the solubility of CO_2 in water. For a water with a given solute composition, the solubility of CO_2 increases with increasing pressure. On the other hand, temperature increase in the same water will decrease CO_2 solubility (Figure 2.5; Carr *et al.*, 2003). The corollary to this behavior is that dissolution of CO_2 in water occurs more readily in sedimentary basins that have low geothermal gradients and pressures above hydrostatic. Finally, increasing salinity will decrease CO_2 solubility because of the decrease in water activity (Figure 2.6; Carr *et al.*, 2003).

2.3.3 Storage Mechanisms and Potential Reactions

Effectively storing CO_2 in geologic formations depends on a combination of physical and geochemical trapping mechanisms that have differing degrees of permanency and storage security (Figure 2.7; Bachu and Adams, 2003; IPCC, 2005). The initial principal means of storage is physical trapping of single-phase CO_2 in stratigraphic or structural traps. Because CO_2 is less dense, it will displace formation water upon injection into the storage reservoir and migrate buoyantly upwards. Effective physical trapping will depend on having thick, low-permeability formations, such as shale or salt beds (stratigraphic traps), and/or folded rocks (structural traps) to act as upward

migration barriers. Hydrodynamic trapping can be extremely effective in saline formations that do not have a closed trap but have long fluid-transport times and distances (IPCC, 2005). In cases where there is an immense distance between the deep injection point and the end of the confining layer, the CO_2 and fluid can be trapped for millions of years (Bachu *et al.*, 1994). This is residual trapping, which refers to retention of CO_2 as an immobile phase in pore space within the storage reservoir. The injected CO_2 forms a plume that spreads vertically and laterally until it is trapped at residual CO_2 saturation (residual trapping), in a local structure, or below a sealing formation.

Another trapping mechanism is solubility trapping in which injected CO_2 dissolves into formation waters. The dissolution forms carbonic acid (H_2CO_3) that subsequently dissociates, resulting in a lowering of pH. The pH response to CO_2 injection can be quick as the dissolution and first dissociation reactions are relatively rapid (Cotton and Wilkinson, 1976; Kharaka *et al.*, 2006). Once CO_2 is dissolved in the formation water it is no longer buoyant, and migration as a discrete phase is no longer an issue. The final and most secure trapping mechanism is mineral trapping. This occurs when HCO_3^- or CO_3^- produced from the reactions above, for example, combines with cations (e.g. Ca^{2+}, Mg^{2+}, Fe^{2+}) to form carbonate minerals and is stored in the solid phase (Gunter *et al.*, 1993; IPCC, 2005; Zerai, 2006).

2.3.4 History of Enhanced Oil Recovery (EOR) in Kentucky

The earliest history of enhanced oil recovery in Kentucky consisted of using natural gas to repressurize reservoirs with the intention of keeping the mobility of the oil in the reservoir from decreasing. The repressurization technique was used by the Petroleum Exploration Company and Ashland Oil Company in the Big Sinking oil field

(1926), Keaton-Mazie oil field (1929), and Haynesville oil pool (1935). By the 1950's water-flooding became the most popular technique used for EOR, and it has remained widely employed in Kentucky to maintain reservoir pressure and sweep oil from the reservoir (Duchscherer, 1965; Miller and Hamilton-Smith, 1998).

Although enhanced oil recovery using CO_2 has been used extensively in west Texas and Wyoming, the CO_2-EOR history in Kentucky is limited to several small-scale projects (Duchscherer, 1965; Miller, 1990; Bardon *et al.*, 1991; Miller *et al.*, 1994; Miller and Hamilton-Smith, 1998). These are single-well cyclic projects in which CO_2 is injected into a single well and then the same well is produced at a later date after a shut-in or "soak" period. During the shut-in period, CO_2 interacts with the oil, reducing its viscosity and making it more mobile in the reservoir. The CO_2-oil interaction is limited because Kentucky oil reservoirs often have reservoir pressures at or below the hydrostatic gradient and the low pressure produces immiscibility between the CO_2 and oil. The reduced recovery efficiency associated with immiscible CO_2-EOR coupled with the historical absence of an affordable and readily available source of CO_2 have limited its use for EOR in Kentucky (Melzer and Miller, 2007).

2.4 Study Area: Sugar Creek Field

The Sugar Creek field was discovered in 1964 in Hopkins County, Kentucky (Figure 2.8). Before injection of CO_2, primary and secondary oil production from the Jackson equaled 895,575 barrels of oil, which represents 33% of the estimated 2.7 million barrels of original-oil-in-place (Gallagher [field operator], unpublished). The oil at Sugar Creek has a gravity of 37 API, is stratigraphically trapped due to a pinch-out of the

Jackson (Figure 2.9), and the primary reservoir drive mechanism is a solution gas drive. Reservoir thickness ranges from 10 to 15 feet, and average porosity and permeability are 16.7% and 15.9 millidarcies, respectively. Average reservoir depth equals 1870 ft. The Sugar Creek CO_2-EOR pilot project was part of a broader pilot program administered by the Midwest Geological Sequestration Consortium and sponsored by the DOE. Goals of the pilot program were to inject CO_2 into several representative oil fields in the Illinois basin, document the influence on oil production, estimate the amount of CO_2 that remained in the reservoir over the course of the project (i.e. CO_2 storage), ascertain the viability of CO_2-EOR, and develop a set of best practices for CO_2-EOR.

Beginning in 1993 and prior to CO_2 injection, the operator implemented a water-flood project as a transition from primary production to secondary recovery. Water for the flood project was taken from a shallow Pennsylvanian sandstone aquifer. This Pennsylvanian formation water is significantly less saline than the formation water in the Jackson and injection has produced variable dilution of the latter. Therefore, Jackson formation water samples from Sugar Creek represent the mixing of Pennsylvanian and Mississippian formation waters. Wilbur-Todd #3 (WT3) was the source of the dilute shallow Pennsylvanian formation water used in the water flood.

From May 11, 2009, to May 13, 2010, 7,268 tons of CO_2 were injected into the Jackson through a central injection well, the Ross-Gentry #5 (RG5), at a rate of 20 to 30 tons per day. Pre-injection reservoir pressure and temperature at RG5 were 700 psi (49 bars) and 28°C, respectively. During CO_2 injection at RG5, pressure increased an additional 1200 psi (84 bars) so that total reservoir pressure equaled 1900 psi (133 bars). Surrounding the RG5 are seven producing wells: Pressley-Hart #1 (PH1), Ross-Gentry #1

(RG1), Ross-Gentry #2 (RG2), Ross-Gentry #3 (RG3), Ross-Gentry #4 (RG4), Wilbur-Todd #4 (WT4), and Wilbur-Todd #9 (WT9). Before, during, and after CO_2 injection, the production wells, in contrast, were pumped at a sufficiently high rate that reservoir pressure equaled approximately 30 psi (2 bars). The horizontal distance between RG5 and production wells ranges from 500 to 1,500 feet. Consequently, a significant horizontal pressure gradient developed in the reservoir where production wells were close to the injection well.

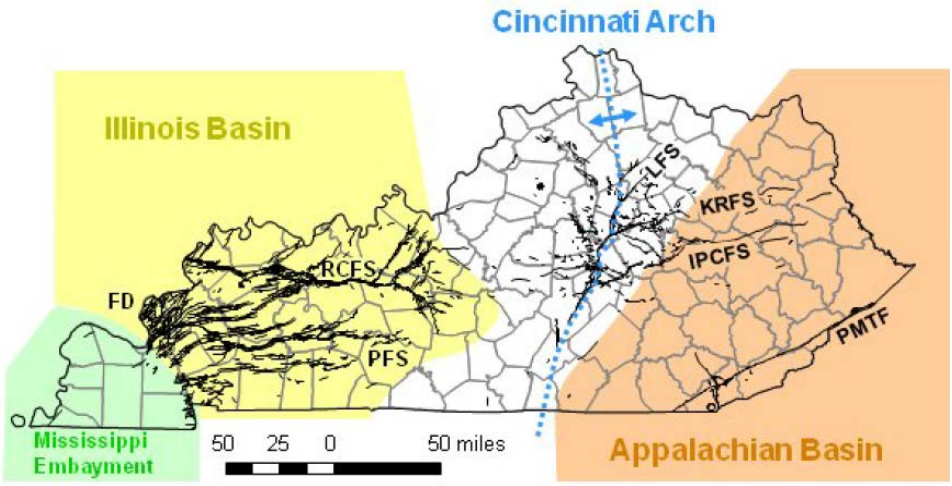

Figure 2.1 Structural setting of Kentucky with faults abbreviated as follows: FD- Fluorspar District, RCFS- Rough Creek Fault System, PFS- Pennyroyal Fault System, LFS- Lexington Fault System, KRFS- Kentucky River Fault System, IPCFS- Irvine-Paint Creek Fault System, and PMTF- Pine Mountain Thrust Fault (Greb and Solis, 2009).

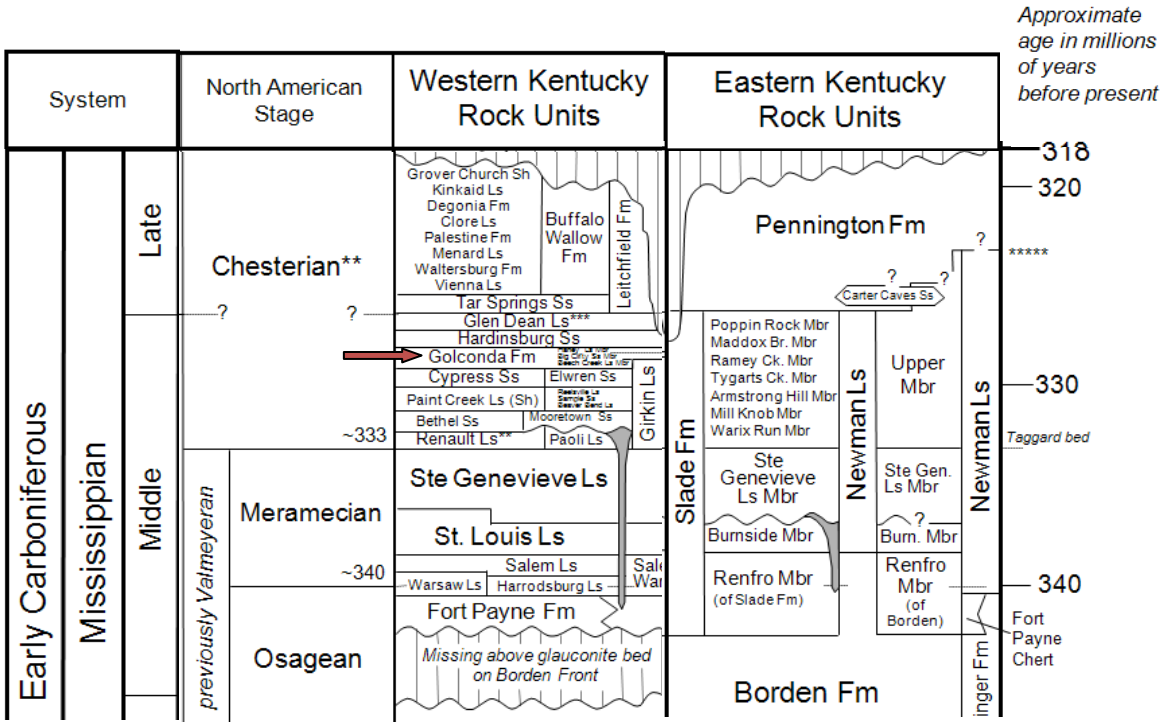

Figure 2.2 Mississippian rock units in eastern and western Kentucky. Bold arrow points to the Golconda Formation that contains the Jackson (Modified from S. Greb, unpublished).

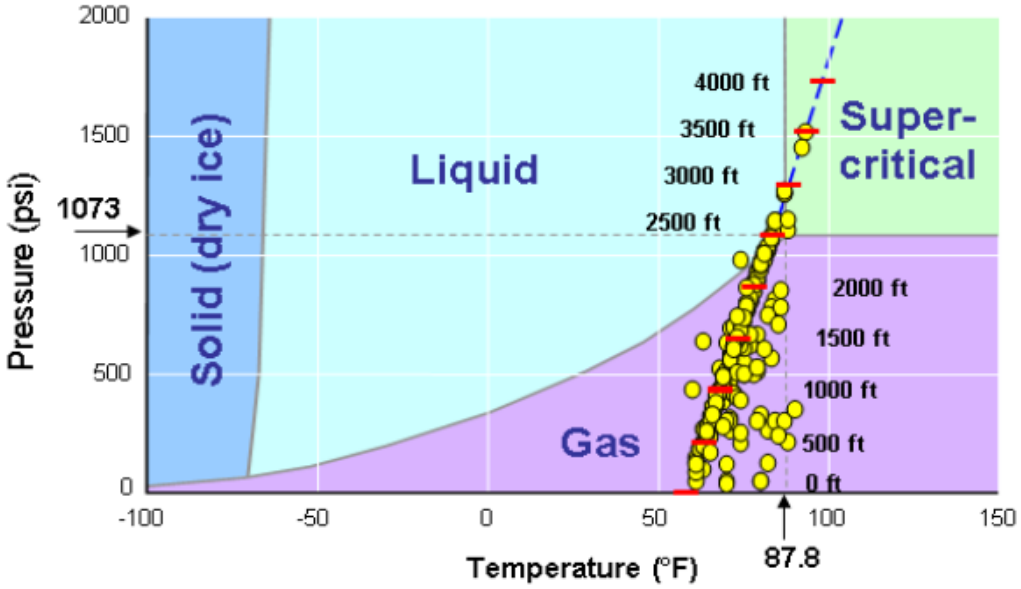

Figure 2.3 Range of temperatures and pressures where CO_2 phases are stable. Circles represent temperatures and pressures for Kentucky oil and gas wells at increasing depths (Greb and Harris, 2009; data compiled by B. C. Nuttall).

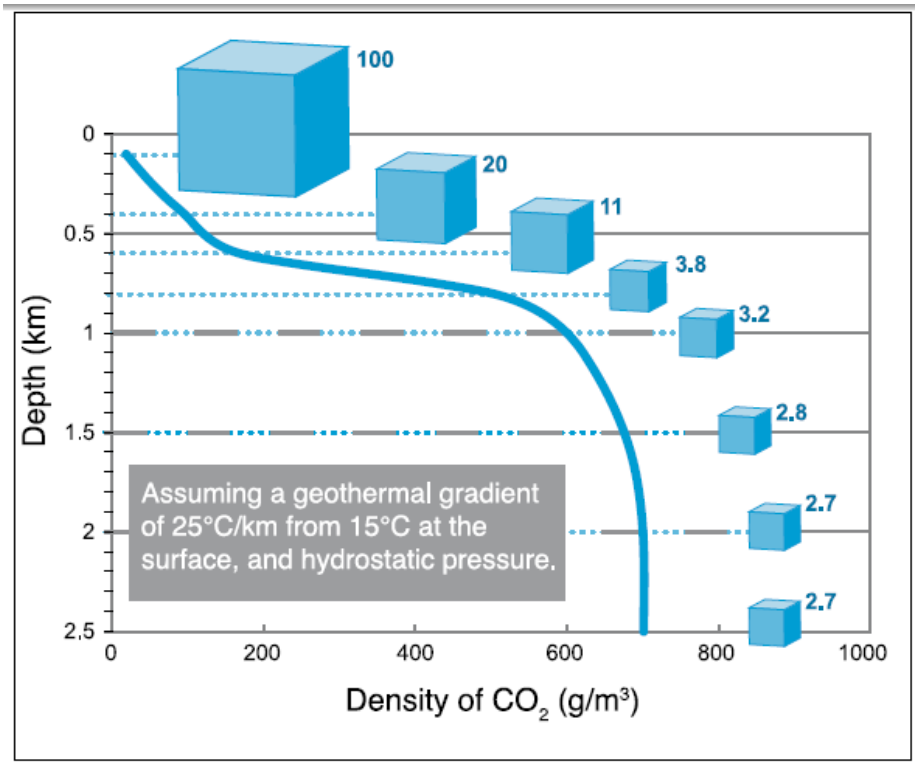

Figure 2.4 Variation of CO_2 density with depth. The change in cube size represents a change in relative volume occupied by the CO_2, not absolute change (from IPCC, 2005).

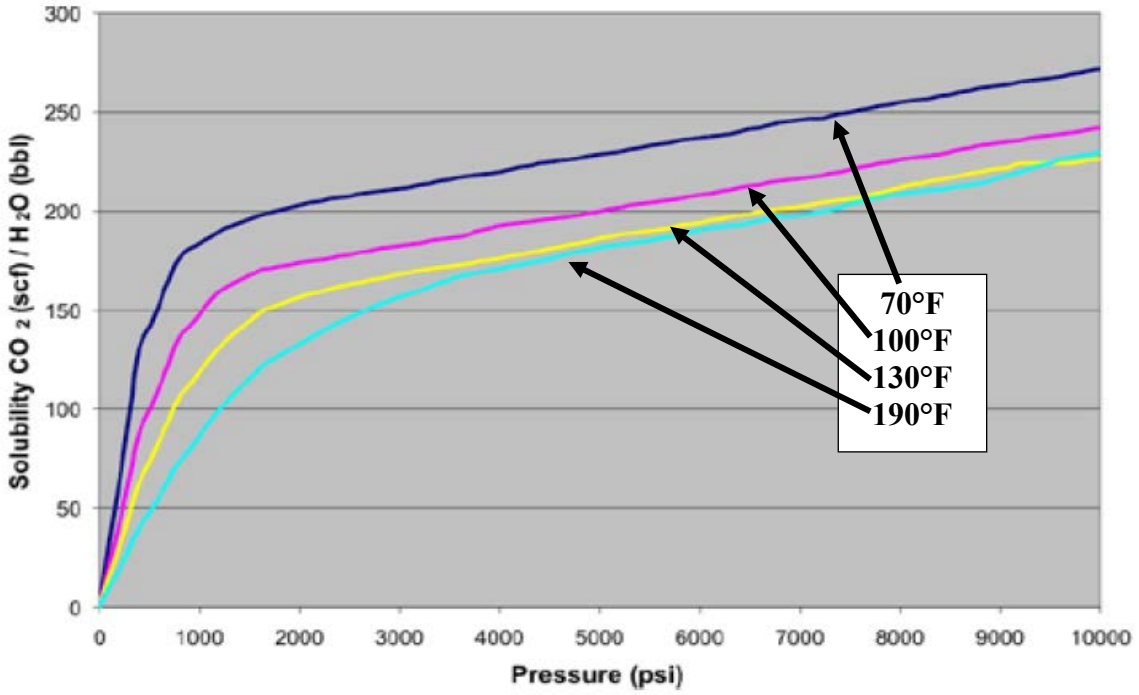

Figure 2.5 CO_2 solubility at different temperatures and pressures (from Carr *et al.*, 2003; Greb and Harris, 2009).

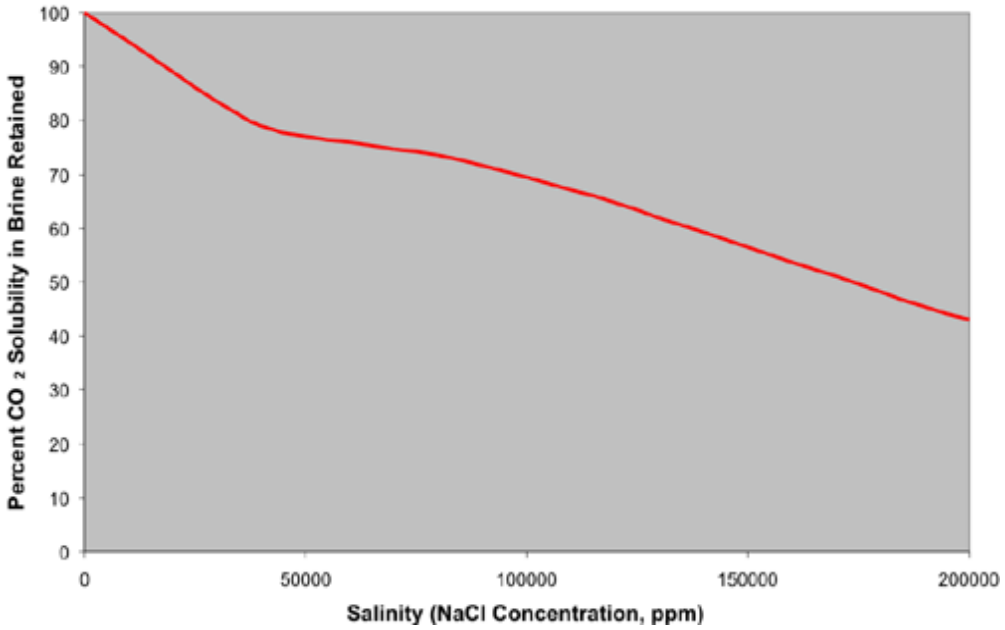

Figure 2.6 Decreasing percent CO_2 solubility versus increasing salinity, which typically increases with depth (from Carr *et al.*, 2003).

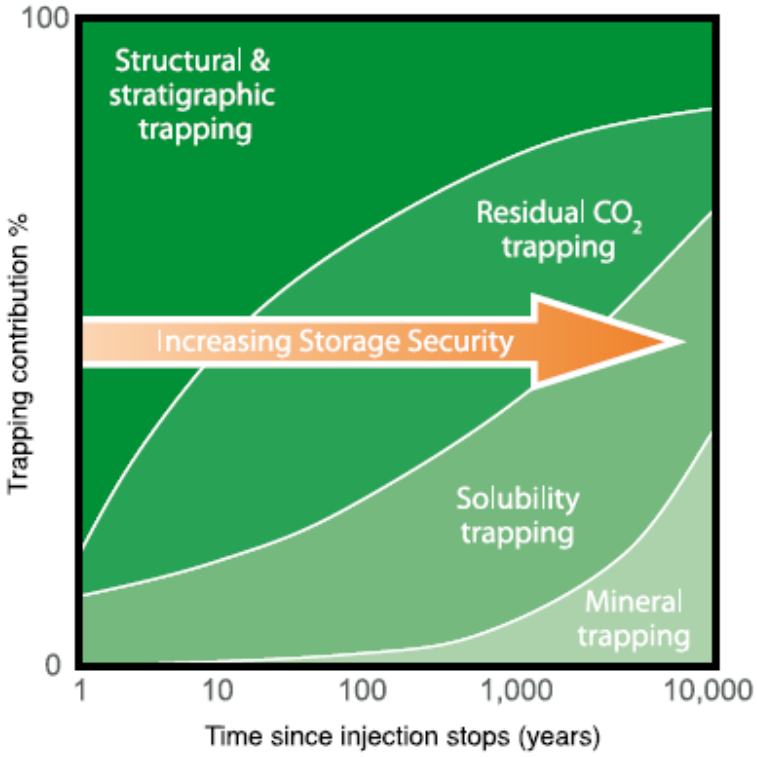

Figure 2.7 CO_2 storage security in the reservoir depends on a combination of both physical and geochemical trapping mechanisms. As time increases, solubility and mineral trapping increase (from IPCC, 2005).

Figure 2.8 Location of the Sugar Creek oil reservoir in Hopkins County, Kentucky (courtesy of R. Locke, ISGS).

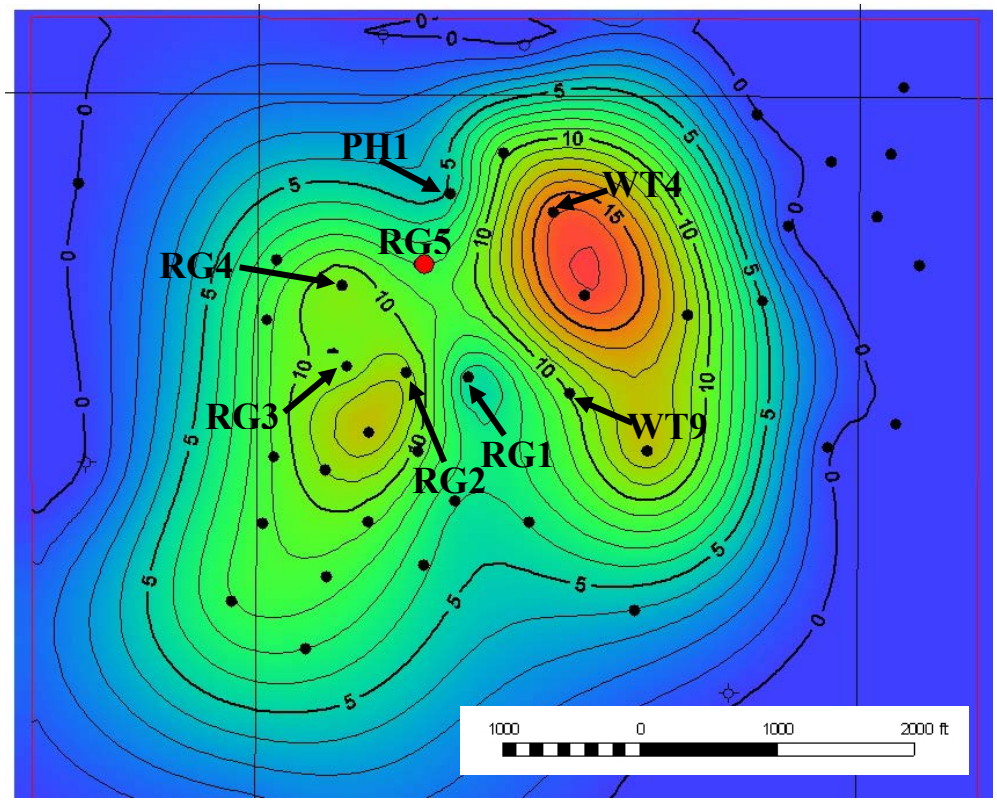

Figure 2.9 Isopach map at Sugar Creek showing thickness of the Jackson in feet. Wells from which formation water and other samples were collected are labeled with abbreviated names (see text). Production wells are shown as black dots and the injection well is a red dot. The WT3 well is not shown on the map (Courtesy of J. Damico *et al.*, ISGS).

Chapter 3: Methods

Accurate characterization of reservoir fluid chemistry and reservoir mineralogy was needed in order to obtain the correct inputs for simulating potential CO_2-water-rock interactions. A total of 62 newly acquired formation fluid samples and measurements from Sugar Creek along with archived water data (collected by KGS and USGS) were used to characterize formation water chemistry. The mineralogy of the reservoir and cap rocks was determined by X-ray diffraction (XRD) measurements on rock core and cuttings samples taken near or in the study field. The collective water chemistry and mineralogical data were then analyzed and input into the GWB for modeling equilibrium state and potential subsurface interactions.

3.1 Formation Water Collection and Laboratory Analysis

Formation waters typically coexist with oil and gas to produce a multi-phase fluid state in hydrocarbon-bearing reservoirs. The Sugar Creek formation water was sampled from the oil reservoir for analysis of various parameters. Each sample was identified by the well name, and a record number was assigned from the KGS oil and gas online database (Table 3.1).

The sampling procedures were adopted and modified from those developed by the Illinois State Geological Survey (ISGS, 1993). The sampled wells were constructed so that all stratigraphic intervals above the oil reservoir were isolated from the wellbore by cement and steel casing. The casing either extended to the top of the reservoir, leaving it exposed to the wellbore (also known as open-hole), or it extended across the reservoir. In the latter example, the casing was perforated to allow fluids to circulate from the

reservoir into the wellbore. Even in the open-hole example, the reservoir interval was typically perforated to facilitate fluid flow into the wellbore. Both examples provided the opportunity to collect discrete samples from the oil reservoir without contamination by mixing with waters from other reservoirs penetrated by the well. Formation water samples were collected using a closed sampling system in which fluids had minimal contact with the atmosphere. This reduced degassing problems and atmospheric contamination. The sampling system consisted of a separation carboy for density segregation of the oil and water, a pre-filter for removing additional oil from the water, and a flow-through cell containing a YSI multi-meter (model 556 MPS) for measuring water properties. These properties included pH, Eh, specific conductance, temperature, and dissolved oxygen (DO). The sampling apparatus was connected to the well head and elements in the sampling system were interconnected with ¼-inch Tygon^{TM} tubing (Figure 3.1). Samples were collected at the point in which water properties, as measured with the YSI multi-meter, became constant and dissolved oxygen levels were less than 1.0 mg/L, which indicated that samples were representative of the formation water.

Samples were then collected for measurement of total CO_2, alkalinity, dissolved inorganic carbon (DIC), anions, metals and cations, and total dissolved solids (TDS) in the KGS lab. Samples were collected in pre-washed Nalgene^{TM} bottles, and all samples, except total CO_2, were filtered with a 0.45 micron filter. Metal and cation samples were acidified with nitric acid to a pH value of 2. After collection, all samples were chilled for transport. Total CO_2 was analyzed according to the American Society for Testing and Materials (ASTM) using a gas-sensing electrode test method (ASTM D 513, 1988). Alkalinity and DIC were analyzed using electrometric titration and a CO_2 coulometer,

respectively (ASTM, 1992; UIC, 2010). A well-mixed sample was dried to 180°C to measure total dissolved solids (ASTM, 1997). Anions and cations in the formation water were analyzed using ion chromatography (ASTM, 1988). Sample collection and measurement quality were monitored using charge balance and only samples with charge balances equal to or less than 10% were used (Table 3.2). Charge balances were calculated using the AquaChem v5.1 software (Schlumberger Water Services, 2010).

3.2 Archived Water Data

Archived hydrochemical data collected in the late 1960's and early 1970's, mostly from oil wells and a few waste disposal and water wells, constituted a supplemental data set. Chemical measurements included major cation and anion concentrations (mg/L), and water property measurements including pH, conductivity, density, and TDS. In addition to the chemical data, the archived records included critical administrative information about the well and its location, and the depth and stratigraphic interval sampled (Parris *et al.*, 2010). For this study, four records from the Jackson Sandstone reservoir in or near the Sugar Creek field were selected to provide representative compositions of Mississippian formation water. Only samples that predated water flood operations were used in order to avoid possible mixing of formation water from different reservoirs. As with the new measurements, only samples with charge balances equal to or less than 10% were used (Table 3.3).

3.3 Mineralogical Analysis

X-ray diffraction (XRD) measurements for mineralogical composition were performed on 17 samples collected from well cuttings near or within the study field. Because of limited amounts of available Jackson cuttings, thin-sections were unable to be produced. When available, geophysical electric logs were used to identify porous and permeable intervals to sample in the reservoir. Of the 17 samples collected, three were from the shaley mudstone upper unit of the Jackson and are referenced henceforth as the seal rocks in Sugar Creek. With lower porosity than the rest of the Jackson, the seal rocks serve as the principal barrier to CO_2 migration.

Mineralogical composition was measured with XRD on the whole-rock and clay fraction (less than 5 microns) by K/T GeoServices. After samples were cleaned of contaminants, XRD measurements were performed using a Rigaku automated diffractometer equipped with a copper X-ray source and a scintillation X-ray detector. Determination of mineral amounts was done by using integrated peak areas and empirical reference intensity ratio factors. The weight percentage data from this method are semi-quantitative and can quantify crystalline material only. The percentages reported for each mineral depend on the percentages for the other materials. One limitation of this method is that if one mineral is underestimated, then the others will be overestimated. Additionally, detection limits differ for each mineral species and are on the order of one to five weight percent (K/T GeoServices, 2008).

3.4 Other Measurements

Though not an explicit part of this study, two additional types of measurements were conducted at Sugar Creek that provide insight into the fate of injected CO_2 and water-rock interactions. The first were stable isotope measurements ($\delta^{18}O$-H_2O, δD-H_2O, $\delta^{13}C$-DIC) of the formation waters. These samples were collected at the same time samples were collected for the bulk chemistry measurements. The second were bulk and isotopic composition measurements ($\delta^{13}C$-CO_2, $\delta^{13}C$-CH_4) of gases co-produced with oil and the formation waters, which was important for calculating gas fugacities and determining the timing of CO_2 break-through. Bulk gas composition was measured in the field with an infrared gas analyzer on gas produced up the wellbore annulus. Gas samples collected from the annulus were used to measure bulk and sable isotopic composition at the Illinois State Geological Survey and Isotech Laboratories.

3.5 Modeling: Geochemist's Workbench Software

Geochemist's Workbench (GWB^{TM}) version 8.0 was used for equilibrium, reaction-path, and kinetic modeling of CO_2-water-rock interactions. GWB is a commercial geochemical reaction and transport modeling package that consists of a suite of modules that solve different types of geochemical problems, and manage and analyze a variety of geochemical data. In order of increasing complexity the modules include SpecE8, React, and X1t and X2t. The SpecE8 module is a speciation or "closed system" model in which mass is not exchanged between the system of interest and its surrounding environment. Measured or inferred fluid chemistry values are used as inputs to predict the

distribution of components among aqueous species. Mineral saturation states are also predicted along with the reaction directions needed to attain equilibrium.

The React module is an “open system” model in which the system exchanges mass or energy with its surrounding environment. Reaction-path models use the speciation calculation as a starting point, but then follow this with a series of speciation calculations to document changes in the composition of the system due to changes in temperature, Eh, pH, gas fugacities, species concentrations, mineral mass, or some combination thereof. This allows for the forward predictions of changes in fluid chemistry and mineral composition and mass along the reaction path.

The X1t (1-dimensional) and X2t (2-dimensional) modules are reactive transport models in which a series of reaction-path models are represented by points distributed over a certain spatial domain. Mass transport in the reaction-path models allows the user to describe the movement of fluid and the transport of chemical species due to advection, dispersion and diffusion. Although no reactive transport modules were used for this study, modeling reactions under no-flow conditions is still an important tool in analyzing and predicting geochemical reactions and the variables that control reaction progress and products (Bethke, 2008).

3.5.1 Conceptual Model and Strategies

To develop an effective geochemical model, the system or process of interest must be conceptualized in a useful manner with the heart of the model being the equilibrium system. In this study the equilibrium system is assumed to be closed at a constant temperature (i.e. isothermal), and contains formation fluids and gases, and reservoir minerals. These components act as the basis species for constructing a

representative geochemical model and provide a starting point for the reaction-path models (open systems) to trace changes in the system's equilibrium state (Bethke, 2008).

As a starting point, it was necessary to define the equilibrium system in the reservoir prior to any chemical changes related to the injection of CO_2. Under isothermal conditions, bulk water chemistry values, gas fugacities, and mineral masses were input into the SpecE8 and React modules to define the equilibrium system. Collectively, these inputs constituted the basis species for the geochemical model. SpecE8 and React used the basis species to describe the composition of all phases and species, charged and uncharged, in the system (Zhu and Anderson, 2002). Once the reservoir or basis was sufficiently characterized, it was used in the React module for reaction-path modeling to trace changes in aqueous species concentrations and the precipitation and dissolution of minerals as CO_2 was introduced into the system.

Because fluid transport was not incorporated into this study, it was not possible to explicitly simulate spatial variations in water-rock interactions due to variation in CO_2 concentration. From a geochemical process perspective, though, variations in CO_2 concentration and their effect on reactions were examined within the context of varying CO_2 fugacity (henceforth called fCO_2). The geochemical system of interest for this study is the reservoir and overlying seal rocks, where fCO_2 varies from a maximum value at and near the injection well to a pre-injection fCO_2 at some distance from the injection well. The fCO_2 was determined by first calculating variations in CO_2 partial pressure at the production and injection wells. The partial pressure of CO_2 equaled the product of reservoir pressure (measured or estimated) and the concentration of CO_2 measured with an infrared gas analyzer in the annular space gas. The fCO_2 equaled the product of CO_2

partial pressure (P_{CO2}) and the fugacity coefficient (φ). Fugacity coefficients for reservoir conditions were calculated using an online calculator (Duan *et al.*, 1992).

Under conditions of active injection it was assumed that gas at and near the injection wells consisted primarily of CO_2 and therefore CO_2 partial pressure equaled total pressure. Table 3.4 shows the pressures and fugacities at Sugar Creek. The bottom-hole injection pressure (1900 psi, 129.2 bars) was continuously recorded with a bottom-hole pressure transducer (Frailey, *et al.*, 2012). Bottom-hole pressures in the Sugar Creek production wells were estimated to be significantly less (30 psi, 2.04 bars) because of field operating procedures (M. Gallagher [field operator], personal communication).

In addition to the calculated fugacities at the injection and production wells, a median fCO_2 and between the injection and production wells was selected to represent geochemical reactions under conditions of intermediate CO_2 concentration (Table 3.4). It should be emphasized, however, that the median fugacity, henceforth called the mid-fugacity, simulation need not correspond with a geographic point midway between the injection well and any given production well. Moreover, gas and water chemistry measurements at Sugar Creek show that the decrease in CO_2 away from the injection well did not occur in a regular radial pattern.

The infrared gas measurements showed that the majority of associated gas in the reservoir prior to CO_2 injection consisted of CH_4. It was assumed that the aqueous reservoir fluid was saturated with respect to CH_4 because it was in contact with hydrocarbons. The saturation value for CH_4 was included in the basis as a fugacity calculation. The composition of CH_4 in the formation water was determined from an online calculator for reservoir temperature (28°C), and the previously mentioned

pressures in 1 m NaCl formation water (Duan and Mao, 2006). Small amounts of CO_2 were also detected in some wells and it too was included in the basis as a fugacity calculation (Table 3.4).

The final step in representing geochemical conditions in the reservoir prior to CO_2 injection was simulated using the React module by adding the reservoir minerals as simple reactants with the formation water containing background levels of CO_2 and CH_4. The resulting equilibrium model provided a starting point for documenting subsequent changes in water properties (e.g. pH, alkalinity) and mineral saturation states due to CO_2 injection.

A sliding fCO_2 model was used to simulate the effects of CO_2 injection on the pre-CO_2 speciated formation water. The fCO_2 was raised to maximum injection pressure with no minerals in the system. The results from this simulation were "picked up" and reservoir minerals were titrated in for 365 days to represent the year of CO_2 injection. Although the order of operations is not completely intuitive relative to how CO_2 injection occurs in real life, to run GWB required CO_2 to be injected into the formation water and then the minerals to be titrated in as separate steps. The post-injection phase of the geochemical model was simulated by sliding fCO_2 back down to a pre-injection value with reservoir minerals treated again as simple reactants.

3.5.2 Model Inputs and Calculations

Several preliminary calculations, such as mineral mass and surface area, were needed to characterize reservoir conditions and quantify model inputs. First, GWB requires the user to define the masses of water and rock in the reaction simulations. This defines the water:rock ratio, which exerts a strong influence on the extent and magnitude

of reactions. The default simulation mass is 1 kg of water, and average porosity and water saturation data (Table 3.5) were used to calculate the reservoir mass and volume needed to hold 1 kg of water. Total reservoir volume ($V_{reservoir}$) is the sum of the rock volume (V_{rock}), oil-saturated volume (V_{oil}), and water-saturated volume (V_{water}). As demonstrated in Figure 3.2a, if total reservoir volume equals "x" then rock, oil, and water volumes represent some fractional "x". Assuming a water density of 1050kg/m^3, the volume occupied by 1 kg of water equals the mass divided by density. Therefore, the volume of reservoir, x, needed to hold 9.5×10^{-4} m^3 of water equals V_{water} (water-saturated pore volume of the reservoir). Previous calculations by the field operator showed oil and water saturation to equal 65% and 35%, respectively (M. Gallagher [field operator], personal communication). Sugar Creek does not have an underlying aquifer and therefore a single water-filled porosity value was applied to the whole Jackson Sandstone reservoir.

Once the reservoir volume was calculated, the rock volume was calculated as the product of the reservoir volume and the fractional rock volume- in this case, 84%. Rock volume was converted to rock mass assuming a density of 2,650 kg/m^3. This density was used since the reservoir is quartz-rich sandstone. The mass of any given mineral in the reservoir equaled the product of total rock mass and relative weight percent of that mineral as determined from the XRD analysis (Figure 3.2b). The same equations were used to calculate volumes and masses in the seal rocks, but a lower porosity (3%) was used and it was assumed to be 100% water saturated. Lower porosity in the seal rocks produced water-rock ratios that were approximately 50% less than that in the reservoir rocks (Table 3.5).

Kinetic simulations in the React module required surface areas and rate constants for minerals in the reservoir and seal rocks (Table 3.6). Rate constants were compiled from a variety of sources (White and Brantley, 1995; Gunter *et al.*, 1997; Pokrovsky and Schott, 2001; Arvidson *et al.*, 2003; Palandri and Kharaka, 2004; Brantley, 2008; Bandstra *et al.*, 2008). Figure 3.3 is an example of the surface area calculation for quartz in the Jackson using the XRD mineral mass determined in Figure 3.2b. To estimate surface area, it was assumed that mineral grains were spherical with a diameter of 0.1875 mm. This grain size diameter equals the median value for fine-grained sand (Wentworth, 1922), which was chosen because the Jackson reservoir consists largely of well-sorted, fine-grained sandstone with well-rounded quartz grains. The density of quartz was multiplied by the sphere volume to get the quartz mass per sphere. The previously calculated total mineral mass (Figure 3.2b) was divided by the mass per sphere to give the number of quartz spheres. Then, the total number of spheres was multiplied by the surface area of a sphere to give an estimated maximum total surface area for quartz in the simulation volume. Similar calculations were applied to other minerals in the reservoir and seal rocks (Table 3.6). It should be noted that this estimate of reactive surface area represents a maximum value as it is assumed that the entire mineral surface area is exposed to fluid and therefore available for reactions. In reality, this is not the case because where the grains contact each other those surfaces are not in contact with fluid.

Table 3.1 Administrative information for wells from which water data were collected and/or analyzed. Record number refers to the KGS database identification number corresponding to each well. Dashes mean that no data were available.

Record No.	Well Name	Field Name	County	Elevation (ft)	Sampled Interval	Remark	Source
53776	Pressley-Hart #1 (PH1)	Sugar Creek	Hopkins	488	Jackson	Production well	This study
53419	Ross Gentry #1 (RG1)	Sugar Creek	Hopkins	497	Jackson	Production well	This study
53418	Ross Gentry #2 (RG2)	Sugar Creek	Hopkins	512	Jackson	Production well	This study
53417	Ross Gentry #3 (RG3)	Sugar Creek	Hopkins	497	Jackson	Production well	This study
53416	Ross Gentry #4 (RG4)	Sugar Creek	Hopkins	510	Jackson	Production well	This study
53415	Ross Gentry #5 (RG5)	Sugar Creek	Hopkins	497	Jackson	Injection well	This study
54162	Wilbur Todd #3 (WT3)	Sugar Creek	Hopkins	430	Jackson	Water injection well	This study
54163	Wilbur Todd #4 (WT4)	Sugar Creek	Hopkins	507	Jackson	Production well	This study
131562	Wilbur Todd #9 (WT9)	Sugar Creek	Hopkins	494	Jackson	Production well	This study
53419	Ross Gentry #1	Sugar Creek	Hopkins	493	Jackson	5/11/70	Archived
10960	Clements #1	-	Hopkins	476	Jackson	-	Archived
2025940	Hoover Hrs. #1	Huntsville CONS	McLean	390	Jackson	8/15/72	Archived
2030172	Delmore Collier #1	Elba West CONS	Muhlenburg	482	Jackson	5/19/1968	Archived

Table 3.2 Charge balance analysis (% electroneutrality) for Jackson formation waters collected in this study. WT3 samples are from a Pennsylvanian sandstone aquifer, which supplied some injection water in the field. Well abbreviations are defined in Table 3.1.

Well Abbrev.	Sample Round	Sample Date	% Electroneutrality
RG1	1	3/16/2009	-3.81
RG1	2	4/8/2009	-6.4
RG1	9	11/9/2009	-0.13
RG1	10	12/10/2009	-2.43
RG1	13	3/2/2010	-1.95
RG2	2	4/8/2009	-4.56
RG2	3	4/28/2009	-0.61
RG2	4	6/2/2009	-4.77
RG3	1	3/17/2009	-5.35
RG3	3	4/28/2009	-1.02
RG3	4	6/2/2009	-1.78
RG3	5	6/29/2009	-4.01
RG3	6	8/10/2009	-0.78
RG3	7	9/8/2009	-2.02
RG3	8	10/12/2009	-1.13
RG3	9	11/10/2009	-0.24
RG3	10	12/10/2009	-0.89
RG3	11	1/13/2010	0.1
RG3	12	2/2/2010	3.04
RG3	13	3/2/2010	-0.98
RG4	1	3/17/2009	-2.22
RG4	2	4/7/2009	0.8
RG4	3	4/27/2009	-0.75
RG4	4	6/2/2009	-0.1
RG4	5	6/29/2009	-2.06
RG4	6	8/10/2009	-3.19
RG4	7	9/8/2009	-2.07
RG4	8	10/12/2009	0.89
RG4	9	11/10/2009	-1.37
RG4	10	12/10/2009	0.49
RG4	11	1/13/2009	0.33
RG4	12	2/2/2010	1.39
RG4	13	3/2/2010	-1.63
RG5	1	3/16/2009	-3.39

Table 3.2 (continued) Charge balance analysis (% electroneutrality) for Jackson formation waters collected in this study. WT3 samples are from a Pennsylvanian sandstone aquifer, which supplied some injection water in the field. Well abbreviations are defined in Table 3.1.

Well Abbrev.	Sample Round	Sample Date	% Electroneutrality
PH1	2	4/8/2009	-5.91
PH1	3	4/28/2009	-1.65
PH1	4	6/3/2009	-6.55
PH1	5	6/29/2009	-4.38
PH1	6	8/10/2009	-4.01
PH1	8	10/13/2009	0.08
WT3	6	8/11/2009	-12.32
WT3	9	11/10/2009	-6.58
WT3	12	2/2/2010	-2.45
WT4	3	4/28/2009	-1.33
WT4	4	6/3/2009	-4.39
WT4	5	6/29/2009	-5.73
WT4	6	8/11/2009	-5.97
WT4	7	9/9/2009	-0.12
WT4	8	10/13/2009	-0.08
WT4	9	11/9/2009	-1.15
WT4	11	1/13/2010	-0.45
WT4	12	2/2/2010	3.42
WT4	13	3/2/2010	-3.2
WT9	3	4/29/2009	-1.2
WT9	4	6/3/2009	21.41
WT9	5	6/29/2009	-0.65
WT9	6	8/11/2009	-12.32
WT9	7	9/9/2009	-3.81
WT9	8	10/13/2009	0.9
WT9	9	11/10/2009	-0.09
WT9	9a	11/18/2009	5.94
WT9	10	12/10/2009	-0.12
WT9	11	1/13/2010	-0.72
WT9	12	2/2/2010	1.91
WT9	13	3/2/2010	1.79

Table 3.3 Charge balance analysis (% electroneutrality) for archived water samples from the Jackson collected near Sugar Creek.

Brine_No.	County	Sampled Interval	% Electroneutrality
Hop29	Hopkins	Jackson	0.00
Hop152	Hopkins	Jackson	-1.26
McL2	McLean	Jackson	-1.24
Muhl4	Muhlenburg	Jackson	-0.28

Table 3.4 Calculated CO_2 fugacity and CH_4 solubility for the pre-injection and CO_2-injection simulations. The CO_2 fugacity co-efficient (Duan *et al.*, 1992) and CH_4 solubility (Duan and Mao, 2006) were determined with an online calculator using input values of reservoir temperature, pressure, and molar concentration of NaCl in the formation water.

		Sugar Creek			
		Injection Well (RG5)	Mid-Fugacity	Avg. Production Wells (RG1-4, WT9)	Avg. Production Wells (WT4/PH1)
Pre-Injection	Total pressure (psi/bar)	700/47.6		30/2.04	
	CO_2 concentration	3.5%			
	CO_2 co-efficient	0.7737		0.9899	
	CO_2 partial pressure (psi/bar)	24.5/1.67		1.05/0.0714	
	CO_2 fugacity (bar)	1.29		0.0707	
	CH_4 solubility (mol/kg)	0.05045		0.00241	0.00208
Injection	Total pressure (psi/bar)	1900/129.2	-	30/2.04	
	CO_2 concentration	100%	-	83%	
	CO_2 co-efficient	0.5921	-	0.9917	
	CO_2 partial pressure (psi/bar)	1200/81.6	-	24.9/1.69	
	CO_2 fugacity	49.6	25.6	1.68	

Table 3.5 Porosity and phase saturation data for reservoir and seal rocks. Total porosity represents an average based on core analysis of the Jackson in the area of Sugar Creek. Oil- and water-filled porosity values are based on phase saturation calculations by the field operator that yielded oil and water saturations equal to 65% and 35%, respectively (M. Gallagher [field operator], personal communication). Note: Values represent conditions at the onset of field development and before the water flood operation.

Sugar Creek	
Reservoir Total Porosity (φ_{total})	16%
Oil Porosity (φ_{oil})	10.4%
Water Porosity (φ_{water})	5.6%
Seal Rock Total Porosity (φ_{total})	3%
Water Porosity (φ_{water})	3%
Water:Rock (reservoir)	0.07
Water:Rock (seal)	0.03

Table 3.6 Inputs for kinetic simulations included surface areas calculated in this study and rate constants compiled from the literature. Dolomite and Chlinochlore-14A were used as substitutes for ankerite and chlorite, respectively, due to lack on thermodynamic data available within the GWB software ([1]Brantley, 2008; [2]Arvidson *et al.*, 2003; [3]Pokrovsky and Schott, 2001; [4]Gunter *et al.*, 1997; [5]Rockware, Inc. GWB Short-course, unpublished, 2009; [6]Palandri and Kharaka, 2004; [7]White and Brantley, 1995).

Mineral	**Surface Area (cm^2/grams)**	**Rate Constant (mol/cm^2 sec)**
[1]Quartz	120.75	7×10^{-17}
[1]K-feldspar	125.00	6×10^{-17}
[1]Albite	122.14	9×10^{-17}
[2]Calcite	118.08	1×10^{-10}
[3]Ankerite (Dolomite)	112.68	1×10^{-12}
[4]Siderite	80.81	1×10^{-10}
[5]Pyrite	63.87	3.05×10^{-17}
[6]Gypsum	139.13	1.62×10^{-7}
[7]Illite	116.36	1×10^{-13}
[5]Smectite	116.36	2.3×10^{-22}
[1]Kaolinite	123.08	8×10^{-19}
[7]Chlorite (Chlinochlore-14A)	100.00	1×10^{-13}
[5]Hematite	60.38	3.05×10^{-17}

Figure 3.1 Photo showing the field setup apparatus used to sample formation waters. Oil was separated from formation water in the separation carboy. The outflow water from the separation carboy was further filtered before entering the flow-through cell for the YSI multi-meter. The large waste carboy on the ground collects overflow (photo by G. Beck, 2009).

(a)

$$V_{rock} + V_{oil} + V_{water} = V_{reservoir}$$

$$0.84x + 0.104x + 0.056x = x$$

Where:

$V_{reservoir} = x$

$V_{rock} = (1- \varphi_{total})x = 0.84x$

$V_{oil} = 0.104x$

$V_{water} = 0.056x$

$\varphi_{total} = 16\%$

$\varphi_{oil} = 10.4\%$

$\varphi_{water} = 5.6\%$

$\rho_{water} = 1054.7$ kg/m^3 (measured density of formation waters in field)

$\rho_{rock} = 2650$ kg/m^3 (density of quartz)

$$V_{water} = 1 \text{ kg} / (1054.7 \text{ kg/m}^3) = 9.48\times10^{-4} \text{ m}^3$$

$$9.48\times10^{-4} \text{ m}^3 = V_{water} = 0.056x;$$

So reservoir volume, $x = 1.69\times10^{-2}$ m^3

$$V_{rock} = 0.84\ (1.69\times10^{-2} \text{ m}^3) = 1.42\times10^{-2} \text{ m}^3$$

$$M_{rock} = (1.42\times10^{-2} \text{ m}^3)(2650 \text{ kg/m}^3) = 37.7 \text{ kg}$$

(b)

To find mineral masses, take M_{rock} and multiply by XRD weight percent results for each mineral:

$$M_{mineral} = (\text{weight percent})(M_{rock})$$

Where:

Quartz = 80.4%

$$\mathbf{M_{quartz} = 0.804\ (37.7 \text{ kg}) = 30.3 \text{ kg}}$$

Figure 3.2 Sample calculations explaining how (a) water-saturated and rock volumes and masses in the reservoir were calculated, and (b) how mineral masses were estimated. The example in (b) is for quartz in the Jackson.

$$V_{mineral} = (4/3)(\prod)(r^3)$$

Where:

$V_{mineral}$ = volume of mineral sphere

r = radius of mineral sphere

$$V_{quartz} = (4/3)\ (\prod)\ (r^3)$$
$$V_{quartz} = (4/3)\ (\prod)\ ((0.009375\text{cm})^3)$$
$$V_{quartz} = 3.45\times10^{-6}\ \text{cm}^3$$

Where:

r = (0.1875 mm / 2) = (0.01875 cm / 2) = 0.009375 cm

$$M_{qtz\ grain} = (\rho_{quartz})\ (V_{quartz})$$
$$M_{qtz\ grain} = (2.65\ \text{g/cm}^3)\ (3.45\times10^{-6}\ \text{cm}^3)$$
$$M_{qtz\ grain} = 9.146\times10^{-6}\ \text{g}$$

Where:

$\rho_{quartz} = 2.65\ \text{g/cm}^3$

$$\text{Number of grains} = M_{total} / M_{qtz\ grain}$$
$$\text{Number of grains} = 30{,}303\ \text{g} / 9.146\times10^{-6}\ \text{g}$$
$$\text{Number of grains} = 3.313\times10^{9}$$

Where:

M_{total} = 30.303 kg = 30,303 g (from Figure 3.2b)

$$\text{Surface Area}_{total} = (4(\prod)(r^2))\ (\text{Number of grains})$$

Where:

Surface Area = surface area per sphere

r = radius of mineral sphere

$$\text{Surface Area}_{total} = (4(\prod)((0.009375\ \text{cm})^2)\ (3.313\times10^{9})$$
$$\text{Surface Area}_{total} = 3.659\times10^{6}\ \text{cm}^2$$

$$\text{Surface Area} = \text{Surface Area}_{total} / M_{total}$$
$$\text{Surface Area} = 3.659\times10^{6}\ \text{cm}^2 / 30{,}303\ \text{g}$$
$$\mathbf{Surface\ Area = 120.75\ cm^2/g}$$

Figure 3.3 Calculations of mineral surface area using quartz as an example.

Chapter 4: Water Chemistry and Mineralogy Results and Discussion

4.1 Formation Water Chemistry

The chemistry of formation waters at Sugar Creek is based on 62 samples collected at eight wells from May 2009 through May 2010. The majority of the samples were collected during injection (ten sample rounds) with a smaller number collected before (three sample rounds). Table 4.1 shows the average values of all the rounds for each well. In addition, four archived samples were used to complement the new samples. The archived water chemistry data are important because they are interpreted to represent pristine Mississippian formation waters and, as such, provide a useful reference in determining to what degree water flooding at Sugar Creek has altered the chemistry of formation waters. Piper plot analysis of formation waters at Sugar Creek shows that they consist primarily of Na^+ and Cl^- (Figure 4.1). The Piper plots also show little difference in the relative proportion of the major cations and anions before and during CO_2 injection (Figure 4.2). The exception is WT3 because it is significantly more enriched in HCO_3 and has lower TDS values of 664 to 936 mg/L.

While the Piper plots are effective in showing variation in the relative proportion of major cations and anions, they do not show changes in absolute concentrations where proportions are relatively constant. This is demonstrated in a plot of Na+Cl versus total dissolved solids (Figure 4.3). Sugar Creek formation waters group into two distinct populations, with the PH1 and WT4 wells having TDS values ranging from 50,420 to 66,640 mg/L, whereas the RG1-RG5 and WT9 wells have significantly lower TDS values on the order of 11,124 to 28,740 mg/L. The WT3 well, with even lower TDS values (664 to 936 mg/L) plots in the upper left corner of Figure 4.3. The variation in water chemistry

shown in Figure 4.3 likely results from varying degrees of mixing between the more dilute Pennsylvanian water from WT3 with more saline Jackson formation water. The differences suggest that Jackson formation water in PH1 and WT4 was minimally impacted, if at all, by water flooding. Therefore, salinity in PH1 and WT4 might represent native formation water salinity. In contrast, salinity was reduced by approximately 50% in WT9 and RG1-RG5 by mixing with less saline Pennsylvanian water from WT3. The bimodal distribution of TDS values provides evidence that the Jackson reservoir is compartmentalized with RG1-RG5 and WT9 being in hydrologic communication with each other, whereas PH1 and WT4 appear to be isolated by some unknown geologic barrier. Despite the differences in salinity and Na+Cl concentration, both the high and low salinity populations show a slight excess of TDS compared to the Na+Cl concentration, indicating the contribution of other cations (Ca^{2+}, Mg^{2+}) and anions (SO_4^{-2}, HCO_3^-) to TDS.

Of the archived data from the Jackson, four out of ten samples collected between 1966 and 1970 have charge balances of 10% or less and were in Hopkins or an adjacent county. Initial Piper plot analysis shows the archived waters to contain primarily Na^+ and Cl^-, which is consistent with results from the newer samples collected from Sugar Creek (Figure 4.4). Plotting Na+Cl versus TDS for the archived samples shows a range of TDS values to be 17,600 to 59,200 mg/L (Figure 4.3). By analogy, the range in TDS and Na+Cl suggests that some of the archived Jackson formation water samples might have also been diluted in the water flood operations in surrounding fields.

4.2 Mineralogy and Petrography

XRD analyses of reservoir and seal rocks in the Jackson allowed identification of potentially reactive minerals and provided semi-quantitative estimates of mineral masses used as inputs for GWB. Macroscopic examination of 14 Jackson reservoir samples shows them to be primarily tan to gray, fine-grained sandstone. Three samples from the upper unit of the Jackson (1730, 1780, and 1810 feet) are medium gray, shaley mudstones. Due to limited Jackson cuttings samples, there was not enough material to send out requests for both XRD analysis and thin section preparation.

In accordance with the macroscopic analysis, the XRD results (Table 4.2) show that samples collected from the Jackson reservoir are predominantly composed of quartz (70.6-89.5%), with lesser amounts of feldspars (1.7-4.4%), carbonates (2.4-19.1%) and clays (3.9-14.8%). Without thin sections the distribution and mode of these minerals is unknown; however, petrographic analysis of Chester sandstone samples elsewhere show that detrital quartz is the main framework grain with smaller amounts of detrital feldspar (Siever, 1953). Additionally, several samples contain large amounts of ankerite and correspond to intervals having high resistivity values. The coincidence suggests that the ankerite might be pore-filling cement because it would reduce the pore space available for pore fluids that have lower resistivity as compared to minerals.

Unlike the reservoir rocks, the three samples from the shaley upper Jackson unit (Table 4.2) contain significantly less quartz (25.7-28.6%), and more clays (44.2-60.2%), feldspars (4.2-5.7%), and carbonates (7.8-21.3%). The more clay-rich section of the Jackson could act as an additional sealing layer above the reservoir.

Table 4.1a Average water properties for Jackson formation water sample. For each well name, the top line of the sample round column represents the samples collected before injection of CO_2 (before May 11, 2009) and the bottom line represents samples collected after CO_2 injection had occurred.

Well Name	No. of Sample Rounds Averaged	pH	Temp (°C)	Cond (mS/cm)	Eh (mV)	DO (mg/L)	Alkalinity (mg/L, $CaCO_3$)	TDS (mg/L)
PH1	2	7.11	18.2	89.1	-188.6	0.55	186	58101
	4	6.77	22.9	87.2	-135.8	1.74	619	61654
WT4	1	6.84	20.4	83.9	-270.3	0.87	310	50420
	9	6.78	19.8	84.1	-244.5	1.39	328	57474
WT9	1	7.12	18.6	37.8	31.3	2.79	858	23720
	11	6.91	17.0	39.0	-246.3	2.08	943	24317
RG1	2	7.26	17.9	41.8	-229.1	1.04	661	21298
	3	5.70	16.5	43.5	-119.1	1.22	1070	28481
RG2	2	6.67	18.6	48.4	-247.5	2.54	850	25818
	1	6.22	27.7	40.9	-182.9	1.77	1997	27284
RG3	2	6.34	18.8	35.1	-122.1	1.36	882	23554
	10	5.95	20.0	40.0	-192.8	1.11	1505	25945
RG4	3	6.88	20.8	25.5	-255.9	2.67	832	19761
	10	6.16	20.8	34.5	-180.5	1.35	1202	21227
RG5	1	7.16	14.0	25.2	-342.9	0.26	689	19108

Table 4.1b Average water properties for Jackson formation water sample. For each well name, the top line of the sample round column represents the samples collected before injection of CO_2 (before May 11, 2009) and the bottom line represents samples collected after CO_2 injection had occurred. Important cation and anion concentrations are listed in milligrams per liter (mg/L).

Well Name	No. Sample Rounds Averaged	Al^{+3}	Ca^{+2}	Ba^{+2}	Fe^{+2}	Li^{+}	Mg^{+2}	Mn^{+2}	K^{+}	Si_{+4}	Na^{+}	Sr^{+2}
PH1	2	-	1555	3.43	184.25	5.45	600	4.43	51	6.76	16775	321
	4	0.15	1668	2.54	27.50	2.49	621	1.36	46	8.05	16825	343
WT4	1	-	1580	5.61	-	2.42	604	0.39	50	4.27	17340	262
	9	0.10	1563	4.99	-	2.23	593	0.20	47	4.57	16980	279
WT9	1	-	453	1.81	21.00	0.97	183	1.63	25	4.20	7860	528
	11	-	471	2.54	-	1.00	191	0.31	28	6.13	7845	563
RG1	2	-	489	2.10	0.02	3.04	173	0.27	19	5.85	6312	317
	3	-	669	3.04	3.01	1.08	238	0.29	28	6.63	8983	450
RG2	2	-	571	4.80	0.01	2.36	219	0.08	26	5.65	7965	483
	1	-	863	4.47	6.23	0.82	240	1.71	24	7.24	7460	596
RG3	2	-	483	5.21	-	2.14	192	0.12	23	6.29	7240	510
	10	-	659	3.26	3.82	0.93	234	0.87	23	6.80	7872	650
RG4	3	-	385	2.22	0.04	2.06	159	0.15	19	5.98	5895	474
	10	0.08	547	2.32	8.23	0.75	202	0.86	19	5.55	6544	536
RG5	1	-	440	2.89	0.01	2.86	172	0.12	17	5.85	5990	284

Table 4.1c Average water properties for Jackson formation water sample. For each well name, the top line of the sample round column represents the samples collected before injection of CO_2 (before May 11, 2009) and the bottom line represents samples collected after CO_2 injection had occurred. Important cation and anion concentrations are listed in milligrams per liter (mg/L).

Well Name	No. Sample Rounds Averaged	HCO_3^-	Br^-	Cl^-	I^-	SO_4^{-2}
PH1	2	227	128	33150	4.6	8.3
	4	755	145	32950	4.7	14.8
WT4	1	378	125	32100	4.0	54.5
	9	400	132	31833	4.2	104.3
WT9	1	1046	52	13600	1.6	60.1
	11	1149	54	12979	1.9	90.2
RG1	2	805	47	12250	0.9	33.5
	3	1305	63	15800	1.9	49.2
RG2	2	1036	55	14450	1.8	30.9
	1	2435	57	14200	1.5	44.2
RG3	2	1075	50	13200	1.8	27.0
	10	1835	57	13650	1.8	40.1
RG4	3	1014	39	10167	1.5	35.8
	10	1466	47	11340	1.5	63.0
RG5	1	840	41	11000	1.6	34.4

Table 4.2 Summary of XRD mineralogic characterization for the Jackson. Values for each mineral are listed in weight percent. *Jackson samples collected immediately above the sandstone reservoir have low porosity and permeability and are treated as the seal rocks for the formation. Abbreviations are as follows: Graden Osburn #1-A (GO1A), Gatlin Harris #3 (GH3), Thomason & Boyd #1 (TB1), Wilbur Todd #2 (WT2), and Dexter Laffoon #1 (DL1), quartz (Qtz), potassium feldspar (K-spar), plagioclase (Plag), ankerite (Ank), calcite (Cal), dolomite (Dol), pyrite (Pyr), gypsum (Gyp), kaolinite (Kao), and chlorite (Chlor). Abbreviations for mixed-layer clays are R0 M-L I/S 90S, randomly ordered mixed-layer illite/smectite with 90% smectite layers, and R1 M-L I/S 30S, randomly ordered mixed-layer illite/smectite with 30% smectite layers.

Sample Depth (ft)	Well Name	Qtz	K-spar	Plag	Ank	Cal	Dol	Pyr	Gyp	R0	R1	Illite & Mica	Kao	Chlor
1840-1845	GO1A	83.5	0.2	2.4	2.6	3.5	1.2	-	-	-	-	2.2	1.2	3.2
1845-1850	GO1A	70.6	0.3	2.3	1.9	14.6	2.6	-	-	-	-	3.6	1.0	3.1
1850-1855	GO1A	84.2	0.3	4.1	1.1	3.4	0.5	-	-	-	-	2.7	1.6	2.1
1795-1800	GH3	85.4	0.5	3.1	-	1.7	1.2	-	-	-	-	1.7	1.6	4.8
1800-1805	GH3	79.5	0.4	3.9	0.8	3.5	-	-	-	-	-	3.9	2.6	5.4
1810-1815	GH3	79.7	0.3	3.7	1.5	5.1	0.3	-	-	-	-	2.9	2.4	4.1
*1810-1815	TB1	25.7	2.4	3.3	1.9	5.9	-	0.6	-	18.5	16.7	18.8	2.7	3.5
1815-1820	TB1	79.3	0.3	1.5	14.3	0.6	-	-	-	-	-	2.2	1.8	-
1820-1825	TB1	80.4	0.3	1.9	12.8	0.4	-	0.2	-	-	-	2.0	2.0	-
*1780-1785	WT2	25.7	2.4	1.8	1.7	8.8	-	0.5	0.4	18.7	15.9	16.2	4.4	3.5
1785-1790	WT2	74.1	0.3	2.6	17.6	0.9	-	0.2	-	-	-	2.1	2.2	-
1790-1795	WT2	75.1	0.2	2.3	12.9	0.7	-	0.3	-	-	-	3.4	3.2	1.9
1795-1800	WT2	87.6	0.2	3.0	1.3	1.2	-	0.1	-	-	-	2.2	2.7	1.7
*1730-1735	WT2	28.6	2.6	2.9	1.9	19.4	-	0.4	-	2.2	17.6	17.9	3.6	2.9
1735-1740	DL1	78.0	0.3	1.4	15.8	0.4	-	0.2	-	-	-	2.1	1.8	-
1740-1745	DL1	78.4	0.2	4.2	1.7	0.7	-	-	-	-	-	3.7	6.5	4.6
1740-1745	DL1	89.5	0.2	2.9	2.1	0.3	-	-	-	-	-	2.1	2.6	0.3

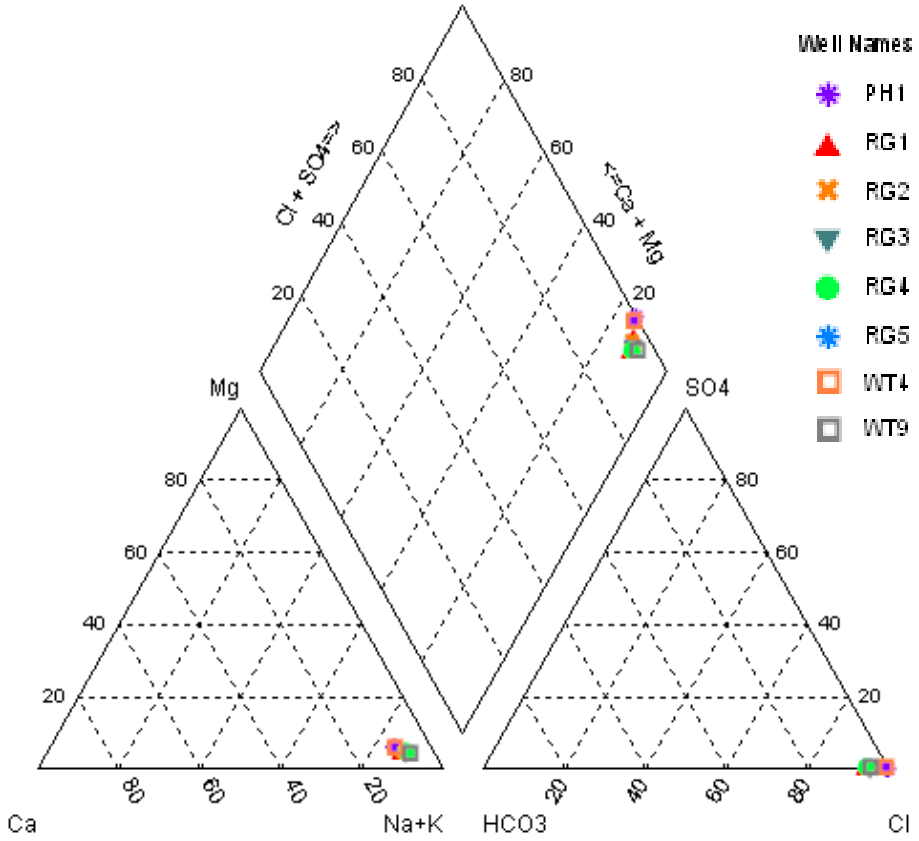

Figure 4.1 Piper plot showing major-ion concentrations in Jackson formation water samples collected before CO_2 injection.

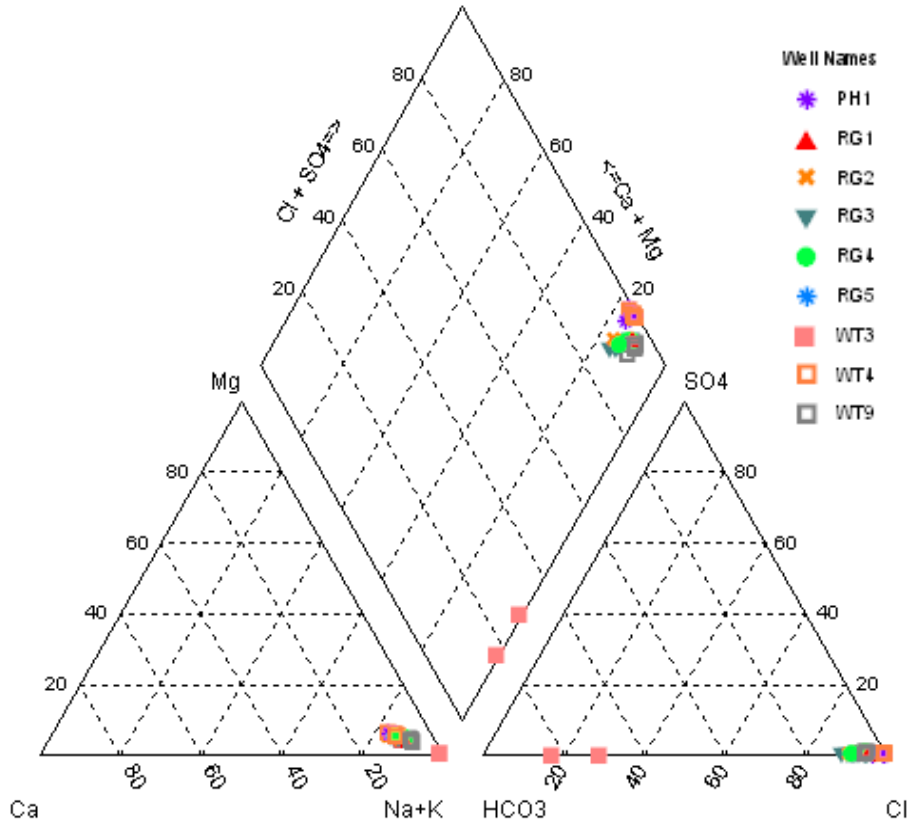

Figure 4.2 Piper plot showing major-ion concentrations for Jackson formation water samples collected during CO_2 injection.

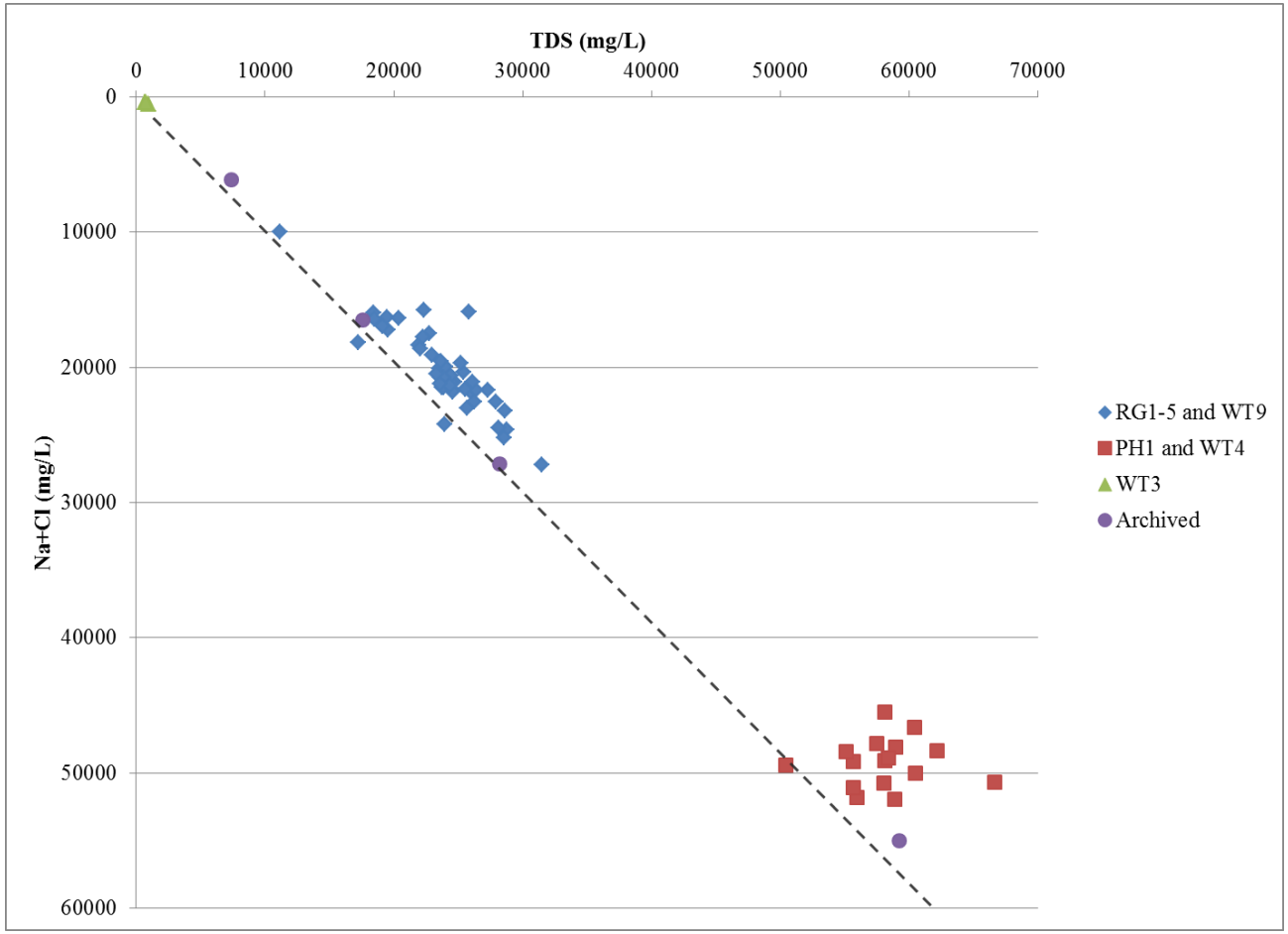

Figure 4.3 Sodium chloride (Na+Cl) versus TDS for Jackson and Pennsylvanian (WT3) formation water samples. Compartmentalization in the reservoir is evidenced by the distinct separation between RG1-5, WT9 and PH1, WT4. The four archived samples were collected from other oil fields near Sugar Creek. The dashed line represents a line of best fit for the archived data, creating a historic trend line for pristine Mississippian formation water in the Jackson.

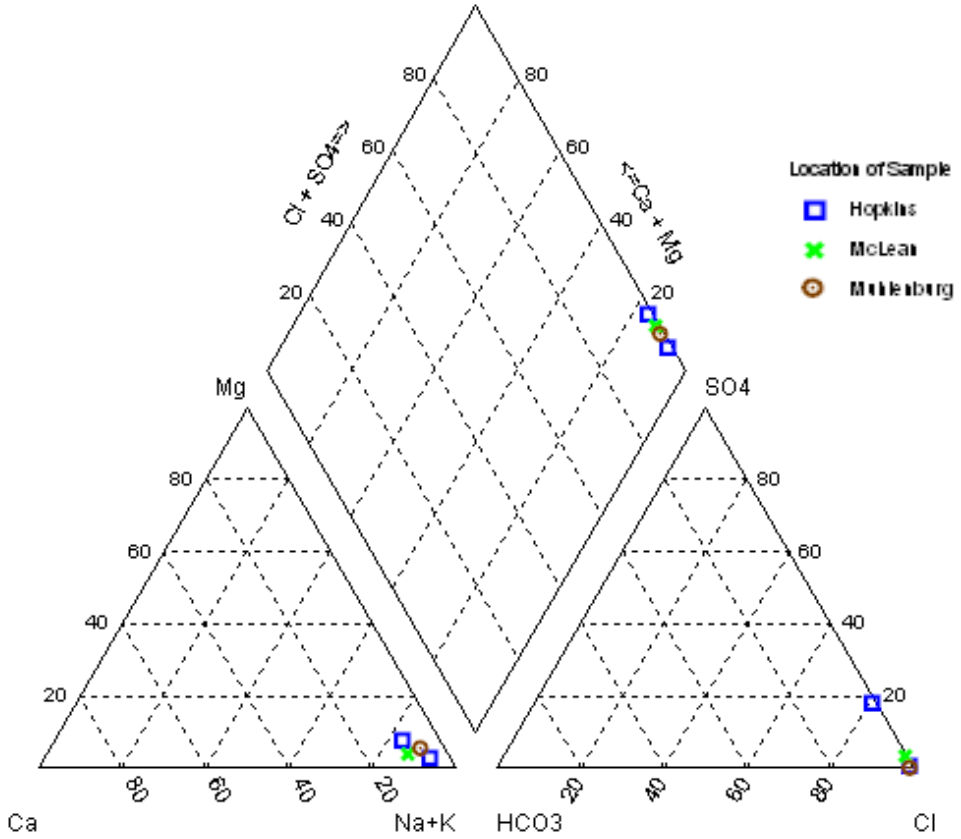

Figure 4.4 Piper plot showing major-ion concentrations for archived Jackson formation water from fields near Sugar Creek.

Chapter 5: GWB Modeling Results

In order to simulate injection of CO_2 into the Jackson reservoir and seal rocks, a mixture of GWB model types (speciation, path of reaction, and kinetic reaction) were used. The models were tailored to fit reservoir temperature and pressure conditions, baseline CO_2 concentrations, injection pressures, and formation-water chemistry. The models for seal rocks and reservoir rocks were separated due to different porosity and mineralogy. As the models were run under conditions of constant temperature equal to 28°C (82°F), the principal variable in the geochemical modeling process was CO_2 fugacity (fCO_2), which represented the variation in pressure and CO_2 concentration in the reservoir and seal rocks throughout the injection process (Tables 5.1a,b). As described in the Methods section, measured reservoir pressure and CO_2 concentration at the injection well and production wells allowed the spatial variation in fCO_2 in the field to be calculated. Simulations were run in which the highest fCO_2 coincided with the injection well and the lowest with the production well. An important aspect of GWB modeling is accounting for the effect of salinity on CO_2 solubility and modifying the database to correct for this salting-out effect. Ignoring these effects overestimates the long-term CO_2 trapping through carbonate mineral precipitation, especially in formation waters with high TDS values (Allen, 2005; Zerai, 2006).

Conceptually, the modeling process was split into distinct phases representing the variation in fCO_2 and reservoir chemistry before, during, and after injection. The configuration of GWB required that the pre-, post-, and injection phases be simulated in four steps. The four phases included: 1) pre-CO_2 injection, 2) CO_2 injection phase I, 3) CO_2 injection phase II, and 4) post-CO_2 injection. The pre-injection phase was simulated

using an equilibrium, or speciation, model in which baseline CO_2 and CH_4 concentrations, as measured in the field and laboratory, were brought into equilibrium with formation water. The results from the pre-injection phase were "picked-up" in GWB and used as the starting point for injection phase I simulation. Injection phase I involved raising fCO_2 to represent CO_2 injection but with no minerals included. Results from injection phase I were again "picked-up" in GWB and used as the starting conditions for simulating injection phase II, in which kinetic minerals were titrated into the system for 365 days, representing the approximate CO_2 injection period for Sugar Creek. Notably, injection phase II was the only simulation step in which time was an explicit variable because the kinetic minerals are partly defined by rate constants. All other simulation steps in which a reaction path was followed (that is, steps 1, 2 and 4) were discriminated against the dimensionless reaction progress. The fourth, or post-injection phase, involved sliding the fCO_2 back down to the pre-injection value. Before reducing fCO_2, minerals that equilibrated during injection phase II were swapped into the basis, which provided the opportunity to simulate how minerals reacted in the post-CO_2 injection phase.

Within the model, important variables that remained constant throughout the simulations include porosity, temperature, and water saturation. Quantitative outputs from the GWB steps are separated into seal and reservoir rocks at the injection well, mid-point fugacity, and production wells. The results include fCO_2 and carbonate equilibrium, mineral saturation (log Q/K values, Tables 5.2a-d), and the masses of reacted minerals (Tables 5.3a-d).

5.1 Pre-CO_2 Injection

Based on field measurements of gas composition and pressure, the highest CO_2 concentrations, and hence fCO_2, are associated with the injection and mid-point fugacity wells (fCO_2 = 1.3), and lowest CO_2 concentration and fCO_2 with the production wells (fCO_2 = 0.071, Tables 5.1a,b). Speciation modeling using these CO_2 fugacities and the water chemistry mentioned in Chapter 4 shows the highest aqueous CO_2 concentrations occur at the injection well with slightly lower values at the mid-fugacity and production wells. According to field measurements, the highest alkalinities were at the injection well (689 mg/kg) and RG1-4, WT9 (557-920 mg/kg). Lowest alkalinities are associated with PH1, WT4 (310-352 mg/kg). Speciation modeling done for the pre-CO_2 injection phase supports the alkalinity distribution found in the field, but with higher values. Simulated pH values equal 5.6 in the injection and mid-point fugacity wells, which is about 1.5 pH units lower than measured at RG5 (Figure 5.1). Simulated pH values for RG1-4, WT9 and PH1, WT4 equal 6.1 and 6.5, respectively. These values are also less than values measured in the field by 0.5 to 1 pH unit. At RG5, the water is highly undersaturated with respect to all of the alumino-silicate minerals (i.e. K-feldspar, plagioclase), slightly undersaturated (close to equilibrium) with respect to calcite, dolomite and quartz, and supersaturated with respect to pyrite (Table 5.2a). Results for the mid-fugacity well are similar but the magnitude of undersaturation and saturation was diminished or increased, respectively (Table 5.2b). In contrast, log Q/K values for RG1-4, WT9 show supersaturation with respect to alumino-silicate minerals except for chlorite, which remains undersaturated; near-equilibrium conditions for quartz; slight undersaturation for calcite and dolomite; and supersaturation for pyrite (Table 5.2c). PH1, WT4 shows even

higher degrees of supersaturation for the alumino-silicate minerals; slight super saturation for calcite, dolomite, and quartz (which is very close to equilibrium); and supersaturation for pyrite (Table 5.2d).

5.2 CO_2 Injection Phase I

During injection phase I, fCO_2 (based on injection pressure and CO_2 concentration) is raised to simulate injection of CO_2 into the reservoir. Tables 5.1a and 5.1b show that fCO_2 is highest at RG5 (49.6 bars), intermediate at the mid-point fugacity (25.6 bars), and lowest at production wells (1.68 bars). The elevated fCO_2 produces corresponding increases in aqueous CO_2 (Tables 5.1a,b). The increased aqueous CO_2 reduces pH to values in the lower 4 range at RG5 and mid-point fugacity, and values in the lower to mid-5 range for the production wells (Figure 5.1). The pH of formation water in the reservoir and seal rocks was similar, but pH values in the latter were approximately a tenth of a pH unit lower as compared to the former. Relative to pre-CO_2 injection values, the fluid response to CO_2 injection shows a decrease in carbonate alkalinity by more than half at RG5 (1050 to 514 mg/kg), a moderate decrease at the mid-point fugacity (795 to 504 mg/kg), and a smaller decrease (704 to 648 mg/kg) at the production wells (Figure 5.2). Differences between aqueous fluid properties at RG1-4, WT9 and PH1, WT4 are a reflection of differences in the pre-CO_2 injection water chemistry caused by the operational water flood and reservoir compartmentalization.

As compared to the pre-CO_2 injection phase, mineral saturation values decrease for most minerals such that most are undersaturated at the end of the phase. Results for saturation states show varying degrees of supersaturation for pyrite (log Q/K range of

1.43 to 8.41). Quartz is near equilibrium, and water in the reservoir rock is undersaturated with respect to calcite, dolomite, K-feldspar, chlorite and albite (Tables 5.2a-d). The decrease in saturation states is especially apparent in PH1,WT4 where minerals that were saturated (e.g. calcite, dolomite, k-feldspar, albite) before CO_2 injection are undersaturated after simulating CO_2 injection phase I (Table 5.2d). Spatially, the degree of undersaturation progressively decreases going from the injection, mid-fugacity, and production wells. Among the production well simulations, however, the degree of undersaturation was greatest for PH1, WT4 as compared to RG1-4, WT9 wells.

5.3 CO_2 Injection Phase II

The elevated fCO_2 values established in CO_2 injection phase I are retained in CO_2 injection phase II, in which the kinetic minerals are titrated into the aqueous fluid. The results at the end of CO_2 injection phase II are important because they include the complete geochemical system of interest; that is, the aqueous fluid with elevated fCO_2, and the reservoir and seal rock minerals (treated kinetically).

When the kinetic minerals are titrated in during CO_2 injection phase II, the aqueous fluid responds with a rapid increase (less than one day) in pH as compared to values in the previous phase (Figure 5.3). The pH values at the end of the 365 day mineral titration range from 4.9 at RG5 to 5.7 at RG1-4, WT9; similarly, alkalinity values range from 3378 mg/kg at RG5 to 804 mg/kg at RG1-4, WT9 and are higher than in CO_2 injection phase I (Table 5.1a, Figure 5.1). Spatially, the magnitude of change in pH and alkalinity values decreases the farther away from the injection well. The response of the

seal rocks at the end of CO_2 injection phase II was similar to the response in the reservoir rocks, but the magnitude of change was less.

Changes in mineral saturation provide the geochemical driver for precipitation and dissolution as minerals are titrated into the CO_2-rich, low pH formation waters. Mineral saturations change rapidly, within days of kinetic mineral titration. With the exception of pyrite, for which saturation decreases from super-saturation to equilibrium, all reservoir and seal mineral saturation states increase (Tables 5.2a-d). Carbonate minerals go to equilibrium quickly from previous conditions of supersaturation (e.g. dolomite at PH1, WT4 and RG1-4, WT9) and undersaturation (e.g. calcite at RG5, mid-fugacity, RG1-4, WT9). Following CO_2-injection phase II, feldspar is undersaturated for most reservoir and seal rocks, except albite, which is at equilibrium in the seal rocks at RG5.

Minerals precipitating at RG5 and the mid-point fugacity within the reservoir include gibbsite, strontianite, and witherite (Table 5.3b). The RG1-4, WT9 wells show gibbsite, strontianite, witherite, and muscovite precipitating and PH1, WT4 wells show strontianite, witherite, siderite, and muscovite (Table 5.3b). Within the seal rocks, the minerals precipitating at RG5 and the mid-point fugacity during the second injection phase include gibbsite, strontianite, and barite (Table 5.3d). Mineral precipitation in seal rocks at RG1-4, WT9 and PH1, WT4 wells includes: strontianite, barite, and muscovite (Table 5.3d). GWB predicts that approximately 5.5 grams of calcite dissolve rapidly (within one day of titration) into the system at RG5, mid-point fugacity (Figure 5.4), and PH1, WT4, and only 2.3 grams dissolve at RG1-4, WT9. Conversely, the highest amount of dolomite rapidly precipitates into the system at PH1, WT4 (3.8 grams), a moderate

amount at mid-point fugacity (1.4 grams, Figure 5.5) and RG1-4, WT9 (1.1 grams), and the lowest at the injection well (0.4 grams). Over all change in mineral mass versus time shows a net dissolution mass change with carbonate minerals (calcite, dolomite and strontianite) as the dominantly controlling minerals which represent the largest change in mass (Figure 5.6).

5.4 Post-CO_2 Injection Phase

The fCO_2 is reduced down to pre-injection values during the post-CO_2 injection phase using a sliding fugacity model, and requires minerals that equilibrated with formation water during the previous phase to be swapped into the basis. For example, dolomite is substituted for Mg^{+2}, calcite for Ca^{+2}, strontianite for Sr^{+2}, gibbsite for Al^{+3}, and pyrite for Fe^{+2}. The simulation proceeds along a non-dimensional reaction path as fCO_2 is reduced.

Results show increasing pH for the formation water in the reservoir rocks, with the largest increase at RG5 (about 1 pH unit), moderate increase for mid-point fugacity and RG1-4, WT9 (about 0.75 pH unit) and the lowest increase at PH1, WT4 (about 0.7 pH unit, Figure 5.1). Carbonate alkalinity decreases and HCO_3^- species are predicted to decrease by an order of magnitude as fCO_2 is decreased. The largest decrease in carbonate alkalinity for reservoir rocks is at RG5 (3739 to 1744 mg/kg), with moderate decreases at mid-point fugacity (2899 to 1264 mg/kg) and RG1-4, WT9 (1063 to 332 mg/kg), and the lowest decrease at PH1, WT4 (903 to 269 mg/kg, Figure 5.2). Formation water in the seal rock shows similar increases in pH and decreases in alkalinity as that in the reservoir. Final pH values in seal rock formation water are slightly less than that in the reservoir

and alkalinities show the same but with a greater magnitude of difference (Tables 5.1a, 5.1b).

Predicted mineral saturation values show the carbonate minerals to be at equilibrium in the reservoir and seal rock simulations (Tables 5.2a-d). The saturation state of quartz in the post-CO_2 injection phase decreases from the preceding simulation phase such that it is undersaturated in the reservoir rock simulations, except for PH1, WT4, where it is at equilibrium. In contrast, quartz attains equilibrium in all of the seal rock simulations. The feldspars are undersaturated in the reservoir and seal rock simulations for all wells, with the exception of albite at RG5 in the seal rock. The only example of where a clay species, kaolinite, is at equilibrium is for the seal rocks at RG5. At the remaining wells, the clay minerals were undersaturated in the post-CO_2 injection phase (Tables 5.2a-d).

During the post-CO_2 injection phase, minerals precipitating at RG5, the mid-point fugacity, and RG1-4, WT9 wells include calcite, dolomite, gibbsite, kaolinite, pyrite, strontianite, and witherite (Tables 5.3a-d). At the PH1, WT4 wells, calcite, dolomite, kaolinite, pyrite, strontianite, witherite, quartz and siderite precipitate (Tables 5.3a-d). Over-all change in mineral mass in grams versus time shows net precipitation, with calcite, dolomite and strontianite as the dominantly controlling minerals (Figure 5.7).

Table 5.1a Variation in calculated fCO_2 during the four GWB simulation phases at different wells for Jackson formation waters in the reservoir. Changes in fCO_2 produce changes in aqueous CO_2, HCO_3^-, carbonated alkalinity, and pH.

Sugar Creek Reservoir Rocks			Pre-injection	Injection Phase I	Injection Phase II	Post-injection
Decreasing CO_2 fugacity ↓	Injection well	fCO_2 (bar)	1.3	49.6	49.6	1.3
		CO_2 (aq) (molal)	0.04334	1.657	1.657	0.04343
		pH (*measured*/modeled)	*7.187*/5.616	4.038	4.903	5.857
		Carbonate alkalinity (mg/kg)	1050	514	3739	1744
		HCO_3^- (molality)	0.01066	0.01077	0.07997	0.01862
	Mid-point fugacity	fCO_2 (bar)	1.3	25.6	25.6	1.3
		CO_2 (aq) (molal)	0.04273	0.8552	0.8552	0.04343
		pH (*measured*/modeled)	*6.379*/5.591	4.293	5.054	5.795
		Carbonate alkalinity (mg/kg)	795	504	2899	1264
		HCO_3^- (molality)	0.01013	0.01021	0.05919	0.01647
	Production wells (RG1-4/WT9)	fCO_2 (bar)	0.071	1.68	1.68	0.071
		CO_2 (aq) (molal)	0.01787	0.05612	0.05612	0.002372
		pH (*measured*/modeled)	*6.418*/6.053	5.558	5.765	6.515
		Carbonate alkalinity (mg/kg)	704	648	1063	332
		HCO_3^- (molality)	0.01212	0.01218	0.01962	0.004653
	Production wells (PH1/WT4)	fCO_2 (bar)	0.071	1.68	1.68	0.071
		CO_2 (aq) (molal)	0.002386	0.05612	0.05612	0.002372
		pH (*measured*/modeled)	*6.823*/6.518	5.165	5.673	6.385
		Carbonate alkalinity (mg/kg)	365	262	903	269
		HCO_3^- (molality)	0.004813	0.00503	0.01621	0.003526

Table 5.1b Variation in calculated fCO_2 during the four GWB simulation phases at different wells for Jackson formation waters in the seal rocks. Changes in fCO_2 produce changes in aqueous CO_2, HCO_3^-, carbonated alkalinity, and pH.

Sugar Creek Seal Rocks			Pre-injection	Injection Phase I	Injection Phase II	Post-injection
Decreasing CO_2 fugacity	Injection well	fCO_2 (bar)	1.3	49.6	49.6	1.3
		CO_2 (aq) (molal)	0.04334	1.657	1.657	0.04343
		pH (*measured*/modeled)	*7.187*/5.616	4.038	4.858	5.734
		Carbonate alkalinity (mg/kg)	1050	514	3378	751
		HCO_3^- (molality)	0.01066	0.01077	0.07261	0.01418
	Mid-point fugacity	fCO_2 (bar)	1.3	25.6	25.6	1.3
		CO_2 (aq) (molal)	0.04273	0.8552	0.8552	0.04343
		pH (*measured*/modeled)	*6.379*/5.591	4.293	5.002	5.700
		Carbonate alkalinity (mg/kg)	795	504	2553	713
		HCO_3^- (molality)	0.01013	0.01021	0.05277	0.01332
	Production wells (RG1-4/WT9)	fCO_2 (bar)	0.071	1.68	1.68	0.071
		CO_2 (aq) (molal)	0.01787	0.05612	0.05612	0.002338
		pH (*measured*/modeled)	*6.418*/6.053	5.558	5.651	6.365
		Carbonate alkalinity (mg/kg)	704	648	804	193
		HCO_3^- (molality)	0.01212	0.01218	0.01525	0.003283
	Production wells (PH1/WT4)	fCO_2 (bar)	0.071	1.68	1.68	0.071
		CO_2 (aq) (molal)	0.002386	0.05612	0.05612	0.002372
		pH (*measured*/modeled)	*6.823*/6.518	5.165	5.598	6.299
		Carbonate alkalinity (mg/kg)	365	262	740	187
		HCO_3^- (molality)	0.004813	0.00503	0.01365	0.002896

Table 5.2a Mineral saturation (log Q/K) values for minerals during each of the four GWB simulation phases at RG5 (injection well). GWB describes the saturation state of minerals with real numbers only for minerals with log Q/K greater than -3. Values greater than zero are super-saturated, equal to zero are at equilibrium, and less than zero are undersaturated. #Represents the saturation state for dolomite, and is a proxy for ankerite, which lakes thermodynamic data in GWB. *Denotes new minerals that precipitate in the system.

	Mineral	Pre-injection	Injection phase I	Injection phase II	Post-injection
Reservoir Rocks	Quartz	-0.0335	-0.0334	0.00	-0.2624
	Calcite	-0.8142	-2.3879	0.00	0.00
	#Dolomite	-0.7185	≤ -3.0	0.00	0.00
	Chlorite	≤ -3.0	≤ -3.0	≤ -3.0	≤ -3.0
	Pyrite	4.1414	1.4342	0.00	0.00
	K-feldspar	≤ -3.0	≤ -3.0	-2.4688	-2.4954
	Albite	≤ -3.0	≤ -3.0	-2.6519	-2.6645
	*Strontianite	1.4909	-0.0829	0.00	0.00
	*Witherite	1.1996	-0.3740	0.00	0.00
Seal Rocks	Quartz	Log Q/K values seal are the same as reservoir rocks in pre-injection and injection phase I		0.1620	0.00
	Calcite			0.00	0.00
	#Dolomite			0.00	0.00
	Chlorite			≤ -3.0	≤ -3.0
	Pyrite			0.00	0.00
	K-feldspar			-2.1535	-1.5740
	Albite			0.00	0.00
	Barite	≤ -3.0	≤ -3.0	-2.4219	-2.2773
	Illite	≤ -3.0	≤ -3.0	-2.2207	-2.1989
	Kaolinite	≤ -3.0	≤ -3.0	0.8486	0.00
	Gypsum	≤ -3.0	≤ -3.0	0.00	-0.0608

Table 5.2b Mineral saturation (log Q/K) values for minerals during each of the four GWB simulation phases at the mid-fugacity. GWB describes the saturation state of minerals with real numbers only for minerals with log Q/K greater than -3. Values greater than zero are super-saturated, equal to zero are at equilibrium, and less than zero are undersaturated. #Represents the saturation state for dolomite, and is a proxy for ankerite, which lakes thermodynamic data in GWB. *Denotes new minerals that precipitate in the system.

	Mineral	Pre-injection	Injection phase I	Injection phase II	Post-injection
Reservoir Rocks	Quartz	-0.0161	-0.0160	0.0674	-0.2636
	Calcite	-0.6982	-1.9930	-0.00	0.00
	#Dolomite	-0.4730	≤ -3.0	0.00	0.00
	Chlorite	≤ -3.0	≤ -3.0	≤ -3.0	≤ -3.0
	Pyrite	7.3726	5.1529	0.00	0.00
	K-feldspar	-0.2828	≤ -3.0	-2.1312	-2.3791
	Albite	-0.4389	≤ -3.0	-2.3254	-2.5641
	*Strontianite	1.6014	0.3065	0.00	0.00
	*Witherite	1.1654	-0.1293	0.00	0.00
Seal Rocks	Quartz	Log Q/K values seal are the same as reservoir rocks in pre-injection and injection phase I		0.1620	0.00
	Calcite			0.00	0.00
	#Dolomite			0.0001	0.00
	Chlorite			≤ -3.0	≤ -3.0
	Pyrite			0.0001	0.00
	K-feldspar			-1.5881	-1.5566
	Albite			-2.1014	-2.1428
	Barite	≤ -3.0	≤ -3.0	0.00	0.00
	Illite	1.7514	≤ -3.0	-1.8060	-2.1868
	Kaolinite	3.6657	-2.4096	0.8509	0.00
	Gypsum	≤ -3.0	≤ -3.0	-0.0002	-0.0473

Table 5.2c Mineral saturation (log Q/K) values for minerals during each of the four GWB simulation phases at RG1-4/WT9. GWB describes the saturation state of minerals with real numbers only for minerals with log Q/K greater than -3. Values greater than zero are super-saturated, equal to zero are at equilibrium, and less than zero are undersaturated. #Represents the saturation state for dolomite, and is a proxy for ankerite, which lakes thermodynamic data in GWB. *Denotes new minerals that precipitate in the system.

	Mineral	Pre-injection	Injection phase I	Injection phase II	Post-injection
Reservoir Rocks	Quartz	-0.0069	-0.0066	0.0653	-0.2628
	Calcite	-0.2609	-0.7540	0.00	0.00
	#Dolomite	0.3794	-0.6067	0.00	0.00
	Chlorite	≤ -3.0	≤ -3.0	≤ -3.0	≤ -3.0
	Pyrite	8.5326	7.7624	0.00	0.00
	K-feldspar	0.3720	-0.4237	-1.4830	-1.7138
	Albite	0.1676	-0.6281	-1.7202	-1.9482
	*Strontianite	2.2388	1.7457	0.00	0.00
	*Witherite	1.6652	1.1721	0.00	0.00
Seal Rocks	Quartz	Log Q/K values seal are the same as reservoir rocks in pre-injection and injection phase I		0.1620	0.00
	Calcite			-0.00	0.00
	#Dolomite			0.00	0.00
	Chlorite			≤ -3.0	≤ -3.0
	Pyrite			0.0001	0.00
	K-feldspar			-1.4575	-0.9574
	Albite			-1.5688	-1.5873
	Barite	≤ -3.0	≤ -3.0	0.00	0.00
	Illite	2.7447	1.5077	-1.4559	-1.5113
	Kaolinite	4.1399	3.5375	0.8240	0.00
	Gypsum	≤ -3.0	≤ -3.0	-0.00	-0.0340

Table 5.2d Mineral saturation (log Q/K) values for minerals during each of the four GWB simulation phases at PH1/WT4. GWB describes the saturation state of minerals with real numbers only for minerals with log Q/K greater than -3. Values greater than zero are super-saturated, equal to zero are at equilibrium, and less than zero are undersaturated. #Represents the saturation state for dolomite, and is a proxy for ankerite, which lakes thermodynamic data in GWB. *Denotes new minerals that precipitate in the system.

	Mineral	Pre-injection	Injection phase I	Injection phase II	Post-injection
Reservoir Rocks	Quartz	0.0227	0.0251	0.0425	0.00
	Calcite	0.0624	-1.2709	-0.00	0.00
	#Dolomite	1.1182	-1.5484	0.00	0.00
	Chlorite	≤ -3.0	≤ -3.0	≤ -3.0	≤ -3.0
	Pyrite	10.4092	8.4131	-0.00	0.00
	K-feldspar	1.2253	-1.0182	-1.4549	-1.0543
	Albite	1.1143	-1.1292	-1.5235	-1.1808
	*Strontianite	1.9332	0.5998	0.00	0.00
	*Witherite	1.7706	0.4374	0.00	0.00
Seal Rocks	Quartz	Log Q/K values seal are the same as reservoir rocks in pre-injection and injection phase I		0.1620	0.00
	Calcite			-0.00	0.00
	#Dolomite			0.0001	0.00
	Chlorite			≤ -3.0	≤ -3.0
	Pyrite			-0.00	0.00
	K-feldspar			-1.2894	-0.9650
	Albite			-1.3298	-1.2747
	Barite	≤ -3.0	≤ -3.0	-0.00	0.00
	Illite	3.6660	0.1206	-1.4991	-1.5120
	Kaolinite	4.2357	2.4438	0.6484	0.00
	Gypsum	≤ -3.0	≤ -3.0	-0.00	-0.0219

Table 5.3a Simulated mineral precipitation and dissolution for reservoir rocks. Positive values are precipitation and negative equal dissolution. *Represents dolomite and ankerite. Abbreviations: “nc” equals no change in mass or volume and “na” indicates mineral did not precipitate for simulation.

Starting Reservoir Minerals		Injection Step II		Post-Injection	
		Mass (g)	Volume (cm^3)	Mass (g)	Volume (cm^3)
Calcite	RG5	-5.42	2.0	3.57	1.32
	Mid-point	-5.49	2.0	2.62	0.97
	RG1-4/WT9	-2.33	0.86	0.83	0.31
	PH1/WT4	-5.34	1.97	0.88	0.33
*Dolomite	RG5	0.41	0.14	0.56	0.20
	Mid-point	1.38	0.48	0.39	0.14
	RG1-4/WT9	1.15	0.4	0.13	0.04
	PH1/WT4	3.82	1.33	0.12	0.04
Quartz	RG5	0.08	0.03	nc	nc
	Mid-point	0.08	0.03	nc	nc
	RG1-4/WT9	0.08	0.03	nc	nc
	PH1/WT4	0.05	0.02	<-0.01	<-0.01
K-feldspar	RG5	<-0.01	<0.01	nc	nc
	Mid-point	<-0.01	<0.01	nc	nc
	RG1-4/WT9	<-0.01	<0.01	nc	nc
	PH1/WT4	<-0.01	<0.01	nc	nc
Albite	RG5	-0.1	0.04	nc	nc
	Mid-point	-0.1	0.04	nc	nc
	RG1-4/WT9	-0.09	0.04	nc	nc
	PH1/WT4	-0.09	0.04	nc	nc
Illite	RG5	-0.01	0.01	nc	nc
	Mid-point	-0.01	0.01	nc	nc
	RG1-4/WT9	-0.01	<0.01	nc	nc
	PH1/WT4	-0.01	<0.01	nc	nc
Kaolinite	RG5	<0.01	<0.01	<0.01	<0.01
	Mid-point	<0.01	<0.01	<0.01	<0.01
	RG1-4/WT9	<0.01	<0.01	<0.01	<0.01
	PH1/WT4	<0.01	<0.01	0.07	0.03
Chlorite	RG5	-0.01	0.01	nc	nc
	Mid-point	-0.01	0.01	nc	nc
	RG1-4/WT9	-0.01	0.01	nc	nc
	PH1/WT4	-0.01	0.01	nc	nc
Pyrite	RG5	<0.01	<0.01	<0.01	<0.01
	Mid-point	<0.01	<0.01	<0.01	<0.01
	RG1-4/WT9	<0.01	<0.01	<0.01	<0.01
	PH1/WT4	0.01	0.01	<0.01	<0.01

Table 5.3b New minerals precipitated in response to CO_2 injection and not part of the original reservoir mineralogy in reservoir rocks. Abbreviations: “nc” equals no change in mass or volume and “na” indicates mineral did not precipitate for simulation.

Starting Reservoir Minerals		CO_2-Injection phase II		Post-CO_2 Injection	
		Mass (g)	Volume (cm^3)	Mass (g)	Volume (cm^3)
Gibbsite	RG5	0.04	0.02	0.03	0.01
	Mid-point	0.04	0.02	0.03	0.01
	RG1-4/WT9	0.04	0.02	0.03	0.01
	PH1/WT4	na	na	na	na
Strontianite	RG5	0.46	0.12	0.47	0.13
	Mid-point	0.79	0.21	0.8	0.21
	RG1-4/WT9	0.92	0.24	0.92	0.24
	PH1/WT4	0.5	0.13	0.5	0.13
Witherite	RG5	<0.01	<0.01	<0.01	<0.01
	Mid-point	<0.01	<0.01	<0.01	<0.01
	RG1-4/WT9	<0.01	<0.01	<0.01	<0.01
	PH1/WT4	<0.01	<0.01	<0.01	<0.01
Siderite	PH1/WT4	0.03	0.01	0.04	0.01

Table 5.3c Simulated mineral precipitation and dissolution for seal rocks. Positive values are precipitation and negative equal dissolution. *Represents dolomite and ankerite. Abbreviations: “nc” equals no change in mass or volume and “na” indicates mineral did not precipitate for simulation.

Starting Seal Minerals		CO_2-Injection phase II		Post-CO_2 Injection	
		Mass (g)	Volume (cm^3)	Mass (g)	Volume (cm^3)
Calcite	RG5	2.27	0.84	3.2	1.18
	Mid-point	0.97	0.36	2.32	0.86
	RG1-4/WT9	-1.42	0.52	0.7	0.26
	PH1/WT4	-4.6	1.7	0.81	0.3
Dolomite*	RG5	0.18	0.06	0.51	0.18
	Mid-point	1.12	0.39	0.35	0.12
	RG1-4/WT9	0.73	0.26	0.11	0.04
	PH1/WT4	3.42	1.20	0.11	0.04
Quartz	RG5	0.16	0.06	-0.09	0.03
	Mid-point	0.16	0.06	-0.08	0.03
	RG1-4/WT9	0.16	0.06	-0.07	0.03
	PH1/WT4	0.16	0.06	-0.07	0.03
K-feldspar	RG5	-0.14	0.05	nc	nc
	Mid-point	-0.13	0.05	nc	nc
	RG1-4/WT9	-0.13	0.06	nc	nc
	PH1/WT4	-0.13	0.05	nc	nc
Albite	RG5	-0.2	0.08	nc	nc
	Mid-point	-0.2	0.08	nc	nc
	RG1-4/WT9	-0.2	0.08	nc	nc
	PH1/WT4	-0.19	0.07	nc	nc
Illite	RG5	-0.48	0.18	nc	nc
	Mid-point	-0.48	0.17	nc	nc
	RG1-4/WT9	-0.47	0.17	nc	nc
	PH1/WT4	-0.47	0.17	nc	nc
Kaolinite	RG5	0.01	0.01	0.55	0.21
	Mid-point	0.01	<0.01	0.54	0.21
	RG1-4/WT9	0.01	<0.01	-0.45	0.17
	PH1/WT4	<0.01	<0.01	-0.36	0.14
Chlorite	RG5	-0.05	0.02	nc	nc
	Mid-point	-0.05	0.02	nc	nc
	RG1-4/WT9	<-0.01	<-0.01	nc	nc
	PH1/WT4	-0.05	0.02	nc	nc
Gypsum	RG5	-16.84	7.31	<-0.01	<-0.01
	Mid-point	-11.97	5.19	-0.03	0.01
	RG1-4/WT9	-6.29	2.73	nc	nc
	PH1/WT4	-7.56	3.28	nc	nc

Table 5.3d New minerals precipitated in response to CO_2 injection and not part of the original mineralogy in seal rocks. Abbreviations: “nc” equals no change in mass or volume and “na” indicates mineral did not precipitate for simulation.

New Seal Minerals		CO_2-injection phase II		Post-CO_2 injection phase	
		Mass (g)	**Volume (cm^3)**	**Mass (g)**	**Volume (cm^3)**
Gibbsite	RG5	0.08	0.03	nc	nc
	Mid-point	0.25	0.1	nc	nc
	RG1-4/WT9	na	na	na	na
	PH1/WT4	na	na	na	na
Strontianite	RG5	0.46	0.12	0.47	0.12
	Mid-point	0.78	0.21	0.79	0.21
	RG1-4/WT9	0.91	0.24	0.91	0.24
	PH1/WT4	0.49	0.13	0.5	0.13
Barite	RG5	<0.01	<0.01	<0.01	<0.01
	Mid-point	<0.01	<0.01	<0.01	<0.01
	RG1-4/WT9	<0.01	<0.01	<0.01	<0.01
	PH1/WT4	<0.01	<0.01	<0.01	<0.01
Alunite	RG5	0.45	0.32	nc	nc
	Mid-point	0.13	0.09	nc	nc
	RG1-4/WT9	na	na	na	na
	PH1/WT4	na	na	na	na

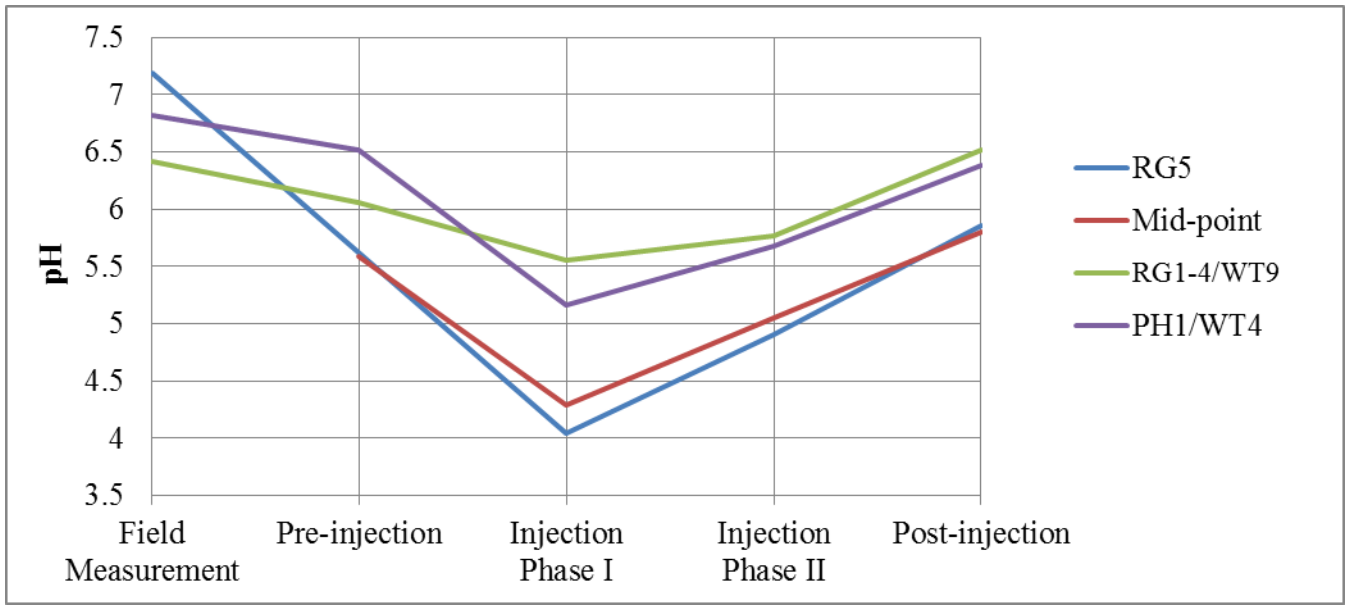

Figure 5.1 pH versus GWB simulation phase for the Jackson reservoir rocks. The pH response within the seal rocks (not shown) follows an identical pattern to the pH change within the reservoir rocks for the first two simulation phases. For the final two phases, the pH in the seal rocks is slightly less than in the reservoir rocks at each of the well locations (Tables 5.1a, 5.1b).

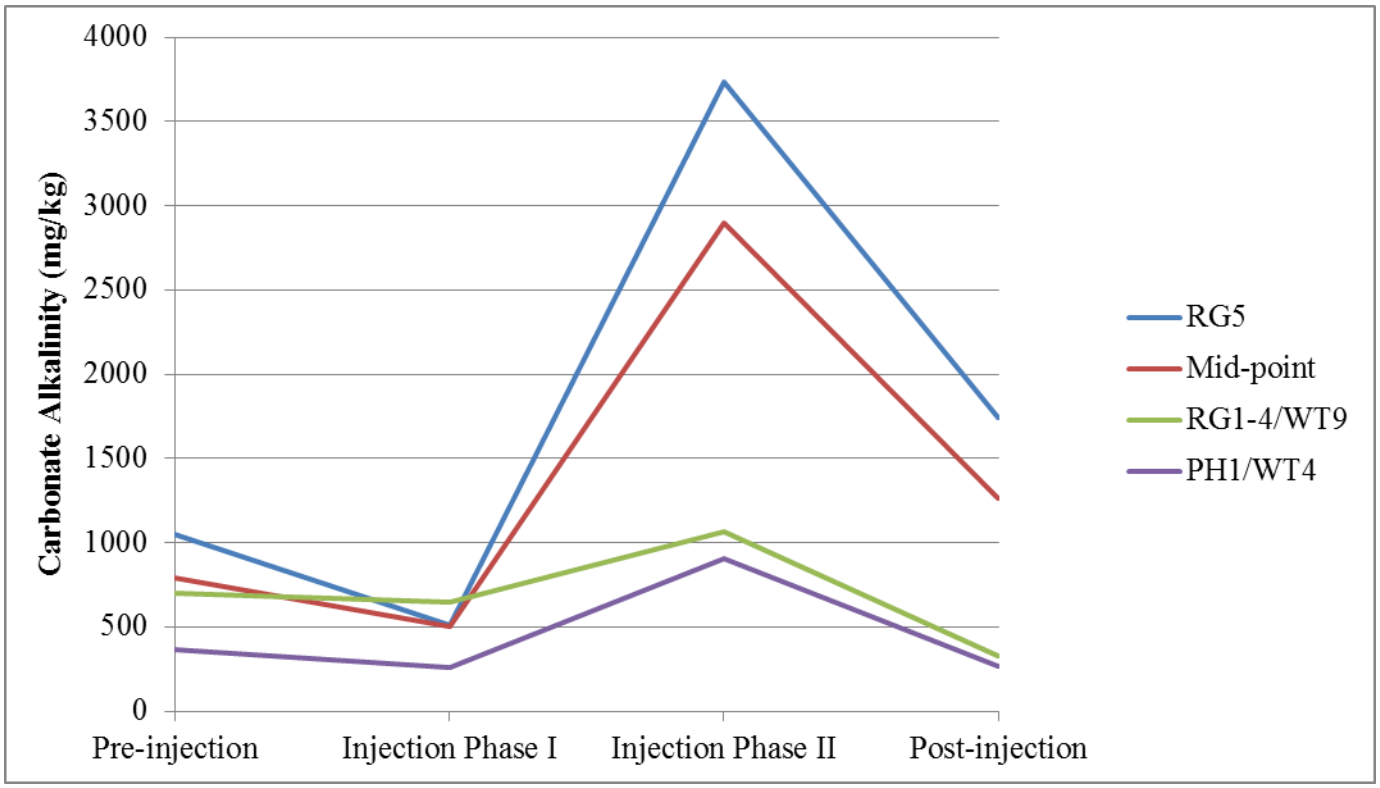

Figure 5.2 Carbonate alkalinity (mg/kg) versus GWB simulation phase for the Jackson reservoir rocks. The carbonate alkalinity response within the seal rocks (not shown) follows an identical pattern to the change within the reservoir rocks for the first two simulation phases. For the final two phases, the carbonate alkalinity in the seal rocks is less than in the reservoir rocks at each of the well locations (Tables 5.1a, 5.1b).

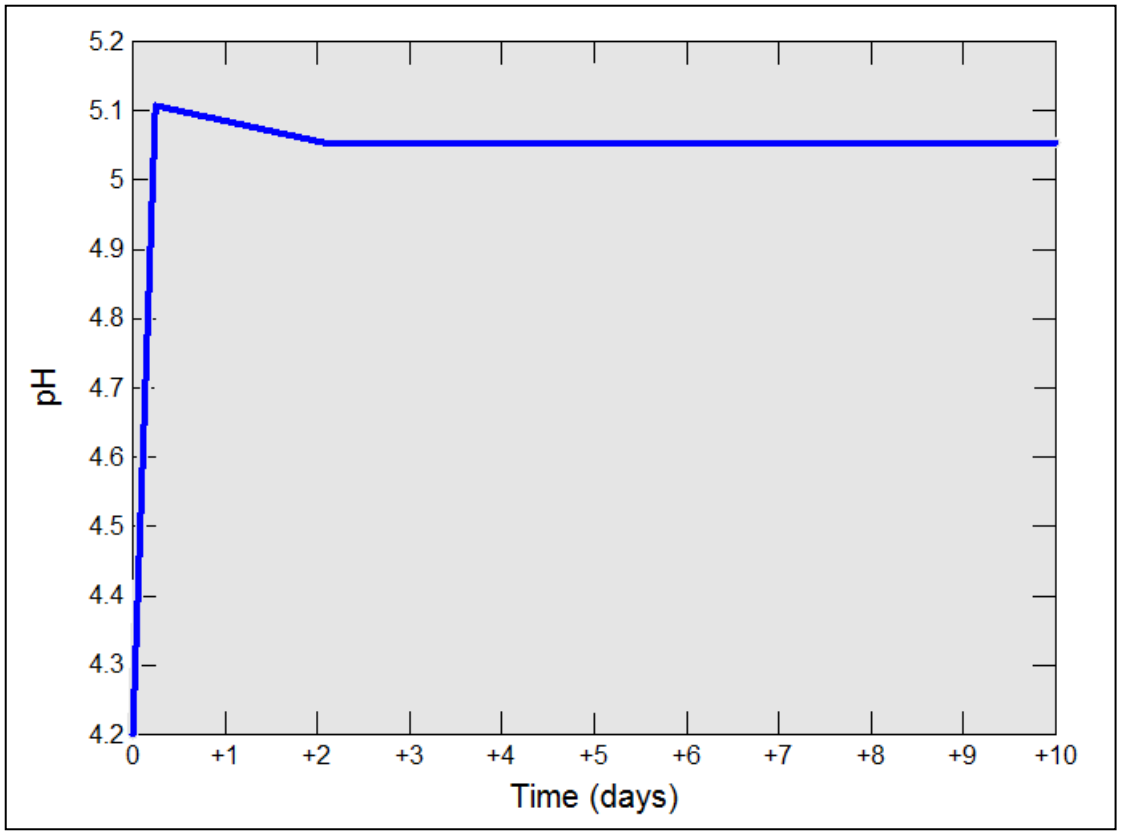

Figure 5.3 pH versus time for mid-fugacity during the CO_2 injection phase II when kinetic minerals were titrated into the system. The model predicts a very rapid pH increase and a similar plot for carbonate alkalinity as well.

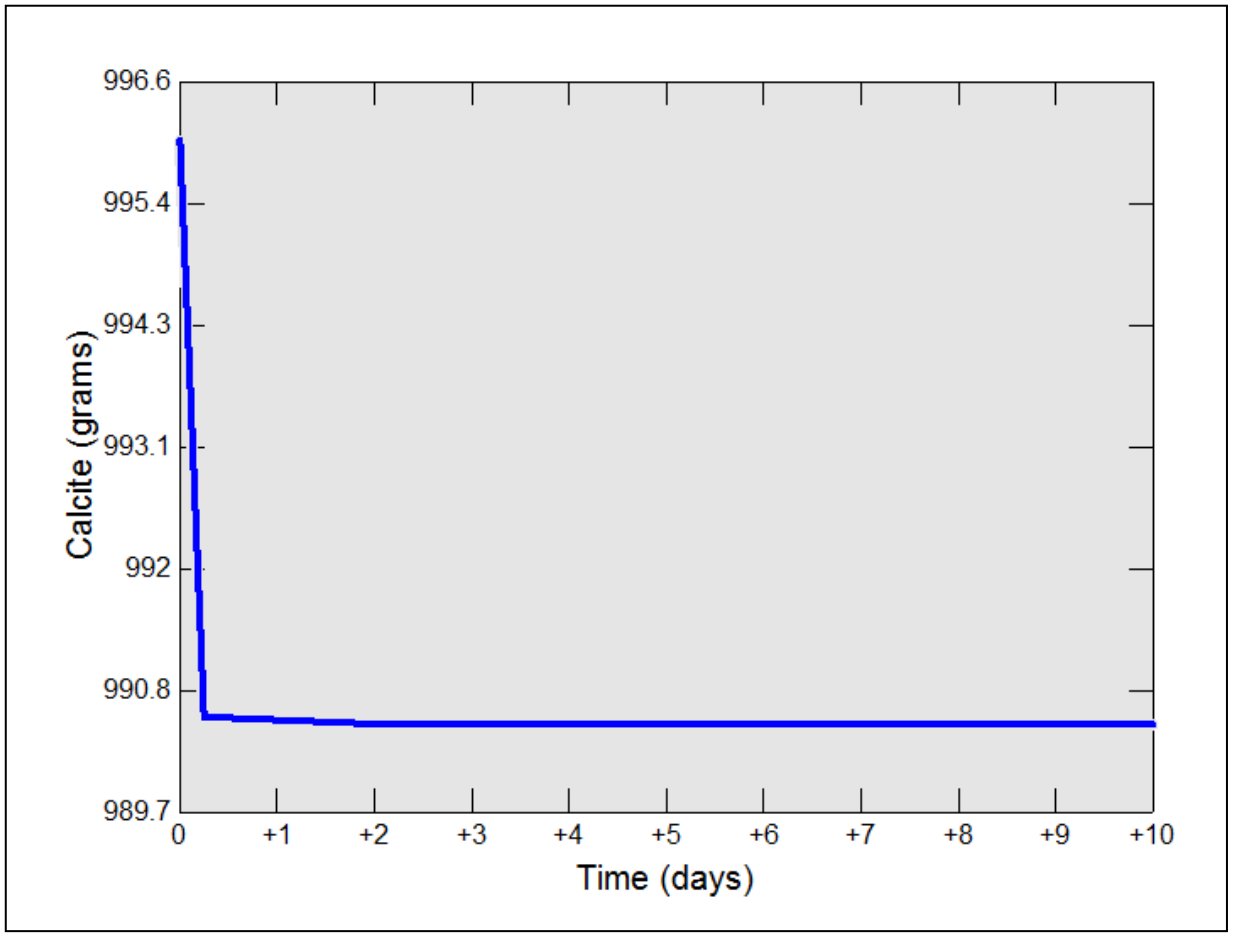

Figure 5.4 Mass of calcite versus time for the mid-fugacity showing the rapid calcite dissolution during the CO_2 injection phase II when kinetic minerals were titrated into the system. The model predicts the dissolution of approximately 5.5 grams of calcite.

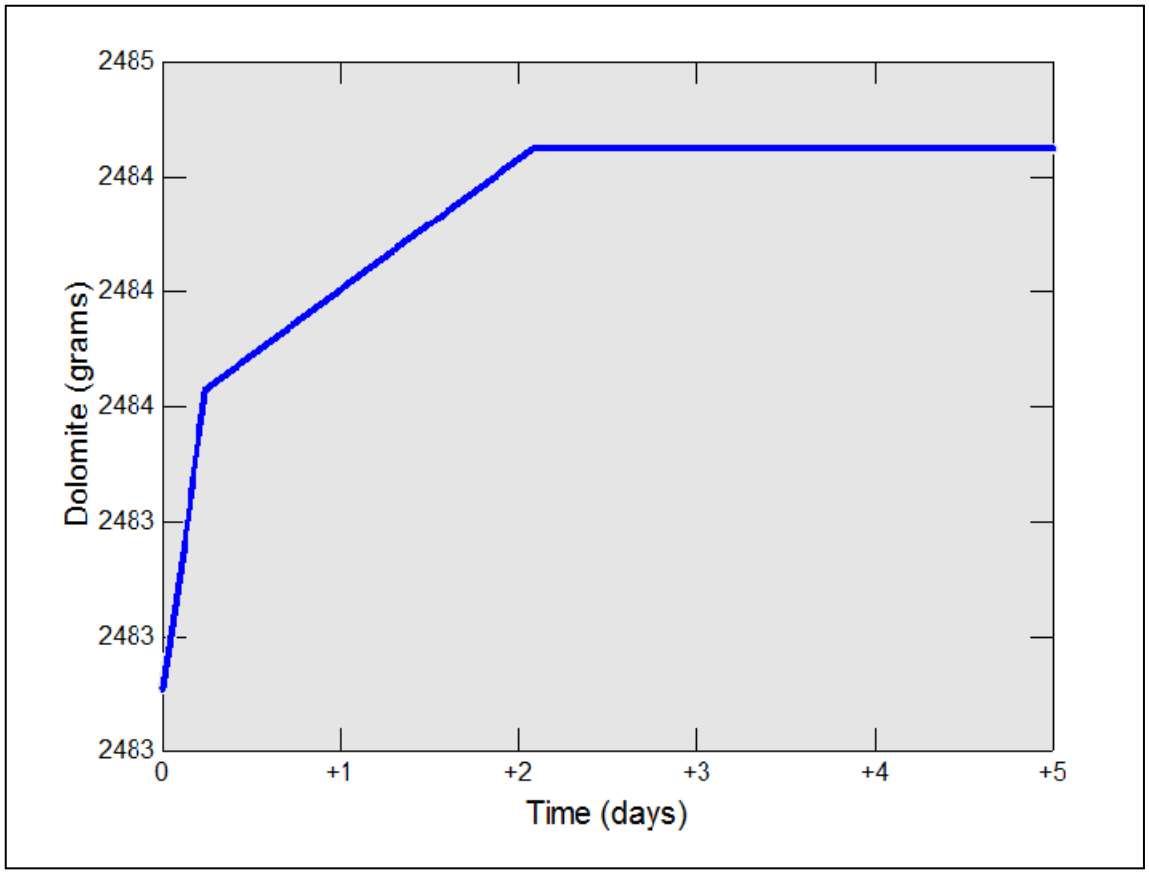

Figure 5.5 Mass of dolomite versus time at the mid-fugacity showing the rapid precipitation of dolomite during CO_2 injection phase II when kinetic minerals were titrated into the system. The model predicts the precipitation of approximately 1.4 grams of dolomite.

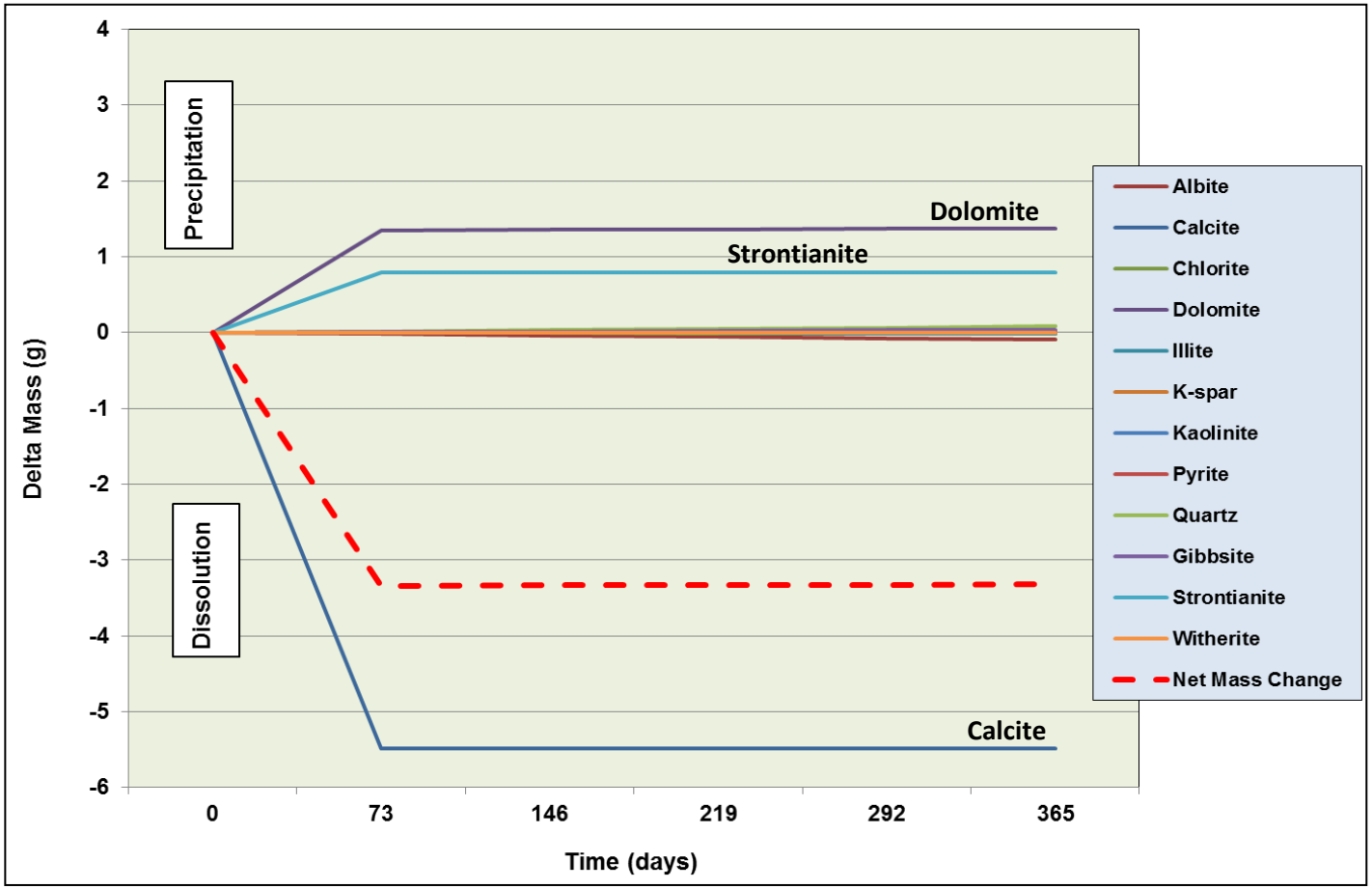

Figure 5.6 Change in mass (delta mass) versus time in days for reservoir rocks at the mid-point fugacity during CO_2 injection phase II. The model shows dissolution of calcite and precipitation of dolomite-ankerite and strontianite. The magnitude and rates of mass change associated with carbonates far exceeds those for alumino-silicate minerals (lines with low gradient slopes near the zero delta mass axis). The magnitude of calcite dissolution exceeds precipitation for all carbonate and alumino-silicate minerals leading to net dissolution. Mass changes for other simulation scenarios follow a similar pattern (Tables 5.3a, b).

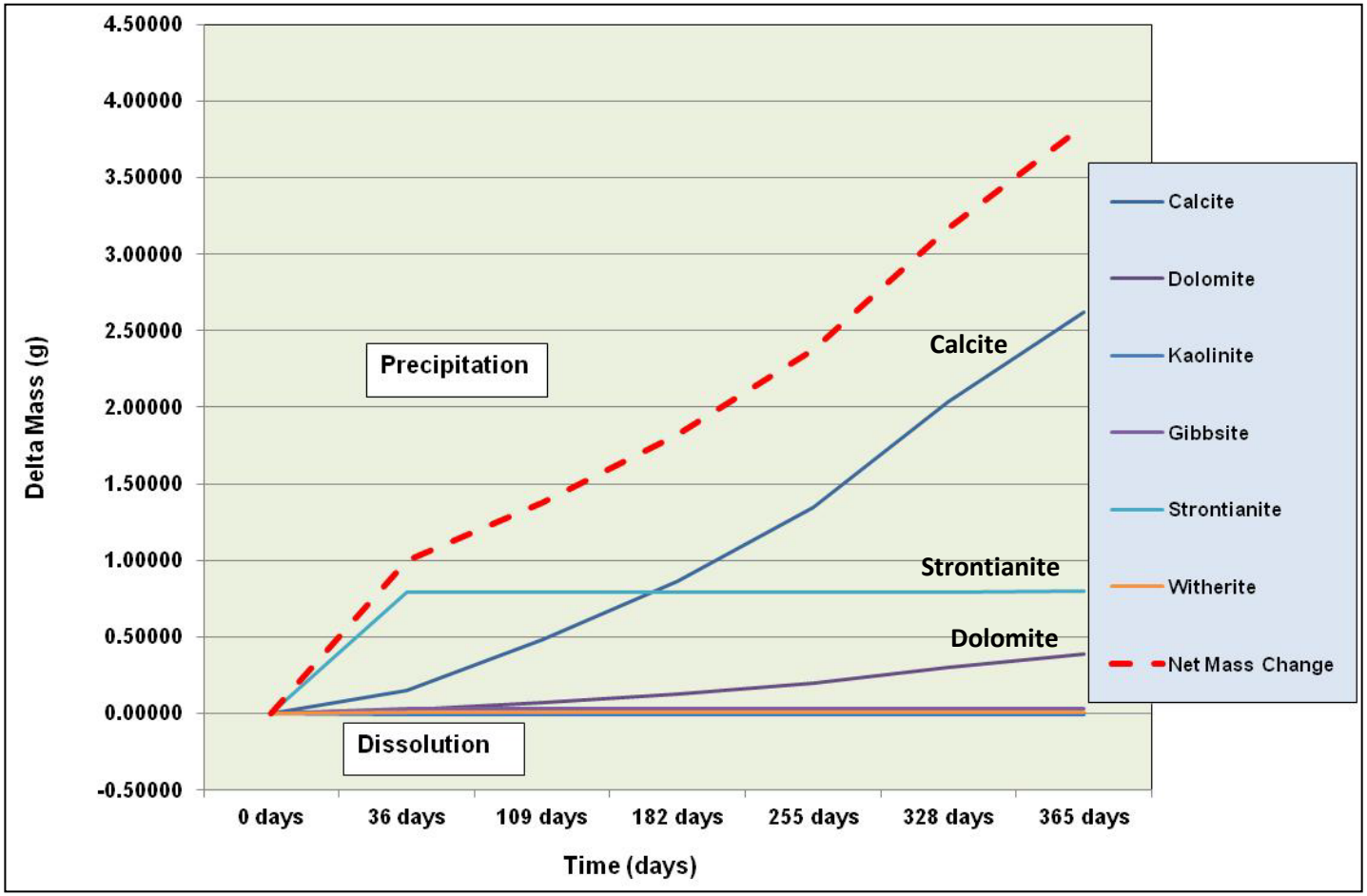

Figure 5.7 Example of change in mass (delta mass) versus time for reservoir rocks at the mid-point fugacity during the post-CO_2 injection phase. The model shows net precipitation as controlled by precipitation of calcite, dolomite and strontianite. As in Figure 5.6, the magnitude and rates of mass change associated with carbonates far exceeds those for alumino-silicate minerals (lines with low gradient slopes near the zero delta mass axis). Mass changes for other simulation scenarios follow a similar pattern (Tables 5.3a, b).

Chapter 6: GWB Modeling Discussion

The simulations completed in this study were conducted under conditions of constant temperature and constant starting mineralogy for the reservoir and seal rocks at each of the four well locations. Therefore, the main variable that influences the types and magnitudes of geochemical subsurface interactions is the variation of fCO_2 to simulate the phases of CO_2 injection. An additional variable that influences geochemical reactions within this study is the variation in formation water chemistry among the wells before CO_2 injection occurred. An examination of how these variables affects water chemistry, mineral saturation, mineral reactions, and porosity is discussed in this section.

As previously noted, water injection of the more dilute, $NaHCO_3$-rich, Pennsylvanian water from WT3 into the reservoir during the water flood results in formation water that is more dilute at RG5, RG1-4, WT9 as compared to PH1, WT4, which are unaffected by the flood (Table 4.1a, Figure 4.3). The PH1, WT4 wells are used as representative of pristine Jackson formation water, and the results provide insight into possible reactions in a Mississippian oil reservoir that was not previously water flooded. This difference in pre-CO_2 aqueous chemistry among the wells affects several variables and is the justification for having distinct simulations for two sets of production wells within the reservoir and seal rocks. For example, the injected $NaHCO_3$-rich Pennsylvanian water explains why higher alkalinities are associated with RG5 and RG1-4, WT9. Additionally, the formation waters from PH1, WT4 have over double the amount of calcium and magnesium as compared to RG1-4, WT9. The elevated amount of carbonate mineral-forming ions in solution at PH1, WT4 indicates a greater potential buffering capacity during CO_2 injection, which will be discussed later on. The dilution of

the Jackson formation water also produces greater degrees of undersaturation, especially for alumino-silicate minerals and carbonates, at RG5, while alumino-silicates and carbonates are slightly saturated and super-saturated at RG1-4, WT9 and PH1, WT4, respectively. Pyrite is super-saturated at all well locations, especially PH1, WT4, likely as a direct result of an anomalously high iron concentration before CO_2 was injected.

For the CO_2 injection phase I simulation it is important to discuss the relationship between pH and changes in fCO_2. Recall that in order to simulate CO_2 injection, fCO_2 is increased, which can be described using following dissociation reaction that produces H^+ ions:

$$CO_2\ (g) \leftrightarrow CO_2\ (aq)$$

$$CO_2\ (aq) + H_2O \leftrightarrow H_2CO_3$$

$$H_2CO_3 \leftrightarrow H^+ + HCO_3^-$$

$$HCO_3^- \leftrightarrow H^+ + CO_3^{-2}$$

The pH is a measure of the H^+ ions in the formation water, so by increasing fCO_2 and aqueous CO_2 during injection phase I, the pH decreases. The rate of pH decrease is rapid early on, and the rate declines with successively higher fCO_2 and aqueous CO_2 values (Figure 5.1). The more gradual pH decrease as fCO_2 increases likely reflects the reaction of H^+ ions and HCO_3^- to produce H_2O and CO_2 (aq):

$$H^+ + HCO_3^- \leftrightarrow CO_2\,(aq) + H_2O.$$

When pH versus reaction progress is examined for each well simulation, none show any significant slope breaks that could be attributed to significant buffering reactions during injection phase I because there are no kinetic minerals included in the system yet. The decrease in alkalinity during injection phase I probably reflects the

consumption of the aqueous HCO_3^- species (the predominant carbonate species at lower pH) due to the previously described reaction with H^+ to form aqueous CO_2 and H_2O. In addition, the concentrations of acetate (CH_3COO), which also contributes to alkalinity, are reduced as acetic acid (HCH_3COO) forms:

$$CH_3COO + H^+ = HCH_3COO.$$

The decrease in alkalinity during injection phase I probably reflects the reaction of HCO_3^- (the predominant carbonate species at lower pH) with H^+ to form CO_2(aq) and H_2O. In addition, CO_3^{-2} and CH_3COO^- (acetate) were also consumed (Figure 6.1) in buffering reactions, with the latter demonstrated by:

$$CH_3COO^- + H^+ = HCH_3COO.$$

Over the simulated pH range, the concentration of aqueous HCO_3^- species was typically one- to two-orders of magnitude greater than CO_3^{-2} and two- to four-orders greater than CH_3COO^-. The previously described pattern of decreased CO_3^{-2}, HCO_3^- and CH_3COO (hence decreased alkalinity), and increased CO_2(aq) and HCH_3COO is similar among all the well simulations with increased fCO_2. The effects of the varying pre-CO_2 injection formation water chemistries are evidenced during injection phase I as well. For example, when fCO_2 is increased to 1.68 bars at the production wells, the result was a greater pH decrease at PH1, WT4 versus RG1-4, WT9 (Tables 5.1a, b). The greater decrease in pH is almost certainly due to the lower alkalinity (and decreased ability to buffer pH) before CO_2 injection at PH1, WT4.

As the kinetic minerals are titrated in and fCO_2 is held constant for the yearlong CO_2 injection phase II, a more effective buffering system is observed and thus represents a more realistic depiction of the aggregate formation water and mineral system. Increases

in pH and carbonate alkalinity at all wells in association with mineral titration underscored the importance of mineral reactions in buffering the formation water in both the reservoir and seal rocks. Analysis of mass changes (Tables 5.3a-d) show that calcite dissolution occurs within day of mineral titration (Figure 5.4) and is largely responsible for buffering, according to the reaction:

$$CaCO_3 + H^+ = Ca^{+2} + HCO_3^-.$$

It is likely that the calcite dissolution also drives the precipitation of both dolomite (Figure 5.5) and strontianite in all the wells. The precipitation of carbonate minerals indicates mineral trapping of CO_2, but the mass of calcite dissolving is greater and causes a net dissolution (Figure 5.6) in the reservoir and seal rocks for all of the well simulations. This suggests that precipitation of these carbonates, despite low pH, is driven by increases in Ca^{+2} and HCO_3^- to varying degrees at all wells, again as a result of differences in formation water chemistry from pre-CO_2 injection. General reactions for precipitation of dolomite and strontianite, respectively, are:

$$Ca^{+2} + Mg^{+2} + 2HCO_3^- = CaMg(CO_3)_2 + 2H^+$$

$$Sr^{+2} + HCO_3^- = SrCO_3 + H^+.$$

It is important to note, however, that ankerite ($CaFe(CO_3)_2$) makes up a significant portion of the carbonate mass in many of the reservoir and seal rock samples. Despite this, ankerite is not included as a mineral in the simulation because thermodynamic data for equilibrium values and kinetic data for reaction rates are lacking for GWB. Consequently, dolomite, which actually represents a smaller part of the carbonate fraction, is used as a proxy for ankerite. Justification for doing this is because ankerite is isostructural with dolomite and the two minerals form a complete solid solution series

(Nesse, 2000). Therefore, it is possible that ankerite precipitation might occur in addition to dolomite for the well simulations during injection phase II in the reservoir and seal rocks.

Analysis of the saturation indices indicate that the formation water is undersaturated with respect to illite, K-feldspar, and albite at the beginning of CO_2 injection phase II at all of the wells in both the reservoir and seal rocks. The undersaturation results in the dissolution of these minerals over the yearlong kinetic mineral titration period. The mass changes (Tables 5.3a-d) show that most dissolution is associated with albite and smaller amounts of K-feldspar, illite, and chlorite (Figure 6.2). The amount of precipitated quartz and gibbsite suggests that these are largely reaction products from albite dissolution in accordance with the general reaction:

$$2NaAlSi_3O_8 \text{ (albite)} + 8H_2O + 2H^+ =$$

$$2Al(OH)_3 \text{ (gibbsite)} + 4Na^+ + 4H_4SiO_4 \text{ (quartz)}.$$

If albite were the only alumino-silicate mineral affected by dissolution, then the mass units dissolved and precipitated could be estimated using the slope-of-line methods in GWB (Bethke, 2008). This is not the case, however, as dissolution of K-feldspar, illite, and chlorite potentially produce some of the same reaction products. Thus, the analysis is restricted to general reactions only, for example:

$$2NaAlSi_3O_8 \text{ (albite)} + 9H_2O + 2H^+ =$$

$$Al_2Si_2O_5(OH)_4 \text{ (kaolinite)} + 4Na^+ + 4H_4SiO_4 \text{ (quartz)}.$$

Despite the number of possible reactions, the overall mass involved in the alumino-silicate reactions is so small (less than 1 gram), due to slow reaction rates (White and Brantley, 1995; Brantley, 2008). Consequently, the formation water in the reservoir and

seal rocks remains undersaturated with respect to the alumino-silicates at the end of CO_2 injection phase II (Tables 5.2a-d).

Recall that the post-CO_2 injection phase at Sugar Creek represents a sliding fCO_2 model in which fCO_2 is reduced back down to pre-CO_2 injection values. Decreasing the fCO_2 causes the pH to increase at all the well locations for both the reservoir and seal rocks, although at differing magnitudes due to the spatial fCO_2 variation and starting formation water chemistry variation among the wells. Analysis of aqueous carbon species for this phase shows that most alkalinity is accounted for by HCO_3^- species. Mass changes for all the well simulations in the reservoir and seal rocks (Tables 5.3a-d) show that the decreased alkalinity can largely be attributed to the removal of HCO_3^- through precipitation of calcite, strontianite, and dolomite (ankerite). Further examination, however, shows no mass changes for most of the alumino-silicate minerals. The reason for this absence represents a limitation of the post-CO_2 injection phase, in which minerals could not be included as reactants. To circumvent this issue, the carbonate minerals are substituted into the basis (e.g. calcite for Ca^{+2}), while the alumino-silicate minerals not in equilibrium with the formation water at the end of CO_2 injection were not substituted into the basis. As discussed in the analysis of mineral precipitation for CO_2-injection phase II, the alumino-silicate reactions might not be important from a mass perspective, but some dissolution of feldspars, illite, and chlorite would likely continue in the post-CO_2 injection phase since they remain undersaturated at all of the wells. Modeling with a sliding-fugacity model without explicitly addressing the alumino-silicate interactions therefore does not provide a complete representation of mass changes in the post-CO_2 injection phase. Though mass changes through dissolution or precipitation of alumino-

silicates might be small, they might have significant effects, especially in the seal rock where porosity is low.

The overall analysis of GWB model predictions for each of the four phases shows numerous similarities between the seal and reservoir rocks. Changes observed in reservoir rocks are mimicked by seal rocks; however, the magnitude of each change is not necessarily equal due to the different starting mineral assemblages. Similarly, changes observed at the injection well, mid-fugacity, and production wells (RG1-4, WT9 and PH1, WT4) all follow a similar pattern, although at different magnitudes as a direct result of the water flood effects on starting formation water chemistry. It should be noted that the GWB model initially predicts the following suite of minerals to precipitate throughout each of the four simulations: dawsonite, dolomite-ord, and dolomite-dis. On a geologic basis, however, a determination was made that they are all unlikely to precipitate under these reservoir conditions within such a short injection time scale. Consequently, they have been suppressed within the system and not allowed to precipitate at all. Several other minerals, including alunite and graphite, are also predicted to precipitate during the modeling process but have been ignored due to the unlikelihood of their occurrence within the reservoir conditions.

6.1 Porosity Effects

Because carbonate reactions account for the greatest changes in mass and volume within the reservoir and seal rocks at the well locations, they also have the greatest influence on porosity. To determine the effects of these geochemical reactions have on porosity, the total change in porosity must be determined. To do that, the total change in

mineral volume is divided by the total volume of the reservoir and seal, respectively. Using the mass change results from the final two phases (CO_2 injection phase II and post-CO_2 injection phase) gives a change in porosity of less than one percent in both the reservoir and seal rocks (Table 6.1). There is a net dissolution and net precipitation within the reservoir rocks during CO_2 injection phase II and post-CO_2 injection phase, respectively. This means that porosity is created during mineral titration whereas the minerals precipitating in the final phase of simulation causes porosity to decrease. In the seal rocks there is a decrease in porosity for both of the aforementioned phases. However, such a minimal change would have negligible effects on both seal integrity and ability to prevent the upward migration of CO_2.

6.2 Model Predictions versus Field Measurements

The monitoring program before, during, and after CO_2 injection pilot project at Sugar Creek allows the opportunity for a comparison between GWB predictions and actual field data. The discrepancy between the measured pH values and the model's pH predictions during the pre-CO_2 injection phase likely represents field error. Although all precautions were taken to avoid contact between the atmosphere and the sampled formation water, sample degassing was unavoidable. Pressure decreased as the sample was brought from the reservoir to the surface, and as a result the concentration of CO_2 (and acidity of the water) decreased. Therefore, the model's prediction for starting pH of the formation water (e.g. 5.62 at RG5) with a concentration of 3.5% CO_2 might be a closer representation than the measured value from the field (e.g. 7.19 at RG5).

During CO_2 injection, the pH decrease (approximately 1 pH unit) occurred very close to the time of CO_2 breakthrough at wells affected by the water flood. One limitation of injection phase II is that the kinetic minerals are titrated into CO_2-rich, low-pH formation water so that reactions start immediately. This results, for example, in the carbonates reacting within days of the mineral titration. The field measurements do reveal a rapid increase in concentrations of Ca^{+2}, Mg^{+2}, Sr^{+2} and Fe^{+2}, which suggests carbonate dissolution and solubility trapping within the reservoir. However, the dissolution occurs within weeks and months as opposed to instantaneously (Frailey *et al.*, 2012). Therefore, the GWB model for injection phase II likely overestimates the degree of geochemical interactions within the reservoir and seal rocks.

After CO_2 injection ceased, the Jackson formation water had persistently low pH values (5.7-6.2) and elevated alkalinity over the yearlong monitoring program (Frailey *et al.*, 2012). As with the GWB model, field results indicate minimal, if any, mineral trapping within the reservoir and solubility trapping as the main mechanism for sequestration of CO_2. Overall, the model is generally successful in predicting the types of reactions occurring before, during, and after CO_2 injection at Sugar Creek; however, aqueous geochemical responses are slower in real time, as evidenced by actual field data as compared to model simulations.

Table 6.1 Calculated change in porosities after CO_2 injection phase II and post-CO_2 injection phase for Jackson reservoir and seal rocks. Positive values indicate a net dissolution (porosity increase) whereas negative values indicate a net precipitation (porosity decrease).

	CO_2 injection phase II	Post-CO_2 injection phase
Reservoir Rocks	0.0078%	-0.0078%
Seal Rocks	-0.00057%	-0.0045%

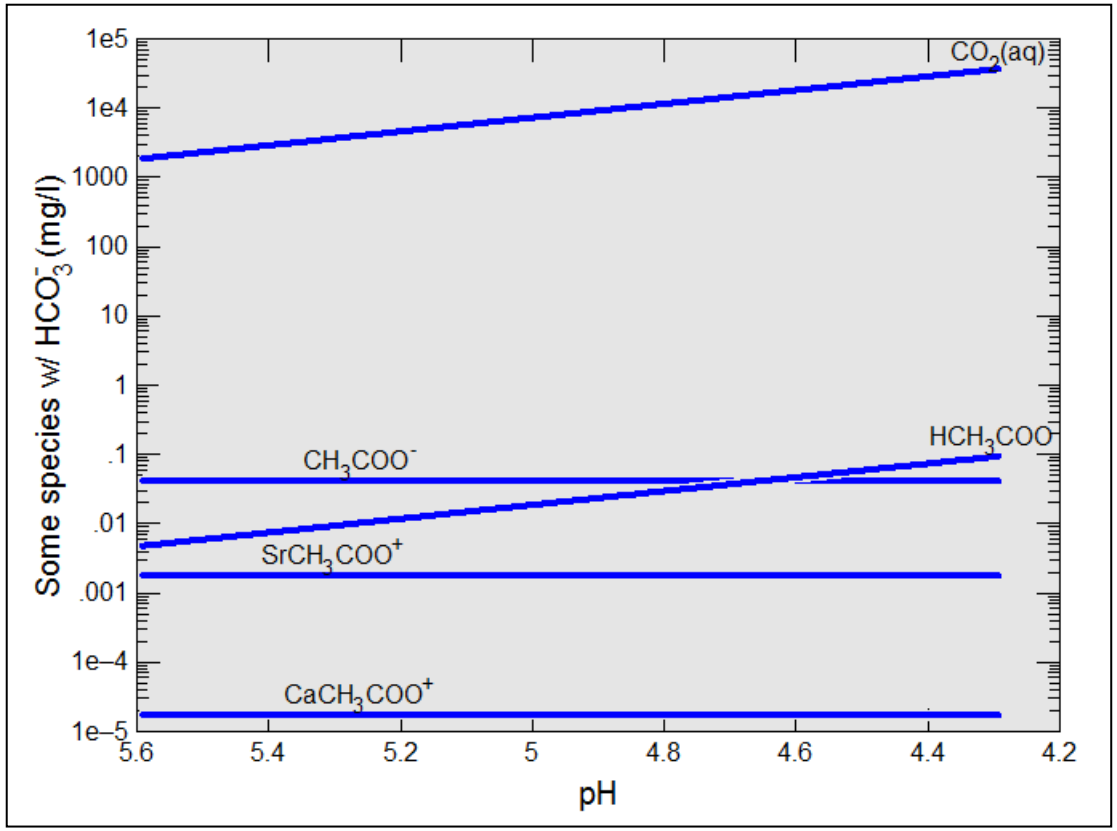

Figure 6.1 Plot from GWB showing HCO_3^- species interactions as pH rapidly decreases during CO_2 injection phase I. Acetate (CH_3COO^-) combines with hydrogen ions (H^+) to form acetic acid (HCH_3COO).

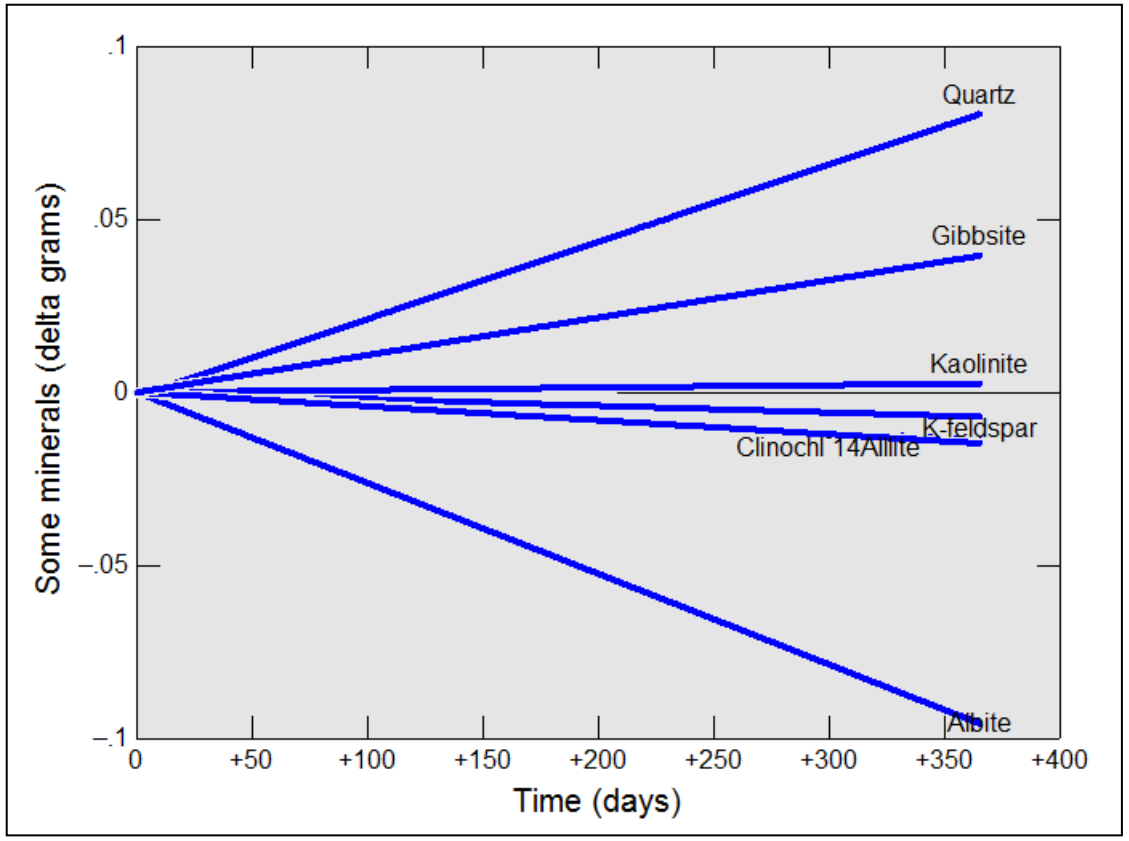

Figure 6.2 Plot from GWB showing delta mass (grams) versus time in days for some alumino-silicate minerals during CO_2 injection phase II for the mid-point fugacity. Chlorite is represented as chlinochlor-14A in the plot.

Chapter 7: Conclusions

Geochemical modeling of CO_2 injection in the Mississippian Jackson sandstone (Jackson) reservoir at Sugar Creek oil field provides insight into geochemical interactions among CO_2, rock-forming minerals, and formation water in the reservoir and seal. Inputs for the GWB model include a robust set of water chemistry data attained from formation water samples collected in and around Sugar Creek field, as well as reservoir and seal mineralogy data collected from XRD analysis of cuttings samples. This study also provides the opportunity to compare modeling results with actual geochemical measurements collected at Sugar Creek as part of a CO_2 injection pilot program administered by the Midwest Geological Sequestration Consortium. CO_2 fugacity (fCO_2), a critical variable in this study, is calculated from pressure and gas composition data collected in the field before, during, and after CO_2 injection (Frailey *et al.*, 2012).

Analysis of formation water in the Jackson reservoir and seal indicates NaCl-rich water, but with a wide range of salinity values. The variation in salinity is likely due to variations in the degree of mixing between original Jackson formation water and fresher water taken from an overlying Pennsylvanian aquifer and used for secondary recovery. The variation in salinity distribution in the field indicates compartmentalization of the Jackson reservoir. XRD analysis coupled with macroscopic examination shows Jackson reservoir samples to be primarily quartz-rich sandstones cemented with quartz, calcite, dolomite, and ankerite. The overlying seal rocks in the upper Jackson and Golconda Formation show a decreased quartz content and increased weight percent of clay, feldspar, and carbonate. The Jackson mineral assemblage is similar to other Chesterian sandstone formations such as the Tar Springs and Hardinsburg (Swann, 1967). Therefore,

the predicted reactions associated with CO_2 injection would likely be similar among the Chesterian sandstone reservoirs. The potential application of CO_2 storage and CO_2-enchaned oil recovery in other Chesterian reservoirs in the southern Illinois basin is further supported by similar temperatures and pressures among them (Takacs *et al.*, 2010; Frailey *et al.*, 2012).

Modeling is accomplished by using four phases: 1) pre-CO_2 injection, 2) CO_2 injection phase I, 3) CO_2 injection phase II, and 4) post-CO_2 injection. During and after CO_2 injection, a variety of reactions are capable of geochemically trapping CO_2 in the Jackson sandstone reservoir. During CO_2 injection, pH values decreased 0.3 to 0.9 pH units, suggesting the dissolution of CO_2 into formation water and subsequent dissociation of carbonic acid. Simulations representing continuous CO_2 injection over one year suggest that dissolution of calcite will be the dominant reaction influencing the change of mass within the reservoir and seal rocks. Dissolution thus predicts that CO_2 will be trapped in solution (solubility trapping). Despite decreases in pH to values ranging from 4.9 to 5.7, calcite dissolution provides Ca^{+2} and HCO_3^- that drives precipitation of dolomite (ankerite) and strontianite. The precipitation of the carbonate minerals thus represents the potential for mineral trapping even as CO_2 is being injected. Analysis of alumino-silicate mass changes shows that most dissolution is associated with albite and smaller amounts of K-feldspar, illite, and chlorite. The overall mass change involved in the alumino-silicate reactions is much smaller than carbonates, which can be attributed to slow reaction rates (White and Brantley, 1995; Brantley, 2008). However, the alumino-silicate reactions might still have significant effects, especially in the seal rock where porosity is low.

The potential for mineral trapping continues into the post-CO_2 period as the calcite and smaller amounts of dolomite (ankerite) and strontianite are predicted to precipitate in the reservoir rocks. The increased alkalinity and cations (i.e. Ca^{+2}, Sr^{+2}, Mg^{+2}) provided by the dissolution of carbonates during the CO_2 injection simulation steps allows calcite, dolomite, and strontianite to precipitate in the post-CO_2 simulation, where fCO_2 is returned to pre-CO_2 injection values. The alumino-silicate minerals, such as K-feldspar, albite, chlorite, and illite are undersaturated at the end of the CO_2 injection simulation steps and therefore are not explicitly included in the basis or as reactants in the post-CO_2 simulation. Consequently, the reaction paths of these minerals are not modeled; however, it is likely that they would continue to dissolve albeit at declining rates as pH increased to pre-CO_2 injection values. The top three minerals (based on volume precipitated) post-CO_2 injection in the seal rocks are calcite, dolomite (ankerite), and kaolinite ($Al_2Si_2O_5(OH)_4$). As with reservoir rocks, the Ca^{+2} and Mg^{+2} needed for calcite and dolomite precipitation are already present in the initial system, and K-feldspar dissolution contributes Al to the system in order to produce kaolinite.

Despite accounting for most of the mass and volume change during CO_2 injection, the carbonate reactions caused porosity to increase and decrease by less than one percent in the reservoir and seal rocks, respectively. After CO_2 injection, the carbonate precipitation reactions caused porosity to decrease by less than one percent in both the reservoir and seal rocks. Although simulated porosity changes were negligible for this study, field projects with longer injection intervals will likely see more significant changes as the CO_2-water-rock reactions in the reservoir and seal intervals will occur

over longer periods of time. Precipitation of carbonate in the seal rocks would further reduce porosity and enhance seal properties.

The post-CO_2 injection phase, in which a sliding fCO_2 model is used, is likely the least effective of the simulation steps in accurately representing the geochemical evolution in the reservoir. The full suite of potential geochemical interactions is not addressed as most of the alumino-silicate minerals are not included. Moreover, the post-CO_2 period at Sugar Creek represents a return to water flood. Geochemically, this is significant, because the injection water mixture includes NaHCO3-rich water that could react with alkaline earth cations (e.g. Ca^{+2}, Sr^{+2}, $Mg^{+}2$) whose values are elevated because of mineral dissolution during CO_2 injection. Because of this, the sliding fugacity model likely underestimates potential mineral trapping. Using GWB's mixing model function would provide a more accurate estimate of geochemical interactions in the post-CO_2 phase.

7.1 Limitations of Geochemical Modeling

Geochemical modeling is a powerful tool that can allow for the analysis of long-term reactions not able to be readily studied within a laboratory. Nevertheless, it is important to note that the model created is only as accurate as the input data provided and the overall understanding of a given system. Although this study provides high quality data from a pilot project and successfully notes important subsurface reactions, additional detailed work is needed. As noted in the previous section, one major limitation to the modeling conducted in this study is that there is no reactive transport component, which integrates geochemical and hydrological processes in complex geologic systems. The

modeling results from this study allow for general statements to be made regarding potential reactions occurring, but they do not explicitly address the distribution of free-phase CO_2, how spatial variations in reservoir properties might influence the timing of geochemical reactions, and how those reactions could affect reservoir properties. Therefore, a more in-depth estimate of the fate of CO_2 should include a transport component. Additionally, the modeling should address transport and reactions where multiple fluid phases are present, such as CO_2, oil, and formation water. Another limitation in the study includes the GWB software itself, which was not designed to simulate reactions under high CO_2 fugacity. The GWB database had to be updated to account for the salting-out effect and other alterations (i.e. kinetic reaction rates) were made in order to allow the system to come to equilibrium (Allen *et al.*, 2005).

7.2 Future Work

Future geochemical reaction studies involving CO_2 injection would benefit by comparing the fate of CO_2 in reservoirs where CO_2 is miscible versus immiscible. In the Illinois basin, the targeted potential EOR resource includes immiscible and miscible oil fields (U.S. DOE, 2012). Successful analysis would require the ability to model reactions with multiple phases. Lastly, although most oil occurs in clastic reservoirs in the Illinois basin, it would be beneficial to compare the differences in geochemical interactions between clastic and carbonate reservoirs, the latter of which are important in other parts of Kentucky.

References

Allen, D. E., B. R. Strazisar, Y. Soong and S. W. Hedges. (2005) Modeling carbon dioxide sequestration in saline aquifers: significance of elevated pressures and salinities. *Fuel Processing Technology*. Vol. 86, pp. 1569-1580.

American Society for Testing and Materials. (1988) Standard test method for anions in water by ion chromatography. D4327-88. *Annual Book of ASTM Standards.* American Society for Testing and Materials, Philadelphia, PA.

American Society for Testing and Materials. (1992) Standard test method for acidity or alkalinity of water. D1067-92. *Annual Book of ASTM Standards.* American Society for Testing and Materials, Philadelphia, PA.

American Society for Testing and Materials. (1997) Standard test method for total dissolved solids dried at 180˚C. 2540C. *Annual Book of ASTM Standards*. American Society for Testing and Materials, Philadelphia, PA.

Arvidson, R. S., I. E. Ertan, J. E. Amonette, and A. Luttge. (2003) Variation in calcite dissolution rates: a fundamental problem?. *Geochimica et Cosmochimica Acta*. Vol. 67, No. 9, pp. 1623-1634.

Bachu, S., W. D. Gunter and E. H. Perkins. (1994) Aquifer disposal of CO_2: hydrodynamic and mineral trapping. *Energy Conversion and Management*. Vol. 35, pp. 269-279.

Bachu, S. (2000) Sequestration of CO_2 in geological media: criteria and approach for site selection in response to climate change. *Energy Conversion and Management*. Vol. 41, pp. 953-970.

Bachu, S. (2002) Sequestration of CO_2 in geological media in response to climate change: road map for site selection using the transform of the geological space into the CO_2 phase space. *Energy Conversion and Management*. Vol. 43, pp. 87-102.

Bachu, S. (2003) Screening and ranking of sedimentary basins for sequestration of CO_2 in geological media in response to climate change. *Environmental Geology*. Vol. 44, pp. 277-289.

Bachu, S. and J. J. Adams. (2003) Sequestration of CO_2 in geological media in response to climate change: capacity of deep saline aquifers to sequester CO_2 in solution. *Energy Conversion and Management*. Vol. 44, No. 20, pp. 3151-3175.

Bachu, S., D. Bonijoly, J. Bradshaw, R. Burress, S. Holloway, N. P. Christensen and O. M. Mathiassen. (2007) CO_2 storage capacity estimation: methodology and gaps. *International Journal of Greenhouse Gas Control*. Vol. 1, pp. 430-443.

Bandstra, J. Z., H. L. Buss, R. K. Campen, L. J. Liermann, J. Moore, E. M. Hausrath, A. K. Navarre-Sitchler, J. Jang, and S. L. Brantley. (2008) Appendix: Compilation of mineral dissolution rates *in* Brantley, S. L., J. D. Kubicki, and A. F. White (eds.), *Kinetics of Water-Rock Interaction.* Springer Science and Business Media, LLC., New York, NY. 833 pages.

Bardon, C., P. Corlay, and D. Longeron. (1991) Interpretation of a CO_2 huff 'n' puff field case in a light-oil-depleted reservoir. *Society of Petroleum Engineers Publication 22650*. 11 pages.

Bergman, P. D. and E. M. Winter. (1995) Disposal of carbon dioxide in aquifers in the U. S. *Energy Conversion and Management*. Vol. 36, No. 6-9, pp. 523-526.

Bethke, C. M. (2008) *Geochemical and Biogeochemical Reaction Modeling*. Cambridge, UK, Cambridge University Press. 2nd ed. 543 pages.

Brantley, S. L. (2008) Chapter 5: Kinetics of mineral dissolution *in* Brantley, S. L., J. D. Kubicki, and A. F. White (eds.), *Kinetics of Water-Rock Interaction*. Springer Science and Business Media, LLC., New York, NY. 833 pages.

Carr, T.R., L. H. Wickstrom, C. P. Korose, R. S. Fisher, W. Solano-Acosta and N. Eaton. (2003) Online tools to evaluate saline aquifers for CO_2 sequestration: Kansas Geological Survey, Open-File Report 2003-33. Available online from: www.midcarb.org/Documents/ofr2003-33.html.

Cook, P. J. (1999) Sustainability and nonrenewable resources. *Environmental Geosciences*. Vol. 6, No. 4, pp. 185–190.

Cotton, F.A. and G. Wilkinson. (1976) *Basic Inorganic Chemistry*. John Wiley and Sons, New York, NY. 579 pages.

Czernichowski-Lauriol, I., B. Sanjuan, C. Rochelle, K. Bateman, J. M. Pearce and P. Blackwell. (1996) Inorganic geochemistry *in* Holloway, S. (ed.), Final report of the Joule II project No. CT92-0031: the underground disposal of carbon dioxide. Keyworth, Nottingham, UK, British Geological Survey, pp. 183-276.

Duan Z.H., N. Moller and J. H. Weare. (1992) An equation of state (EOS) for CH_4-CO_2-H_2O I: pure systems from 0 to 1000 C and from 0 to 8000 bar. *Geochimica et Cosmochica Acta.*, Vol. 56, pp. 2605-2617.

Duan Z.H. and S.D. Mao. (2006) A thermodynamic model for calculating methane solubility, density and gas phase composition of methane-bearing aqueous fluids from 273 to 523 K and from 1 to 2000 bar. *Geochimica et Cosmochimca. Acta*. Vol. 70, No. 13, pp. 3369-3386. Available online from: http://www.geochem-model.org/models/h2o_ch4_nacl/.

Duchscherer, W. (1965) Secondary recovery by inert gas injection in the Spring Grove Pool, Union County, Kentucky *in* Wilson, E.N. (ed.), Proceedings of the technical sessions. Kentucky Oil and Gas Association, Kentucky Geological Survey, Series 10, Special Publication 10. pp. 7-17.

Frailey, S. M., T. M. Parris, J. R. Damico, R. T. Okwen and R. W. McKaskle. (2012) Carbon storage and enhanced oil recovery: Sugar Creek oil field test site, Hopkins County, Kentucky. Monson, C. C. and J. H. Goodwin (eds.), Illinois State Geological Survey, Open File Series 2012-4. 236 pages.

Fritz, A. J. (1967) Typical lenticular sandstone development and oil entrapment: the Jackson sand in Gibson County, Indiana *in* Geology and Petroleum Production of the Illinois Basin, volume 1. Joint publication of the Illinois and Indiana-Kentucky Geological Societies. pp. 23-28.

Gale, J. and P. Freund. (2001) Coal-bed methane enhancement with CO_2 sequestration worldwide potential. *Environmental Geosciences*. Vol. 8, No. 3, pp. 210-217.

Gale, J. (2002) Geological storage of CO_2: what's known, where are the gaps and what more needs to be done. Paper presented at the 6th International Conference on Greenhouse Gas Control Technologies, Kyoto, Japan, October 2002. 6 pages.

Gaus, I., P. Audigane, L. André, J. Lions, N. Jacquemet, P. Durst, I. Czernichowski-Lauriol and M. Azaroual. (2008) Geochemical modeling and solute transport modeling for CO_2 storage, what to expect from it? *International Journal of Greenhouse Gas Control*. Vol. 2, pp. 605–625.

Gaus, I. (2010) Role and impact of CO_2-rock interactions during CO_2 storage in sedimentary rocks. *International Journal of Greenhouse Gas Control*. Vol. 4, pp. 73-89.

Grabowski Jr., G. J. (2001) Stratigraphy: Mississippian System *in* McDowell, R. C. (ed.), The geology of Kentucky—a text to accompany the geologic map of Kentucky. *USGS Professional Paper 1151-H*. 68 pages. Available from http://pubs.usgs.gov/pp/p1151h/miss.html.

Greb, S. F. and D.C. Harris. (2009) Introduction and background material *in* Parris, T. M., S. F. Greb, and B. C. Nuttall (principal investigators), Evaluation of geologic CO_2 sequestration potential and CO_2 enhanced oil recovery in Kentucky. Final Report for Kentucky Energy and Environment Cabinet, Department of Energy Development and Independence Contract No. PO2-855-0700010071, Kentucky Geological Survey. 327 pages.

Greb, S.F. and M. P. Solis. (2009) Geologic carbon storage (sequestration) potential in Kentucky *in* Parris, T. M., S. F. Greb, and B. C. Nuttall (principal investigators), Evaluation of geologic CO_2 sequestration potential and CO_2 enhanced oil recovery in Kentucky. Final Report for Kentucky Energy and Environment Cabinet, Department of Energy Development and Independence Contract No. PO2-855-0700010071, Kentucky Geological Survey. 327 pages.

Gunter, W. D., E. H. Perkins and T. J. McCann. (1993) Aquifer disposal of CO_2-rich gases: reaction design for added capacity. *Energy Conversion and Management*. Vol. 34, pp. 941-948.

Gunter, W. D., B. Wiwchar and E. H. Perkins. (1997) Aquifer disposal of CO_2-rich greenhouse gases: extension of the time scale of experiment for CO_2-sequestering reactions by geochemical modeling. *Contributions to Mineralogy and Petrology*. Vol. 59, pp. 121-140.

Gupta, N. and E. S. Bair. (1997) Variable-density flow in the midcontinent basins and arches region of the United States. *Water Resources Research*. Vol. 33, No. 8, pp. 1785-1802.

Hanor, J. S. (1994) Physical and chemical controls on the composition of waters in sedimentary basins. *Marine and Petroleum Geology*. Vol. 11, No. 1, pp. 31-45.

Holloway, S. (2005) Underground sequestration of carbon dioxide: a viable greenhouse gas mitigation option. *Energy*. Vol. 30, pp. 2318-2333.

Holloway, S. and R. van der Straaten. (1995) The Joule II Project: the underground disposal of carbon dioxide. *Energy Conversion and Management*. Vol. 36, No. 6-9, pp. 519-522.

IPCC (2001) *Climate Change 2001: Synthesis Report*. A Contribution of Working Groups I, II, and III to the Third Assessment Report of the Intergovernmental Panel on Climate Change [Watson, R.T. and the Core Writing Team (eds.)]. Cambridge University Press, New York. 398 pages.

IPCC (2005) IPCC Special Report on *Carbon Dioxide Capture and Storage*. Prepared by Working Group III of the Intergovernmental Panel on Climate Change [Metz, B., O. Davidson, H. C. de Conick, M. Loos and L. A. Meyer (eds.)]. Cambridge University Press, New York. 431 pages.

ISGS Oil and Gas Section. (1993) Improved and enhanced oil recovery in Illinois by reservoir characterization: standard operating and QA/QC procedures. Illinois State Geological Survey, Open File Series. 1993-17. 174 pages.

Kharaka, Y. K., L. M. Law, W. W. Carothers and D. F. Goerlitz. (1986) Role of organic species dissolved in formation waters from sedimentary basins in mineral diagenesis *in* D. Gautier (ed.), Relationship of organic matter and mineral diagenesis. *Society of Economic Paleontologists and Mineralogists*. Special Vol., No. 38, pp. 111-122.

Kharaka, Y. K., D. R. Cole, S. D. Hovorka, W. D. Gunter, K. G. Knauss and B. M. Freifeld. (2006) Gas-water-rock interactions in Frio Formation following CO_2 injection: implications for the storage of greenhouse gases in sedimentary basins. *Geology*. Vol. 34, No. 7, pp. 577-580.

Kolata, D. R. and W. J. Nelson. (1991) Tectonic history of the Illinois basin *in* Leighton, M. W., D. R. Kolata, D. F. Oltz, and J. J. Eidel (eds.), Interior Cratonic Basins: American Association of Petroleum Geologists Memoir. No. 51, pp. 263-285.

K/T GeoServices. (2008) Whole rock and clay fraction XRD: discussion of terminology, limitations, sample preparation, and analytical procedures. K/T GeoServices Report Z08227. 5 pages.

McDowell, R.C. (2001) The geology of Kentucky: structural geology—a text to accompany the geologic map of Kentucky. *USGS Professional Paper 1151-H*. 68 pages. Digital copies available from http://pubs.usgs.gov/prof/p1151h/contents.html

Melzer, S. and B. Miller. (2007) EOR and the expanding field of carbon dioxide flooding. American Association of Petroleum Geologists - Eastern Section Annual meeting. Lexington, Ky., September 16, 2007. Short course.

Miller, B. J. (1990) Design and results of a shallow, light oil field-wide application of CO_2 huff 'n' puff process. *Society of Petroleum Engineers/Department of Energy Publication 20268*. 8 pages.

Miller, B. J., C.P Bardon, and P. Corlay. (1994) CO_2 huff 'n' puff field case: Five-year program update. *Society of Petroleum Engineers Publication 27677*. 7 pages.

Miller, B.J. and T. Hamilton-Smith. (1998) Field case: cyclic gas recovery for light oil-using carbon dioxide/nitrogen/natural gas. *Society of Petroleum Engineers Publication 49169*. 6 pages.

Nesse, W.D. (2000) *Introduction to Mineralogy*. Oxford University Press, New York, NY, USA. 442 pages.

Pacala, S. and R. Socolow. (2004) Stabilization wedges: solving the climate problem for the next 50 years with current technologies. *Science*. Vol. 305, pp. 968-972

Palandri, J. L. and Y. K. Kharaka. (2004) A compilation of rate parameters of water-mineral interaction kinetics for application to geochemical modeling. *USGS Open File Report 2004-1068*. 70 pages.

Parris, T. M., D. J. Webb, K. G. Takacs, and N. Fedorchuk. (2010) Chapter 3: Geochemical characterization of formation waters in Kentucky and implications for geologic carbon storage *in* Parris, T. M., S. F. Greb, and B. C. Nuttall (principal investigators), Evaluation of geologic sequestration potential and enhanced oil recovery in Kentucky. KGS Report of Investigations 17414. 244 pages.

Potter, P. E., E. Noscow, N. M. Smith, D. H. Swann and F. H. Walker. (1958) Chester cross-bedding and sandstone trends in Illinois Basin. *AAPG Bulletin*. Vol. 45, No. 5, pp. 1013-1046.

Pokrovsky, O. S., and J. Schott. (2001) Kinetics and mechanism of dolomite dissolution in neutral to alkaline solutions revisited. *American Journal of Science*. Vol. 301, pp. 597-626.

Russell, W. L. (1932) Geology of oil and gas fields of western Kentucky. *AAPG Bulletin*. Vol. 16, No. 3, pp. 231-254.

RockWare, Inc. (2009) GWB Modeling Short Course materials. Denver, CO. June 4-5, 2009. 146 pages.

Schlumberger Water Services. (2010) *AquaChem*. Computer software. Vers. 5.1. Available online from: www.swstechnology.com.

Siever, R. (1953) Petrology and sedimentation of upper Chester sandstones. Journal of Sedimentary Research. Vol. 23, No. 4, pp. 207-219.

Stueber, A. M., L. M. Walter, T. J. Huston and P. Pushkar. (1993) Formation waters from Mississippian-Pennsylvanian reservoirs, Illinois basin, USA: Chemical and isotopic constraints on evolution and migration. *Geochimica et Cosmochimica Acta*. Vol. 57, pp. 763-784.

Swann, D.H. (1967) A summary geological history of the Illinois basin *in* Geology and Petroleum Production of the Illinois Basin, volume 1. Joint publication of the Illinois and Indiana-Kentucky Geological Societies. pp 3-27.

Takacs, K. G., B. C. Nuttall and T. M. Parris. (2010) Assessment of Kentucky fields for CO_2-enhanced oil recovery *in* Parris, T. M., S. F. Greb and B. C. Nuttall (principal investigators) Evaluation of geologic sequestration potential and enhanced oil recovery in Kentucky. KGS Report of Investigations 17414. 244 pages.

UIC, Incorporated. (2010) Application note 1: carbon dioxide coulometer. Available online from http://www.uicinc.com/CANs/CarbAppNote_01.pdf.

U.S. Department of Energy (1999) Carbon sequestration research and development: Office of Fossil Energy, Office of Science, Washington, D. C., December. 195 pages. Available online from: www.netl.doe.gov/technologies/carbon_seq/index.html

U.S. Department of Energy (2004) Carbon sequestration technology roadmap and program plan: National Energy Technology Laboratory. 24 pages. Available online from: www.fe.gov/programs/sequestration/publications/programplans/2004/SequestrationRoadmap4-29-04.pdf

U.S. Department of Energy (2012) The 2012 United States carbon utilization and storage atlas: National Energy Technology Laboratory. 4th ed. 130 pages. Available online from: http://www.netl.doe.gov/technologies/carbon_seq/refshelf/atlasIV/Atlas-IV-2012.pdf

Voormeij, D. A. and G. J. Simandl. (2002) Geological, ocean and mineral CO_2 sequestration options: a technical review. *Geoscience Canada*. Vol. 31, No. 1, pp. 11–22.

Wentworth, C. K. (1922) A scale of grade and class terms for clastic sediments. *Journal of Geology*. Vol. 30, pp. 377-392.

White, A.F. and S. L Brantley. (1995) Chapter 1: Chemical weathering rates of silicate minerals, an overview *in* White, A.F. and S.L. Brantley (eds.) Chemical weathering rates of silicate minerals. *Reviews in Mineralogy*. Vol. 31, pp. 1-22.

Wildenborg, A. F. B. and L. G. H. van der Meer. (2002) The use of oil, gas and coal fields as CO_2 sinks. Proceedings of the IPCC Workshop on Carbon Dioxide Capture and Storage, Regina, Canada, 18–21 November.

Zhang, W., Y. Li, T. Xu, H. Cheng, Y. Zheng and P. Xiong. (2009) Long-term variation of CO_2 trapped in different mechanisms in deep saline formations: a case study of the Songlio basin, China. *International Journal of Greenhouse Gas Control*. Vol. 3, pp. 161-180.

Zhu, C. and G.M. Anderson. (2002) *Environmental Applications of Geochemical Modeling*. Cambridge University Press, London, United Kingdom. 304 pages.

Zerai, B. (2006) CO_2 sequestration in saline aquifer: geochemical modeling, reactive transport simulation and single-phase flow experiment. Dissertation, Case Western Reserve University. 269 pages.

Vita

Anne Schumacher

Born in Kalamazoo, MI

Prior Education

- Bachelor of Arts, Geology from Albion College, Albion, MI

Prior Experience

- Geologist, Rhino Resource Partners LP (Lexington, KY)
- Student Researcher, Kentucky Geological Survey (Lexington, KY)
- Teaching Assistant, Department of Earth and Environmental Sciences, University of Kentucky (Lexington, KY)
- Field Hydrogeologist, Bureau of Land Management (Durango, CO)

Professional Memberships

- Geological Society of America
- American Association of Petroleum Geologists
- National Groundwater Association

Professional Publications and Presentations

- **Schumacher, A.M.**, T. M. Parris, A. E. Fryar, E. G. Beck, and K. G. Takacs. (2010) Modeling of CO_2-water-rock interactions in Mississippian sandstone reservoirs of Kentucky. AAPG Eastern Section Meeting, Kalamazoo, MI.
- **Schumacher, A. M.**, T. M. Parris, and A. E. Fryar. (2010) Modeling of CO_2-water-rock interactions in Mississippian sandstone and carbonate reservoirs of Kentucky. GSA North-Central and South-Central Section Joint Meeting, Branson, MO.
- **Schumacher, A. M.**, T. M. Parris, E. G. Beck, K. G. Takacs, and A. E. Fryar. (2010) Modeling of CO_2-water-rock interactions in Mississippian sandstone reservoirs of Kentucky. KWRRI Annual Symposium, Lexington, KY.
- Phillips, J. D., S. McCormack, J. Duan, J. P. Russo, **A. M. Schumacher**, G. N. Tripathi, R. B. Brockman, A. B. Mays, and S. Pulugurtha. (2010) Origin and interpretation of knickpoints in the Big South Fork River basin, Kentucky-Tennessee. *Geomorphology*. Vol. 114, No. 3, pp. 188-198.
- Parris, T. M., D. J. Webb, N. Fedorchuk, S. Daugherty, K. G. Takacs, and **A. M. Schumacher**. (2009) Brine chemistry in the Illinois and Appalachian basins of Kentucky—Implications for Geologic Carbon Sequestration: AAPG Eastern Section Meeting, Evansville, IN.